AD_____

Award Number: W81XWH-08-1-0787

TITLE: SEPT9_v1 Functions in Breast Cancer Cell Division

PRINCIPAL INVESTIGATOR: Qicong Hu

CONTRACTING ORGANIZATION: Leland Stanford Junior University
Stanford, CA 94305

REPORT DATE: January 2012

TYPE OF REPORT: Revised Annual Summary

PREPARED FOR: U.S. Army Medical Research and Materiel Command
Fort Detrick, Maryland 21702-5012

DISTRIBUTION STATEMENT: Approved for public release;
Distribution unlimited

REPORT DOCUMENTATION PAGE

Form Approved
OMB No. 0704-0188

1. REPORT DATE *(DD-MM-YYYY)*	2. REPORT TYPE	3. DATES COVERED *(From - To)*
January 2012	Annual Summary	1 January 2009 - 31 December 2011

4. TITLE AND SUBTITLE

SEPT9_v1 Functions in Breast Cancer Cell Division

5a. CONTRACT NUMBER

5b. GRANT NUMBER
W81XWH-08-1-0787

5c. PROGRAM ELEMENT NUMBER

6. AUTHOR(S)
Qicong Hu

E-Mail: wjnelson@stanford.edu

5d. PROJECT NUMBER

5e. TASK NUMBER

5f. WORK UNIT NUMBER

7. PERFORMING ORGANIZATION NAME(S) AND ADDRESS(ES)
Leland Stanford Junior University
Stanford, CA 94305

8. PERFORMING ORGANIZATION REPORT NUMBER

9. SPONSORING / MONITORING AGENCY NAME(S) AND ADDRESS(ES)
U.S. Army Medical Research and Materiel Command
Fort Detrick, Maryland 21702-5012

10. SPONSOR/MONITOR'S ACRONYM(S)

11. SPONSOR/MONITOR'S REPORT NUMBER(S)

12. DISTRIBUTION / AVAILABILITY STATEMENT
Approved for Public Release; Distribution Unlimited

13. SUPPLEMENTARY NOTES

14. ABSTRACT

Septins comprise a large, conserved family of GTPases that fassemble into apolar filaments, bundles and rings. Septins play important roles in mitosis, cell migration, and cell morphogenesis by forming scaffolds and diffusion barriers. Defects in septin expression, organization and function are implicated in many human diseases including cancer and neuropathies. During this period of funding: 1). We tested the effect of a plant cytokinin, Forchlorfenuron (FCF), on mammalian septins, and showed that FCF effects septin assembly, and induced mitotic and cell migration defects; 2). We showed that in mammalian epithelial cells that vesicles containing apical or basolateral proteins exit the Golgi complex along SEPT2/polyGlu microtubule tracks, and that these tracks are required for the proper morphogenesis of polarized epithelia; 3). We showed that SEPT2 is part of a diffusion barrier at the base of the primary cilium, which transduces extracellular signals through signaling receptors localized in the ciliary membrane, and is essential for retaining receptor-signaling pathways in the primary cilium. In summary, the results of this funding have provided significant advances in defining new functions for septins that provide novel insights into cellular functions and defects that could occur in human diseases.

15. SUBJECT TERMS
None Provided.

16. SECURITY CLASSIFICATION OF:			17. LIMITATION OF ABSTRACT	18. NUMBER OF PAGES	19a. NAME OF RESPONSIBLE PERSON
a. REPORT	b. ABSTRACT	c. THIS PAGE			USAMRMC
U	U	U	UU	42	19b. TELEPHONE NUMBER *(include area code)*

Table of Contents

ABSTRACT continued:
Septins comprise a large, conserved family of GTPases that form linear heterotrimers in mammalian cells that assemble into apolar filaments, bundles and rings. Septins play important roles in mitosis, cell migration, and cell morphogenesis by forming scaffolds and diffusion barriers. Defects in septin expression, organization and function are implicated in many human diseases including cancer and neuropathies. During this period of funding: 1). We tested the effect of a plant cytokinin, Forchlorfenuron (FCF), on mammalian septins. We showed that FCF effects septin assembly, and induced mitotic and cell migration defects, indicating that FCF is a promising tool to study mammalian septin organization and functions; 2). We showed that in mammalian epithelial cells that vesicles containing apical or basolateral proteins exit the Golgi complex along SEPT2/polyGlu microtubule tracks, and that these tracks are required for the proper morphogenesis of polarized epithelia; 3). We showed that SEPT2 is part of a diffusion barrier at the base of the primary cilium, which transduces extracellular signals through signaling receptors localized in the ciliary membrane, and is essential for retaining receptor-signaling pathways in the primary cilium. In summary, the results of this funding have provided significant advances in defining new functions for septins that provide novel insights into cellular functions and defects that could occur in human diseases.

INTRODUCTION:
The major components of the mammalian cytoskeleton comprise three types of filamentous polymers: actin microfilaments, microtubules and intermediate filaments. Based on their fibrous organization, septins have been identified as a fourth type of cytoskeleton. Do septins comprise a unique cytoskeleton with functions distinct from those of the other three types of filaments, or do they regulate functions of the cytoskeleton elements with which they are associated? The properties of septins indicate that they provide a skeleton-like scaffold that structurally supports membranes, however they also appear to function as regulatory scaffolds in the organization and function of the microtubule cytoskeleton. The goals of the work were to understand the interactions and functions of septins with the microtubule cytoskeleton in different cellular processes. This was accomplished by: 1). Studying the effects of a small molecule inhibitor (FCF); 2). Examining the roles of septins and microtubules in vesicle trafficking and epithelial morphogenesis; and 3). Discovering a role of septins in regulating signaling by the primary cilium. The results provide novel insights into the regulation and function of septin filaments, and define new mechanisms regulating important cellular functions.

BODY:

1). Study the effects of a small molecule inhibitor Forchlorfenuron (FCF) on septin oirganization and function (*see attached Publication_1.pdf*):

Small molecules that reversibly perturb septin organization and function would be valuable tools for dissecting septin functions and could be used for therapeutic treatment of septin-related diseases. An earlier study showed that the small molecule compound Forchlorfenuron (FCF, a plant cytokinin) disrupted septin organization and caused cytokinesis defects in budding yeast. However, that study did not show whether FCF acted directly and specifically on septins, and if so, how FCF acted on septins and whether FCF could be used as a tool to study mammalian septin organization and functions.

Our results show that FCF specifically altered septin assembly in vitro but did not affect actin or tubulin polymerization (*see Figures 1 & 2, Publication_1.pdf*). These observations are in agreement with our studies in mammalian cells showing that FCF induced changes in septin organization from short, thin fibrilla to long, thick bundle-like filaments. These effects of FCF in cells were reversible. To elucidate how FCF acts on septins, we examined SEPT2 dynamics in vivo using FRAP (*see Figure 3, Publication_1.pdf*). The results reveal that FCF increased both the half-time of recovery and the immobile fraction, indicating an increase in the stability of septin filaments. This is consistent with the FCF-induced changes in septin organization observed both in vitro and in cells (*see Figures 1 & 2, Publication_1.pdf*). Moreover, our FRAP data indicate that the thick bundle-like septin filaments induced by FCF arise from a decrease in the koff of septin assembly (lower dissociation rate), which progressively results in accumulation of abnormally large filamentous structures. FCF-induced changes in septin dynamics and organization resulted in defects in cell mitosis (*see Figure 4, Publication_1.pdf*) and migration (*see Figure 5, Publication_1.pdf*). We suggest that stabilization of septin filaments by FCF reduces the turnover rate of septin filaments and therefore the relative abundance of cytoplasmic and filamentous

septins, which is critical for their function. These results are in accordance with the effects of septin depletion or over-expression, which alter overall septin organization and function. FCF provides a high degree of temporal control over septin function, acting within 1 h, and is reversible (*see Figure 2, Publication_1.pdf*); therefore, it may prove more useful than siRNA as a probe for septin functions.

In summary, our results show that FCF alters mammalian septin assembly in vitro and alters septin organization and dynamics in cells by stabilizing septin filaments. These results suggest that FCF will be useful as a tool to study septin biology. With low levels of cytotoxicity, anti-mitotic, and anti-migratory efficacies, FCF could be considered as a septin-based anti-tumorigenic agent.

1). Examine the roles of septins and microtubules in vesicle trafficking and epithelial morphogenesis (*see attached Publication_2.pdf*):

The plasma membrane of polarized columnar-shaped epithelial cells is segregated into functionally distinct apical and basolateral domains that face different biological compartments and regulate vectorial transport of ions and solutes. Biogenesis of these membrane domains and maintenance of cell shape depend on protein sorting during vesicle budding from the TGN and endosomes, transport of vesicles along the actin and microtubule cytoskeleton, and their fusion with the appropriate membrane domain. The microtubule cytoskeleton is involved in long-range transport of vesicular carriers and in the morphogenesis of columnar-shaped, polarized epithelial cells. How release and transport of vesicles from the Golgi complex to the plasma membrane are coordinated with microtubule organization is unknown. In the budding yeast *Saccharomyces cerevisiae*, polarized membrane growth is spatiotemporally coordinated by septins. In mammalian cells, septins bind to microtubules, but the functional significance of this association in interphase cells and the role of septins in the morphogenesis of polarized epithelia are unknown. Therefore, we examined the distribution and function of the mammalian SEPT2 with respect to the microtubule cytoskeleton of Madin-Darby canine kidney (MDCK) cells.

Immunofluorescence and live cell imaging of nonpolarized MDCK cells revealed a juxtanuclear tuft of SEPT2 fibers closely apposed to the Golgi complex, that SEPT2 fibers co-aligned with a subset of microtubules containing poly-glutamylated (polyGlu) tubulin (*Figure 3, Publication_2.pdf*), and their distribution was dependent on microtubule structural integrity (*see Figure 1, Publication_2.pdf*). Significantly, the majority of transport vesicles exiting the Golgi complex appeared to move along septin/polyGlu microtubule tracks (*Figure 2, Publication_2.pdf*), and disruption of septin filaments or polyGlu microtubules resulted in greatly reduced trafficking of vesicles form the Golgi to the plasma membrane (*Figure 2, Publication_2.pdf*). Having shown that SEPT2 plays roles in vesicular transport, we tested whether SEPT2 is required for the establishment of epithelial membrane polarity and columnar cell shape. We depleted endogenous SEPT2 from nonpolarized, and then assayed cell polarity and shape in monolayers of polarized cells (*Figure 5, Publication_2.pdf*). Significantly, SEPT2-depleted cells lacked an apical dome and honeycomb morphology characteristic of a polarized, columnar epithelium, and were elongated along their long axis and were shorter compared with control cells. Moreover, in SEPT2- depleted cells, levels of endogenous apical (gp135/podocalyxin) and basolateral (Na/K-ATPase) membrane markers were significantly reduced from their respective membrane domains, and these proteins accumulated intracellularly in punctate structures (*Figure 5, Publication_2.pdf*).

In summary, SEPT2 binding to polyglutamylated microtubules appears to specify a functionally distinct subset of microtubule tracks on which " fast track " vesicle transport occurs. The rate of vesicle trafficking may be regulated further by the assembly of "speed bumps" along polyGlu microtubules by accessory proteins (eg., MAP4). Therefore, the balance between the levels of polyGlu microtubules, SEPT2, and MAP4 may control the amount of vesicle transport to the plasma membrane. For example, different amounts of vesicle transport may be required for rapid membrane growth during morphogenesis of a columnar epithelium compared with those required to maintain homeostasis or in response to physiological stress (wound healing).

3). A role of septins in regulating signaling by the primary cilium (*see attached Publications_3 & 4.pdf*):

The primary cilium in mammals was first identified over 100 years ago (Zimmermann 1898). However, it was considered a vestigial appendage of little importance and was largely ignored until the last decade when

studies began to link ciliary dysfunction with genetic diseases such as polycystic kidney disease (PKD). Recent studies have revealed that the primary cilium is the cell's antenna which receives and transmits extracellular signals through specific receptors on the ciliary membrane that initiate cell signaling cascades critical for normal development and homeostasis. Heritable diseases, called ciliopathies, are associated with ciliary dysfunction, and include cystic kidneys, retinal degeneration, hearing loss, situs inversus, and other defects (*for a review, see Publication_3.pdf*).

The ciliary membrane is contiguous with the surrounding plasma membrane but retains a distinct composition of lipids and proteins required for cilia-mediated sensing/signaling events, ciliary membrane trafficking and ciliogenesis. However, mechanisms for retaining these proteins and lipids in the primary cilia are not clear. We directly tested the presence of a diffusion barrier using fluorescence recovery after photobleaching (FRAP; *Figure 1, Publication_4.pdf*). Photobleaching of part or the whole cilium or plasma membrane pool revealed that four membrane proteins in the apical plasma membrane and ciliary membrane were mobile, but did not exchange, indicating the presence of a physical barrier that blocked the free diffusion of those membrane proteins between these two adjacent plasma membrane compartments. To identify molecular components of this ciliary membrane diffusion barrier we focused on septins. SEPT2 localized to the base of the cilium at the boundary between the ciliary and periciliary membrane in IMCD3 cells, and in MEFs stably expressing Smo^{YFP} (*Figure 2, Publication_4.pdf*). In some optical sections SEPT2 staining appeared as a ring-like structure of ~500nm diameter reminiscent of structures formed by recombinant septins in vitro, and as two fused dots similar to septin staining at the sperm annulus. SEPT2 localized between the ciliary axoneme (marked by acetylated a-tubulin, ^{Ac}Tub) and structures marked by the distal appendage protein CEP164, the subdistal/distal appendage protein outer dense fiber 2 (Odf2), and the pericentriolar protein pericentrin (PeriCT) (*Figure 2, Publication_4.pdf*).

To test whether SEPT2 is part of a diffusion barrier at the base of the ciliary membrane, we measured ciliary membrane protein mobility in the 10-15% of the stable SEPT2-depleted IMCD3 cells. We detected a significant increase in the diffusional mobility of 4 ciliary membrane proteins when the whole cilium was photobleached in SEPT2-depleted cells compared to controls (*Figure 4, Publication_4.pdf*). Furthermore, the Barrier Index, defined as the ratio of mean fluorescence intensity of these proteins in the ciliary membrane to surrounding periciliary membrane, was reduced significantly in SEPT2-depleted cells compared to controls (*Figure 4, Publication_4.pdf*). finally, we tested whether loss of the ciliary membrane diffusion barrier following SEPT2 depletion affected cilium-dependent receptor signal transduction. Shh signaling requires enrichment of Smo in the ciliary membrane, and signal transduction results in increased *Gli1* and *Patched1* (*Ptc1*) mRNA levels. In SEPT2-depleted cells, Smo accumulation in cilia was reduced, although total cellular levels were unaffected. After induction with Shh or Smo agonist (SAG), *Gli1* and *Ptc1* mRNA levels were reduced significantly in SEPT2-depleted cells compared to controls (*Figure 4, Publication_4.pdf*). Thus, the SEPT2 diffusion barrier is required for cilium-dependent Shh signal transduction.

In summary, we identified a septin-containing diffusion barrier at the base of the ciliary membrane that is required to retain receptor-signaling pathways in the primary cilium. This diffusion barrier restricts the diffusion of ciliary membrane proteins between the ciliary and periciliary membrane, but permits the diffusion of ciliary transport proteins. Thus, septins appear to have evolutionarily conserved roles from fungi to animals in the functional compartmentalization of membrane domains.

KEY RESEARCH ACCOMPLISHMENTS:

- Identified and characterized a small molecule inhibitor (FCF) that affects septin assembly, organization and epithelial polarity and morphogenesis;
- Defined mechanisms involving the roles of septins and microtubules in vesicle trafficking and epithelial morphogenesis;
- Discovered a role of septins as a diffusion barrier at the base of the primary cilium, and its sole in regulating signaling by the primary cilium.
- Overall, these results provide novel insights into the regulation and function of septin filaments, and define new mechanisms regulating important cellular functions that are defective in a variety of human diseases.

REPORTABLE OUTCOMES

A. Manuscripts:

1. **Hu, Q.**, Nelson, W. J. and Spiliotis, E. T. (2008). Forchlorfenuron alters mammalian septin assembly, organization, and dynamics. *J. Biol. Chem.* **283**, 29563-29571. *PMCID: PMC3143192*
2. Spiliotis, E., Hunt, V. S., **Hu, Q.**, Kinoshita, M. and Nelson, W. J. (2008). Epithelial polarity requires septin coupling of vesicle transport to polyglutamylated microtubules. *J. Cell Biol.* **180**, 295-303. *PMCID: PMC2213583*
3. **Hu, Q.**, Milenkovic, L., Jin, H., Scott, M. P., Nachury, M., Spiliotis, E. T. and Nelson, W. J. (2010). A septin diffusion barrier at the base of the primary cilium maintains ciliary protein distributions. *Science*. **329**, 436-439. *PMCID: PMC3092790*
4. **Hu, Q.** and Nelson, W. J. (2011). Ciliary diffusion barrier: the gatekeeper for the primary cilium compartment. Cytoskeleton **68**, 313-324.

B. Degrees obtained:

Qicong Hu was awarded a Ph.D. from Stanford University in 2012

C. Development of Cell Lines:

All reagents developed from these studies (plasmids, antibodies and cell lines) are available to all science colleagues without questions or charge. For example, the novel cell lines reported in *Science*. **329**, 436-439 (2010) have been sent to >10 laboratories world-wide.

D. Funding Applied for:

A Program Project (PO1) application (NIH PO1 GM102089-01; *Mechanisms of cilium-based signaling*) has been submitted to the NIH.

CONCLUSIONS:

The goals of the work were to understand the interactions and functions of septins with the microtubule cytoskeleton in different cellular processes. This was accomplished by: 1). Studying the effects of a small molecule inhibitor (FCF); 2). Examining the roles of septins and microtubules in vesicle trafficking and epithelial morphogenesis; and 3). Discovering a role of septins in regulating signaling by the primary cilium. The results provide novel insights into the regulation and function of septin filaments, and define new mechanisms regulating important cellular functions. The knowledge gained by these studies have identified key functions of septins in membrane trafficking, signaling and epithelial morphogenesis and functions. The results have identified ways to inhibit septin organization and function including a small molecule inhibitor (Forchlorfenuron) and si/shRNAs that could be applied in the future to test the role of septins in diseases and as a therapy when septins are over- or mis-expressed.

LIST OF PERSONNEL:

Qicong Hu (PI/Fellow), Graduate Student
W. James Nelson (mentor), Professor of Molecular and Cellular Physiology
Elias T. Spiliotis, postdoctoral fellow (now an Assistant Professor at Drexel University)
Maxence V. Nachury, Assistant Professor of Molecular and Cellular Physiology
Matthew P. Scott, Professor of Developmental Biology, Genetics and Bioengineering
Ljiljana Milenkovic
Hua Jin

APPENDICES:

1. **Publication_1.pdf:** Hu, Q., Nelson, W. J. and Spiliotis, E. T. (2008). Forchlorfenuron alters mammalian septin assembly, organization, and dynamics. *J. Biol. Chem.* **283**, 29563-29571. *PMCID: PMC3143192*
2. **Publication_2.pdf:** Spiliotis, E., Hunt, V. S., **Hu, Q.**, Kinoshita, M. and Nelson, W. J. (2008). Epithelial polarity requires septin coupling of vesicle transport to polyglutamylated microtubules. *J. Cell Biol.* **180**, 295-303. *PMCID: PMC2213583*
3. **Publication_3.pdf:** Hu, Q. and Nelson, W. J. (2011). Ciliary diffusion barrier: the gatekeeper for the primary cilium compartment. Cytoskeleton **68**, 313-324.
4. **Publication_4.pdf:** Hu, Q., Milenkovic, L., Jin, H., Scott, M. P., Nachury, M., Spiliotis, E. T. and Nelson, W. J. (2010). A septin diffusion barrier at the base of the primary cilium maintains ciliary protein distributions. *Science*. **329**, 436-439. *PMCID: PMC3092790*

THE JOURNAL OF BIOLOGICAL CHEMISTRY VOL. 283, NO. 43, pp. 29563–29571, October 24, 2008

Forchlorfenuron Alters Mammalian Septin Assembly, Organization, and Dynamics*[S]

Received for publication, June 30, 2008, and in revised form, August 15, 2008 Published, JBC Papers in Press, August 18, 2008, DOI 10.1074/jbc.M804962200

Qicong Hu[‡], W. James Nelson[‡§], and Elias T. Spiliotis[‡1]

From the Departments of [‡]Biology and [§]Molecular and Cellular Physiology, Stanford University, Stanford, California 94305

Septins are filamentous GTPases that associate with cell membranes and the cytoskeleton and play essential roles in cell division and cellular morphogenesis. Septins are implicated in many human diseases including cancer and neuropathies. Small molecules that reversibly perturb septin organization and function would be valuable tools for dissecting septin functions and could be used for therapeutic treatment of septin-related diseases. Forchlorfenuron (FCF) is a plant cytokinin previously shown to disrupt septin localization in budding yeast. However, it is unknown whether FCF directly targets septins and whether it affects septin organization and functions in mammalian cells. Here, we show that FCF alters septin assembly *in vitro* without affecting either actin or tubulin polymerization. In live mammalian cells, FCF dampens septin dynamics and induces the assembly of abnormally large septin structures. FCF has a low level of cytotoxicity, and these effects are reversed upon FCF washout. Significantly, FCF treatment induces mitotic and cell migration defects that phenocopy the effects of septin depletion by small interfering RNA. We conclude that FCF is a promising tool to study mammalian septin organization and functions.

Septins were originally identified in screens for genes that regulate the cell cycle in budding yeast *Saccharomyces cerevisiae* (1). In this organism, septins function as scaffolds and diffusion barriers to localize many proteins required for bud site selection, cell cycle progression, and cell division (2–6). Septins have since been identified in many other eukaryotes ranging from fungi to animals (7, 8). In mammalian cells, septins regulate cytoskeleton organization (9–14) and membrane traffic and fusion (15–17), and during mitosis, they are required for proper chromosome alignment, segregation (18, 19), and cytokinesis (13, 20, 21).

Septins are guanine nucleotide-binding proteins that form filaments associated with membranes and the cytoskeleton (22, 23). Mammalian septin filaments assemble from heteromeric complexes, whose composition varies depending on cell type and level of expression (22, 24). Mammalian septin complexes have been purified from mouse brain and tissue culture cells (9, 16), and the ubiquitously expressed Septin 2 (SEPT2) has been reconstituted *in vitro* into filamentous structures by itself and in a complex with SEPT6 and SEPT7 (9, 25–27). Recently, x-ray crystallography and electron microscopy revealed that SEPT2, SEPT6, and SEPT7 assemble into filaments through their GTP binding domains (27).

An increasing body of evidence implicates the mammalian septin family in the pathogenesis of diverse disease states including neoplasia, neurodegenerative conditions, and infections (28, 29). Many septin isoforms are abnormally expressed in carcinomas (30–34), and altered levels of septin expression strongly correlate with tumorigenic phenotypes such as increased cell growth, motility and invasiveness, and resistance to microtubule-disrupting reagents (35, 36). In neurodegenerative disorders (*e.g.* Alzheimer disease), septins are present in cytosplasmic inclusions and neurofibrillary tangles, and a septin isoform (SEPT4) was recently shown to suppress α-synuclein neurotoxicity in Parkinson disease (37–39). Finally, some septins have been identified as host proteins involved in viral and bacterial infections (40, 41).

Various tools have been developed to study septin organization and functions, including function-blocking antibodies and RNA interference. However, these reagents are not readily reversible, and we have, therefore, turned to small molecule compounds, which could also be of therapeutic value in translational research. A recent study showed that the plant cytokinin forchlorfenuron (FCF;[2] 1-(2-chloro-4-pyridyl)-3-phenylurea, 4PU300) disrupted septin localization and caused cytokinesis defects in budding yeast (42). However, it was unclear whether FCF directly and specifically affected septins, and if so, how FCF affected septin organization and functions. Here, we analyzed the effects of FCF on mammalian septins using recombinant SEPT2/6/7 as an *in vitro* septin assembly system and mammalian cells to study effects *in vivo*. Our studies show that FCF directly alters septin assembly *in vitro* and affects septin organization in mammalian cells by stabilizing septin filaments; these effects of FCF in cells are reversible upon FCF washout. Cells treated with FCF display mitosis defects

* This work was supported, in whole or in part, by National Institutes of Health Grant GM35527 (to W. J. N.). This work was also supported by a Cell and Molecular Biology Training Grant and by grants from the Department of Defense Breast Cancer Research Program Predoctoral Fellowship BC083077 (to Q. H.) and the Stanford Digestive Disease Center (N. G.). The costs of publication of this article were defrayed in part by the payment of page charges. This article must therefore be hereby marked "*advertisement*" in accordance with 18 U.S.C. Section 1734 solely to indicate this fact.

[S] The on-line version of this article (available at http://www.jbc.org) contains three supplemental figures and nine supplemental movies.

[1] To whom correspondence should be addressed: Dept. of Bioscience and Biotechnology, Drexel University, Philadelphia, PA 19104. E-mail: ets33@drexel.edu.

[2] The abbreviations used are: FCF, forchlorfenuron; MDCK, madin-darby canine kidney; FRAP, fluorescence recovery after photobleaching; CENP-E, centromere associated protein E; DMSO, dimethyl sulfoxide; siRNA, small interfering RNA; DMEM, Dulbecco's modified Eagle's medium; FBS, fetal bovine serum; GFP, green fluorescent protein; YFP, yellow fluorescent protein; FI, fluorescence intensities; PIPES, 1,4-piperazinediethanesulfonic acid; DAPI, 4′,6-diamidino-2-phenylindole.

and decreased cell migration that phenocopy the effects of septin knockdown by siRNAs.

EXPERIMENTAL PROCEDURES

Cell Culture, Cell Synchronization, and siRNA Transfections—Madin-Darby canine kidney (MDCK) clone II and HeLa (ATCC CCL-2) cells were maintained as described previously (18). HeLa S3 cells were maintained in high glucose DMEM supplemented with 10% fetal bovine serum (FBS). MDCK-SEPT2-YFP (18), MDCK-actin-GFP (43), and HeLa-α-tubulin-GFP (a gift from L. Wordeman, University of Washington) cells were maintained in DMEM (Sigma-Aldrich) supplemented with 10% FBS and 0.5 mg/ml G418. HeLa S3 cells were synchronized in mitosis by blocking with 2 mM thymidine (Sigma) for 18 h followed by a 4-h release into regular media, and a 12-h incubation with nocodazole (Sigma; 40 ng/ml). HeLa cells were transfected with siCONTROL non-targeting siRNA and SEPT2 siRNAs as described previously (18).

Assembly of Recombinant SEPT2/6/7 in Vitro—Recombinant His-SEPT2/6/7 was purified from insect cells and assembled into filamentous structures as described previously (9). Briefly, His-SEPT2/6/7 was clarified by centrifugation at 100,000 × *g*, diluted to ~0.2 mg/ml, and dialyzed against low salt buffer (5 mM potassium phosphate buffer (pH 7.2), 50 mM KCl, 10% glycerol, 2 mM $MgCl_2$, and 1 mM dithiothreitol) in the presence of FCF (Sigma) or DMSO (Sigma) at 4 °C. Assembly of higher-order SEPT2/6/7 filaments was reversed by dialysis in high salt buffer (5 mM potassium phosphate buffer (pH 7.2), 1 M KCl, 10% glycerol, 2 mM $MgCl_2$, and 1 mM dithiothreitol) for 12 h. Septin structures were transferred to poly-L-lysine-coated glass coverslips and fixed with 3% paraformaldehyde (EM Sciences) in phosphate-buffered saline for 10 min, blocked with 2% bovine serum albumin, and stained with anti-SEPT2 (N5N; rabbit polyclonal antibody). The surface area of septin structures was quantified using the ImageJ software. Negative stain electron microscopy was performed by adsorbing His-SEPT2/6/7 complexes onto glow-discharged carbon-coated copper grids (200 mesh copper hexagonal) for 2 min. Samples were washed twice with water and stained with 1% uranyl acetate for 2 min. Following staining, samples were dried and examined with a CM-12 Philips transmission electron microscope. In pelleting assays of recombinant septin assembly, higher-ordered filamentous structures were centrifuged at 16,000 × *g* for 10 min. Supernatants and pellets were then analyzed by SDS-PAGE and Coomassie Brilliant Blue staining.

Actin and Microtubule Polymerization Assays—Pyrene actin (Cytoskeleton, Inc.) polymerization assay was performed according to the manufacturer's instructions in the presence of different concentrations of FCF or DMSO. Fluorescence intensity was measured using a fluorescence plate reader (Tecan Group Ltd.; excitation 360 nm, emission 405 nm). A bovine tubulin (Cytoskeleton, Inc.) polymerization assay was performed according to the manufacturer's instructions in the presence of various concentrations of FCF or DMSO. Turbidity was measured at 340 nm using a plate reader (Tecan Group Ltd.).

Immunofluorescence Microscopy—Subconfluent cells were fixed with warm PHEM (60 mM Pipes-KOH, pH 6.9, 25 mM Hepes, 10 mM EGTA, and 1 mM $MgCl_2$) containing 3% paraformaldehyde (EM Sciences) and 0.1% Triton X-100 and stained with antisera to SEPT2 (N5N; rabbit polyclonal antibody), SEPT7 (anti-SEPT7; rabbit polyclonal antibody), α-tubulin (DM1α; Sigma-Aldrich), and secondary fluorescein isothiocyanate- or rhodamine red X-conjugated $F(ab')_2$ goat anti-mouse or anti-rabbit IgGs (Jackson ImmunoResearch Laboratories). Microfilaments were stained with Alexa Fluor-355-conjugated phalloidin (Invitrogen). Samples were mounted in VECTASHIELD mounting medium (Vector Laboratories) and imaged with an inverted Zeiss microscope (Axiovert 200) or the Marianas system (Intelligent Imaging Innovations). Cell morphology (axis length ratio) was quantified using the Statistics module in the Slidebook 4.2 software. Staining of MDCK cells for centromere-associated protein E (CENP-E) and CREST serum was performed as described previously (18). Images were captured and deconvolved with an Applied Precision Delta Vision wide field deconvolution system (×63 oil objective; ×1.5 optovar). Quantification of CENP-E-containing kinetochores (n = ~100 per cell) was performed in every fourth optical section from a deconvolved z-stack.

Cytotoxicity Assays—HeLa or MDCK cells were plated overnight on collagen-coated 35-mm tissue culture dishes and then treated with DMSO or FCF for 4 h. Cells were trypsinized, resuspended in DMEM supplemented with 10% FBS, and mixed in a 1:1 ratio with trypan blue (Invitrogen) at room temperature for 1 min. Blue and non-blue cells were counted using a hemocytometer. For alamarBlue assays, HeLa cells (1×10^4/well) were plated onto a 96-well plate (Costar) and cultured overnight. Cells were then treated with FCF or DMSO, and 50 μl of medium was removed and mixed with 5.5 μl of alamarBlue reagent (AbD Serotec) for 2 h. Fluorescence intensities were measured using a plate reader (Tecan Group Ltd.; excitation 560 nm, emission 590 nm). Each measurement was performed in quadruplicates.

Live Cell Imaging and FRAP—Cells were grown on collagen-coated coverslips for 24 h at subconfluent density and imaged in phenol red-free DMEM supplemented with 10% FBS, 25 mM Hepes (Invitrogen) using the Marianas system (Intelligent Imaging Innovations) equipped with the MicroPoint fluorescence recovery after photobleaching (FRAP) laser system (Photonic Instruments). Photobleaching experiments were carried out using the FRAP module of the Marianas system. Equivalent laser intensity, repetition, and exposure time were used for FRAP measurements in FCF- or DMSO-treated samples. Bleached areas were accurately positioned along septin filaments, actin stress fibers, or microtubule bundles. Images were taken 5 s before photobleaching and 5 min after photobleaching at a rate of one frame per second. Fluorescence intensities were quantified after background subtraction and normalization against unbleached areas using the Slidebook 4.2 software as described previously (43). Fluorescence intensities (FI) were plotted against time (t) and fitted to an exponential recovery curve: $FI = FI_{st} - (FI_{st} - FI_{blch})\exp^{(-\ln 2 \times T/t_{1/2})}$ in which FI_{blch} is the fluorescence intensity at the time of bleaching, and FI_{st} is the fluorescence intensity at the final steady status. From this equation, half-times of fluorescence recovery ($t_{1/2}$) were derived. The k_{off} was calculated as $\ln 2/t_{1/2}$, and recovery percentage was

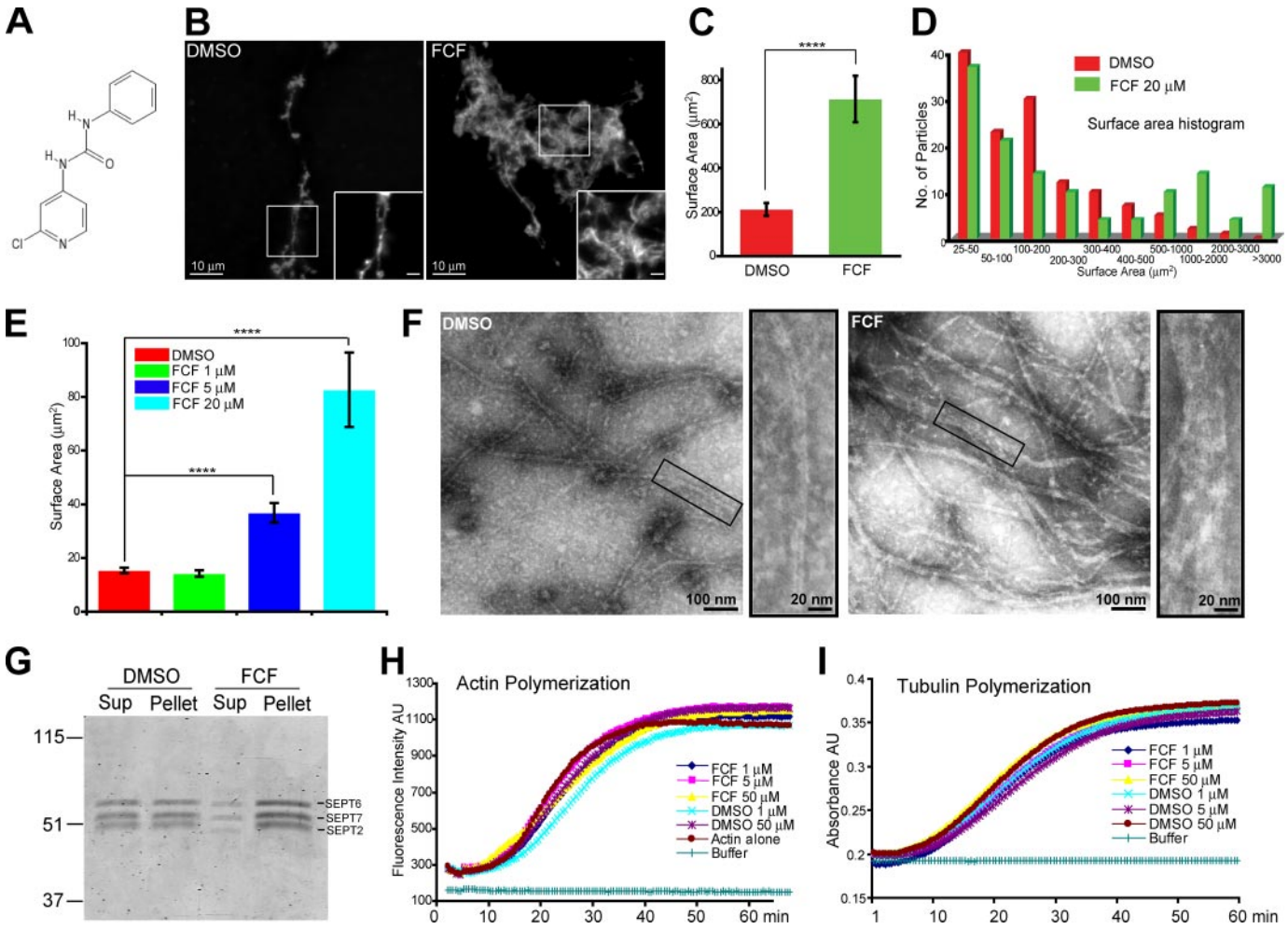

FIGURE 1. **FCF alters SEPT2/6/7 assembly *in vitro*.** *A*, the chemical structure of FCF. *B*, SEPT2/6/7 complexes (0.2 μg/μl) were dialyzed for 2 h in low salt buffer containing FCF (20 μM) or DMSO to induce septin filament assembly. Immunofluorescence images show filamentous structures stained for SEPT2. *Insets* show magnified images of selected regions; *scale bars*, 2 μm. *C*, the bar graph shows the surface areas (mean ± S.E.) of septin filaments after dialysis in DMSO (*red*, $n = 132$) or FCF (*green*, $n = 129$); ****, $p < 0.0001$. *D*, the surface area histogram of septin filaments formed in DMSO (*red*) or FCF (*green*). *E*, the bar graph shows the surface areas (mean ± S.E.) of septin filaments after 1 h dialysis of SEPT2/6/7 (0.1 μg/μl) in low salt buffer containing various concentrations of DMSO (*red*) or FCF (*green*, 1 μM; *blue*, 5 μM; *cyan*, 20 μM); ****, $p < 0.0001$. *F*, representative images of negative stained septin filaments after dialysis in DMSO (*left panel*) or 20 μM FCF (*right panel*). *G*, septin filaments formed in DMSO or FCF were spun at 16,000 × *g*. Supernatant (*Sup*) and pellet (*Pellet*) fractions were resuspended in SDS-sample buffer, analyzed by SDS-PAGE, and stained with Coomassie Blue. *H* and *I*, pyrene actin (*H*) and tubulin (*I*) polymerization assays in the presence of FCF or DMSO.

calculated as: $((FI_{st} - FI_{blch})/(FI_{prebleach} - FI_{blch})) \times 100$ in which $FI_{prebleach}$ is the fluorescence intensity before photobleaching (44, 45). Plots and curve fittings were performed with the Origin 6.1 software.

Cell Motility and Wound-healing Assays—A modified cell motility assay was used (46). Fluorescent beads (1 μm FluoSpheres; Invitrogen) were vortexed, sonicated, and plated onto 18-mm coverslips precoated with collagen and incubated at 4 °C overnight. Excess beads were washed off, and HeLa cells (3×10^3) were plated for 16 h at 37 °C in DMEM and 10% FBS. Cells were fixed, random images were taken, and the surface areas covered by single cells were quantified using the ImageJ software. For wound-healing assays, HeLa cells (2×10^6) were grown on 35-mm dishes overnight in DMEM and 10% FBS. MDCK cells were first plated in low calcium DMEM (5 μM Ca^{2+}) and 10% dialyzed FBS for 75 min, and then the medium was exchanged for DMEM with 10% FBS. Confluent monolayers were scratched with a pipette tip. HeLa and MDCK cells were imaged for 8 and 14 h, respectively. Displacement surface areas (ΔArea) were calculated as $S_i - S_t$ in which S_i is the initial wounded surface area and S_t is the wounded surface area at time point t. The surface areas were quantified using ImageJ.

RESULTS

FCF Alters SEPT2/6/7 Assembly in Vitro—To determine whether FCF (Fig. 1*A*) has a direct effect on mammalian septin assembly, we used recombinant SEPT2/6/7 complex purified from insect cells (9). SEPT2/6/7 complexes were dialyzed in the presence of FCF or DMSO (the vehicle for FCF) in low salt buffer to induce septin self-assembly into higher-order structures, which were analyzed by immunofluorescence microscopy (Fig. 1*B*) or transmission electron microscopy (Fig. 1*F*). Under control conditions (DMSO), SEPT2/6/7 complexes assembled into filamentous structures as reported previously (9). In the presence of 20 μM FCF, SEPT2/6/7 complexes formed structures that were larger and denser than those

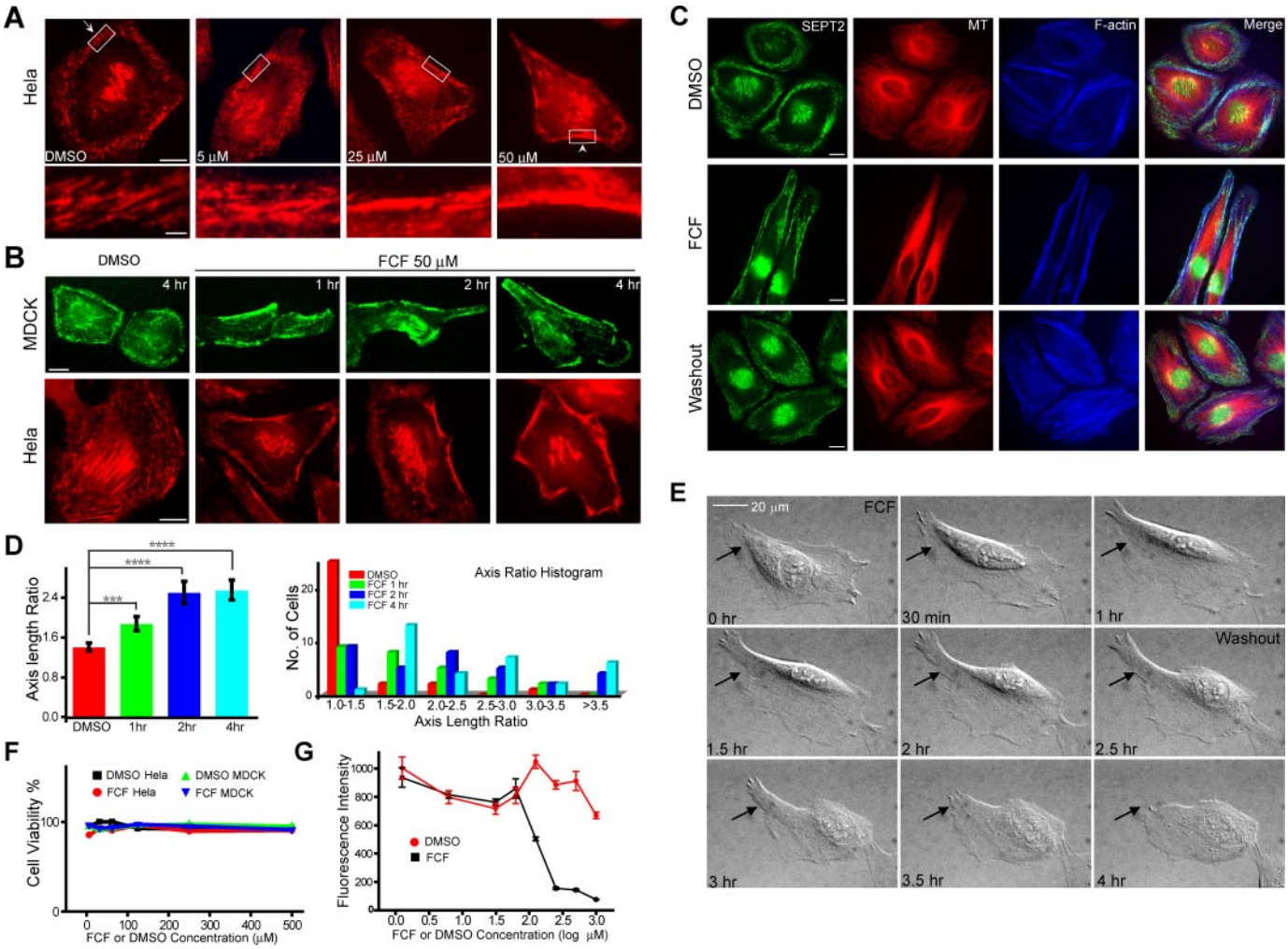

FIGURE 2. **FCF reversibly alters septin organization in HeLa and MDCK cells.** *A*, immunofluorescence images of HeLa cells stained for SEPT2 after treatment with 5, 25, or 50 μM FCF or DMSO for 2 h; *scale bars*, 10 μm. *Lower panels* show the boxed regions at higher magnification; *scale bar*, 2 μm. *B*, MDCK and HeLa cells were treated with DMSO for 4 h or FCF for 1, 2, or 4 h and stained for SEPT2; *scale bars*, 10 μm. *C*, immunofluorescence images of HeLa cells stained for SEPT2 (*green*), α-tubulin (*red*), and F-actin (*blue*) after treatment with DMSO for 4 h (*top panel*) or 50 μM FCF for 4 h (*middle panel*) followed by a 2-h washout with regular cell medium (*bottom panel*); *scale bars*, 10 μm. *D*, the bar graph (*left panel*) shows ratios (mean ± S.E.) of lengths of major cell axes to lengths of minor cell axes for MDCK cells treated with DMSO (*red*) or 50 μM FCF for 1 (*green*), 2 (*blue*), and 4 h (*cyan*); ***, $p = 0.0049$; ****, $p < 0.0001$. The histogram (*right panel*) shows the distribution of axis ratio values after DMSO and FCF treatments. *E*, differential interference contrast images from time-lapse microscopy (supplemental movies 1 and 2) of HeLa cells. FCF was added at 0 h and washed out at 2.5 h. *Arrows* point to a cell region that becomes elongated during FCF treatment and retracts upon FCF washout. *F*, a trypan blue cytotoxicity assay of HeLa or MDCK cells treated with various concentrations of DMSO or FCF (6.25–500 μM) for 4 h. Trypsinized cells were stained with trypan blue reagent and counted as the percentage of total cells ($n = \sim 200$). *G*, an alamarBlue cytotoxicity assay of HeLa cells treated with various concentrations of DMSO (*red circles*) or FCF (1.25 μM–1 mM; *black squares*) for 24 h. Cell medium was incubated with alamarBlue reagent, and fluorescence intensities (mean ± S.E.) were plotted as a function of time. All measurements were performed in quadruplicates.

formed in DMSO (Fig. 1*B*). These structures were highly intertwined (Fig. 1*B*, see *inset*) and had significantly larger surface area than control filaments (Fig. 1, *C* and D), giving rise to a higher percentage (30.2% *versus* 6.2%) of structures with a surface area greater than 500 μm^2 (Fig. 1*D*). The effect of FCF on SEPT2/6/7 assembly was concentration-dependent, with a significant effect at a concentration as low as 5 μM (Fig. 1*E*), and was reversible upon dialysis of filaments in high salt buffer without FCF (supplemental Fig. 1).

The ultrastructure of septin filaments assembled *in vitro* in the presence or absence of FCF was examined by transmission electron microscopy. In DMSO, SEPT2/6/7 formed extended fibers with an average diameter of 10.9 ± 0.3 nm ($n = 40$) that appeared to be composed of two parallel filaments (Fig. 1*F*, *left panel*, see *inset*). The morphology of these septin structures is similar to that formed by recombinant septins and septin complexes purified from mammalian cells (9, 25, 26). In FCF, SEPT2/6/7 formed much thicker filaments with an average diameter of 21.0 ± 1.1 nm ($n = 40$) that appear to comprise many parallel filaments (Fig. 1*F*, *right panel*, see *inset*). This change in septin assembly was confirmed by analyzing the ratio of septins in the supernatant and pellet after centrifugation at 16,000 × *g*. After dialysis in the presence of FCF, more SEPT2/6/7 was pelleted (~90% *versus* ~50%) (Fig. 1*G*).

We also examined whether FCF has similar effects on the assembly of other filamentous cytoskeleton polymers such as actin and tubulin. *In vitro* actin and tubulin polymerization assays were performed in the presence of a range of FCF or DMSO concentrations. FCF did not affect the rate or steady state amount of actin or tubulin polymerization (Fig. 1, *H* and *I*).

Taken together, these results show that FCF alters SEPT2/6/7 assembly and formation of higher-order structures in a dose-dependent manner. FCF did not affect actin or tubulin polymerization *in vitro* under the same conditions.

FCF Alters Septin Organization in HeLa and MDCK Cells Reversibly—We next tested whether FCF affected septin organization in mammalian cells. HeLa cells were treated with increasing concentrations of FCF for 2 h and stained for SEPT2 (Fig. 2*A*). SEPT2 organization changed from thin, short fibrillar structures (Fig. 2*A*, *arrow*, see magnified image of the *boxed region* in the *lower panel*) to thick, long filamentous structures localized at the cell periphery (Fig. 2*A*, *arrowhead*, see magnified image of the *boxed region* in the *lower panel*). These effects were dose-dependent and pronounced at 50 μM FCF (Fig. 2*A*). To examine the time course of FCF effects, HeLa and MDCK cells were treated with 50 μM FCF and fixed after 1, 2, or 4 h. FCF began to induce the reorganization of septins after 1 h of treatment (Fig. 2*B*) with a concomitant increase in SEPT2 filament length and width (supplemental Fig. 2, *A* and *B*). Significantly, FCF-induced changes in septin organization were reversed upon FCF washout (2 h; Fig. 2*C*), demonstrating that the effects of FCF were not permanent and that septins were dynamic and could reorganize within 2 h. We also examined whether septins other than SEPT2 were affected by FCF and found that organization of SEPT7 was also affected during FCF treatment similar to that of SEPT2 (supplemental Fig. 2*C*).

We observed that FCF-treated cells had elongated morphology (Fig. 2, *A*–*C*). We used the axis-length ratio (major axis length/minor axis length) to measure cell morphology (Fig. 2*D*). Quantification of the axis-length ratio of MDCK cells treated with FCF or DMSO revealed a time-dependent effect of FCF on cell morphology (Fig. 2*D*); this time course of changes in cell shape paralleled changes in septin organization observed by immunofluorescence microscopy (Fig. 2*B*). Live cell imaging of HeLa cells treated with FCF also showed gradual changes in cell morphology, which were reversed upon FCF washout (Fig. 2*E*, *arrows*, and see supplemental movies 1 and 2).

Although the effects of FCF were reversible, indicating that cells were viable, we evaluated the cytotoxicity of FCF using trypan blue and alamarBlue assays. The trypan blue assay shows that the viability of HeLa and MDCK cells was unaffected even at FCF concentrations as high as 500 μM for 4 h (Fig. 2*F*). The alamarBlue assay indicates that after 24 h of treatment, FCF-treated HeLa cells were as viable as DMSO-treated cells at a concentration of FCF $\leq$ 62.5 μM. However, HeLa cells began to show decreasing viability at higher FCF concentrations (Fig. 2*G*). The results show that FCF is not toxic over short time periods even at high concentrations, and for long treatments, FCF is not toxic at a concentration of FCF $\leq$ 62.5 μM.

FCF Dampens SEPT2 Dynamics—To explore how FCF acts on septins, we measured septin filament dynamics using FRAP in MDCK

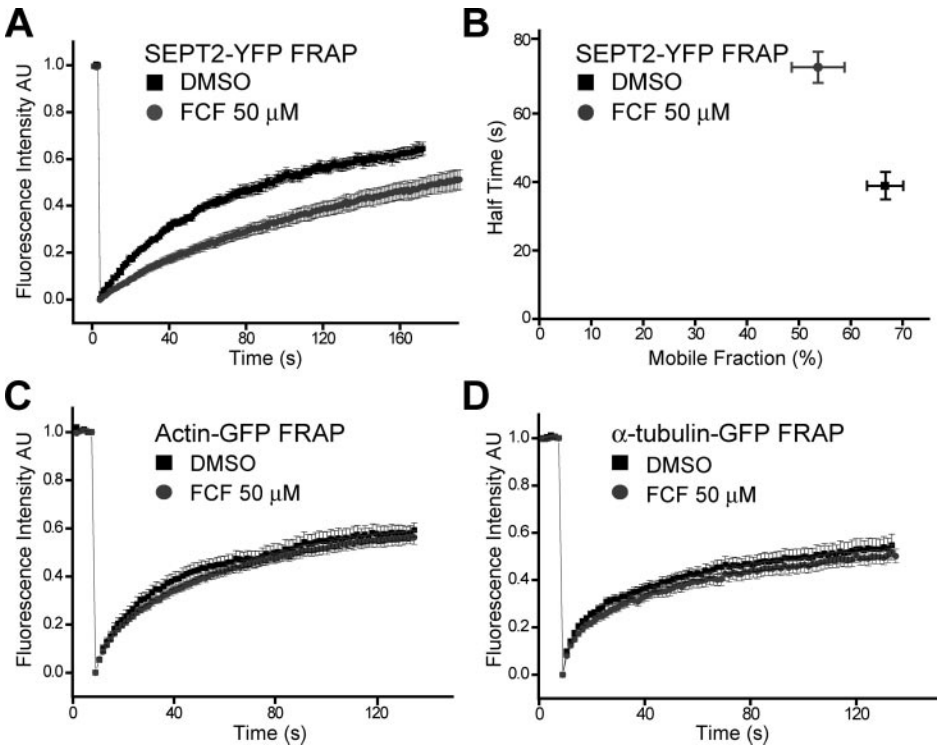

FIGURE 3. **FCF dampens SEPT2 dynamics in MDCK cells.** *A*, normalized FRAP curves for SEPT2-YFP in MDCK cells treated with DMSO (n = 10; supplemental movie 3) or 50 μM FCF (n = 15; supplemental movie 4). *AU*, arbitrary units. *B*, the plot shows half-times of SEPT2-YFP fluorescence recovery (mean ± S.E.; *y* axis) and the percentage of SEPT2-YFP mobile fraction (mean ± S.E.; *x* axis) in MDCK cells treated with DMSO (n = 10; *black squares*) or 50 μM FCF (n = 15; *gray circles*). *C*, normalized FRAP curves for actin-GFP in MDCK cells treated with DMSO (n = 13) or FCF 50 μM (n = 15). *D*, normalized FRAP curves for α-tubulin-GFP in HeLa cells treated with DMSO (n = 14) or FCF 50 μM (n = 14). All *error bars* represent S.E.

TABLE 1

Half time of recovery ($t_{1/2}$) and percentage recovery of SEPT2 filaments, actin microfilaments, and microtubules

All values for $t_{1/2}$ and % recovery represent mean ± S.E.

Subject	Treatment	$t_{1/2}$	Recovery	Number	p value
		s	%		
SEPT2-YFP filaments	DMSO	38.9 ± 4.0	66.6 ± 3.5	10	$t_{1/2} < 0.001$
	FCF 50 μM	73.5 ± 4.5	53.7 ± 5.1	15	Recovery 0.0268
Actin-GFP bundles	DMSO	20.1 ± 1.9	59.3 ± 3.0	13	$t_{1/2}$ 0.8112
	FCF 50 μM	20.6 ± 1.1	56.5 ± 2.9	15	Recovery 0.5060
α-tubulin-GFP microtubules	DMSO	13.5 ± 2.0	54.6 ± 4.6	14	$t_{1/2}$ 0.5477
	FCF 50 μM	15.1 ± 1.7	51.4 ± 3.0	14	Recovery 0.5651

cells stably expressing SEPT2-YFP (18). From the profile of fluorescence recovery, we calculated the mobile fraction and half-time of fluorescence recovery ($t_{1/2}$) of SEPT2-YFP (see "Experimental Procedures"). The mobile fraction of SEPT2-YFP filaments was 66.6 ± 3.5% in the presence of DMSO when compared with 53.7 ± 5.1% in the presence of FCF (Fig. 3, *A* and *B*, and Table 1). The difference in the mobile fraction indicates that FCF increased the stable, immobile fraction of septin filaments. FCF treatment also resulted in a doubling of the half-time of fluorescence recovery (73.5 ± 4.5 s *versus* 38.9 ± 4.0 s, Fig. 3, *A* and *B*, Table 1, and supplemental movies 3 and 4). Since SEPT2-YFP dynamics reflect mainly the association and dissociation of septin complexes into filamentous structures (the recovery is much slower than free cytoplasmic diffusion), we derived the dissociation rate constant k_{off} ($k_{off} = \ln 2/t_{1/2}$) of SEPT2-YFP as described previously for FRAP analysis of cytoskeleton-binding proteins (44, 45). SEPT2-YFP in FCF-treated cells had a k_{off} of $9.8 \pm 0.6 \times 10^{-3}$ s^{-1} when compared with $14.8 \pm 1.1 \times 10^{-3}$ s^{-1} in DMSO-treated cells. This further suggests that FCF stabilizes septin complexes into higher-order, less dynamic filamentous structures.

To test the specificity of FCF on septins, similar experiments were performed in cells stably expressing actin-GFP or α-tubulin-GFP. FCF had no effect on actin microfilament or microtubule dynamics when compared with the DMSO control (Fig. 3, *C* and *D*, and Table 1).

These FRAP studies on septin filaments, actin, and microtubule filaments demonstrate that FCF stabilizes septin filaments by decreasing the mobile fraction and k_{off} of septins and that neither actin microfilament nor microtubule dynamics is affected by FCF. This result is consistent with our observations that FCF caused increased assembly of septin complexes into large filamentous

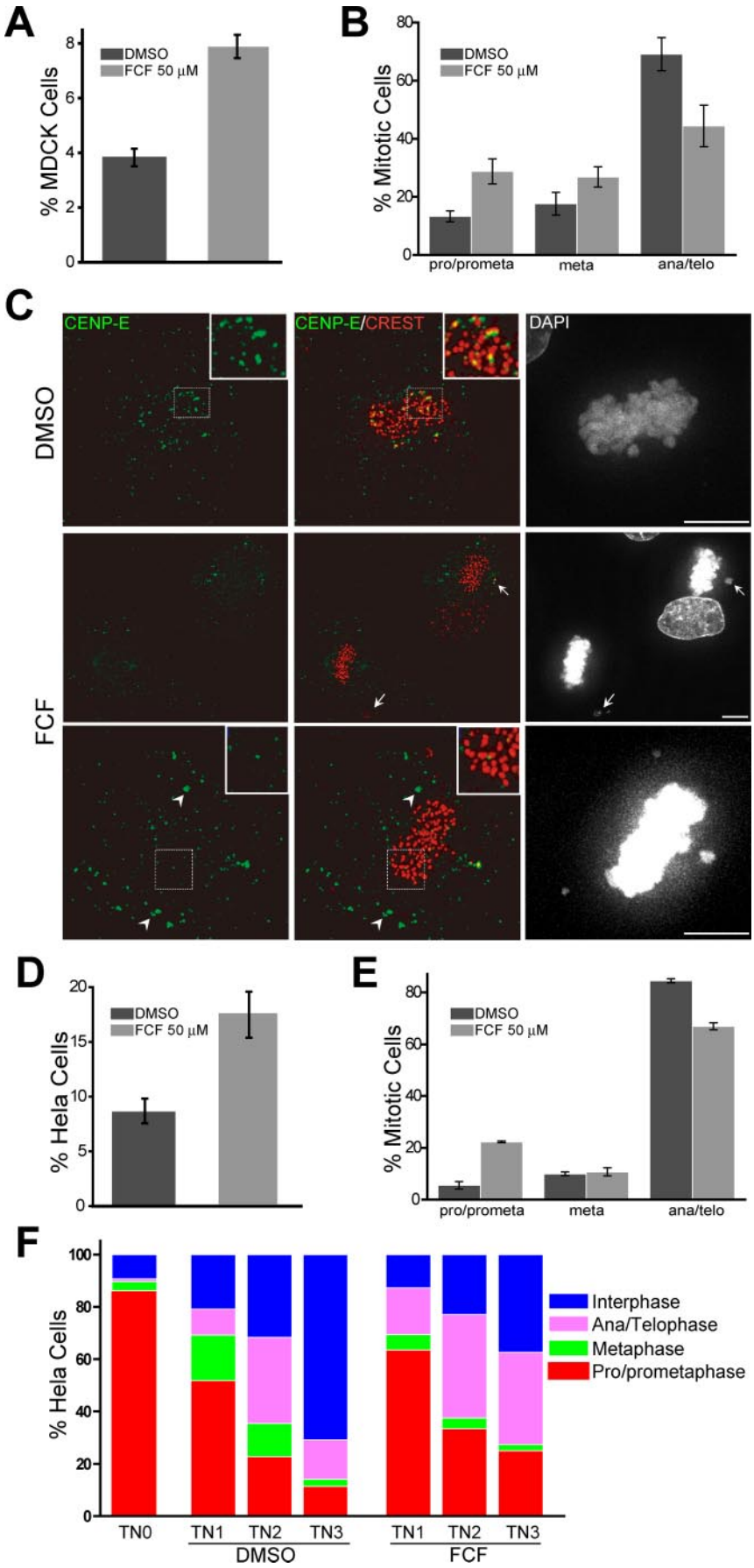

structures *in vitro* but had little effect on either actin or tubulin polymerization (Fig. 1).

FCF Causes Mitotic Defects—Given that septins have important functions in mitosis (13, 18, 19) and FCF is able to change septin organization and dynamics, we sought to examine whether FCF caused mitotic defects. FCF treatment of MDCK and HeLa cells for 8 h caused an increase in the percentage of mitotic cells (Fig. 4, *A* and *D*). These cells appeared to be delayed in prophase/prometaphase (Fig. 4, *B* and *E*). Time-lapse microscopy of HeLa cells expressing histone 2B-GFP revealed an increase in the average duration of mitosis in FCF-treated cells (125 ± 8.7 min; $n = 70$) when compared with DMSO-treated cells (81.7 ± 3.9 min; $n = 70$). In these movies, histone 2B-GFP labeled chromosomes of the cells treated with FCF failed to properly congress and align at the metaphase plate (supplemental movies 5–7). Similar failure in chromosome congression and alignment was observed in FCF-treated MDCK cells (Fig. 4*C*, *arrows*). These data resemble the effects of SEPT2 and SEPT7 depletion in chromosome alignment (18, 19), which are caused by mislocalization of CENP-E, a mitotic motor that is required for proper kinetochore-microtubule attachment. To examine whether the localization of CENP-E is disrupted upon FCF treatment, mitotic MDCK cells were stained for CENP-E and the kinetochore marker protein CREST (Fig. 4*C*). Quantitative analysis of these images revealed a reduction in the percentage of kinetochores that contained CENP-E (20.8 ± 0.7% in FCF-treated cells *versus* 40.6 ± 1.9% in DMSO-treated cells; $n = 10$). In addition, CENP-E was often observed to mislocalize outside the kinetochore regions of mitotic chromosomes (Fig. 4*C*, *arrowheads*).

Since previous studies have shown that septin disruption results in cytokinesis defects (20, 21), we tested whether FCF has similar effects downstream of chromosome alignment. Synchronized HeLa cells were arrested in prophase/prometaphase and treated with FCF at various time points after release into mitosis (Fig. 4*F*). Although early FCF treatments delayed the transition from prophase/prometaphase to metaphase, FCF treatments after a 2.5-h release into mitosis delayed the transition from telophase/cytokinesis to interphase. These data are consistent with a septin function in cytokinesis (13, 20, 21). In summary, our results indicate that FCF may cause mitotic defects by disrupting septin organization and dynamics during cell division.

FCF Impairs Cell Migration—Having investigated the specific effects of FCF on septin organization and dynamics, we examined whether FCF affects cell migration, which has been previously shown to be disrupted by septin mutants (47). We used a single cell motility assay (Fig. 5, *A* and *B*) and a "wound-healing" assay (Fig. 5, *C* and *D*) to evaluate the effects of FCF on cell migration. In the single cell motility assay, HeLa cells were plated on fluorescent beads and treated with 50 μM FCF or DMSO for 16 h; as the cells migrate during this time, they remove beads by endocytosis, leaving behind a cleared area devoid of beads that is a direct measure of the area covered by the cell (Fig. 5*A*, areas outlined by the *red lines*). Quantification of the surface areas covered by HeLa cells clearly indicates that FCF inhibited cell migration (Fig. 5*B*). In the wound-healing assay, cell monolayers were scratched to remove a line of cells, which were then filled in by cells migrating in from the edges of the monolayer. This assay also reveals that FCF decreased the rate of MDCK and HeLa cell migration (Fig. 5, *C* and *D*, and supplemental movies 8 and 9).

To test directly whether septins are involved in cell migration, we knocked down SEPT2 in HeLa cells and performed the single cell motility assay. We found that upon SEPT2 knockdown, the average surface area traveled by knockdown cells was reduced by ~50% when compared with control cells (supplemental Fig. 3). These data are consistent with previous studies showing cell motility defects upon exogenous expression of septin mutants (47). Taken together, these results show that disruption of septin organization and dynamics by FCF treatment results in defects in cell migration that phenocopy the effects of septin depletion by siRNA.

DISCUSSION

Septins comprise a filamentous system with regulatory and structural properties for diverse cellular functions. Function-blocking antibodies and siRNAs have been used to study septin functions, but these reagents are not readily reversible, and the time scale of their use leads to cumulative effects. Therefore, small molecules that perturb septin organization quickly and reversibly would be powerful tools to dissect septin organization and functions.

An earlier study showed that the small molecule compound FCF disrupted septin organization and caused cytokinesis defects in budding yeast (42). However, that study did not show whether FCF acted directly and specifically on septins, and if so, how FCF acted on septins and whether FCF could be used as a tool to study mammalian septin organization and functions. Our results show that FCF specifically altered septin assembly *in vitro* but did not affect actin or tubulin polymerization. These observations are in agreement with our studies in mammalian cells showing that FCF induced changes in septin organization from short, thin fibrilla to long, thick bundle-like filaments. These effects of FCF in cells were reversible. In summary, FCF targets the filamentous assembly of divergent septin isoforms

FIGURE 4. **FCF causes mitotic defects.** *A*, the bar graph shows the mitotic index (mean ± S.E.) of MDCK cells after treatment with DMSO or 50 μM FCF for 8 h. Mitotic cells were identified by staining with DAPI and anti-α-tubulin and calculated as the percentage of total MDCK cells ($n = \sim1800$; three independent experiments). *B*, the bar graph shows the percentage (mean ± S.E.) of DMSO- ($n = \sim100$) and FCF-treated ($n = \sim150$) mitotic cells in prophase/prometaphase (*pro/prometa*), metaphase (*meta*), and anaphase/telophase (*ana/telo*). Results are representative of three independent experiments. *C*, maximum intensity projections of deconvolved optical sections from FCF- and DMSO-treated (50 μM; 8 h) MDCK cells stained for CENP-E, CREST and DNA (DAPI). *Arrows* point to misaligned chromosomes; *arrowheads* point to CENP-E accumulations outside the kinetochore regions. *Scale bars*, 5 μm. *D*, the bar graph shows the mitotic index (mean ± S.E.) of HeLa cells after treatment with DMSO ($n = \sim800$) or 50 μM FCF ($n = \sim500$) for 8 h. Results are representative of three independent experiments. *E*, the bar graph shows the percentage (mean ± S.E.) of DMSO- ($n = \sim150$) and FCF-treated ($n = \sim150$) mitotic cells in prophase/pro-metaphase, metaphase, and anaphase/telophase. Results are representative of three independent experiments. *F*, after a thymidine-nocodazole block, HeLa S3 cells were released into mitosis for 1 (*TN1*), 2 (*TN2*), and 3 (*TN3*) h. For each time point, FCF (50 μM) or DMSO was added in the medium 30 min prior to fixation and staining with DAPI. The stack bar graphs show the percentage of HeLa cells ($n = \sim400$) in interphase and each phase of mitosis.

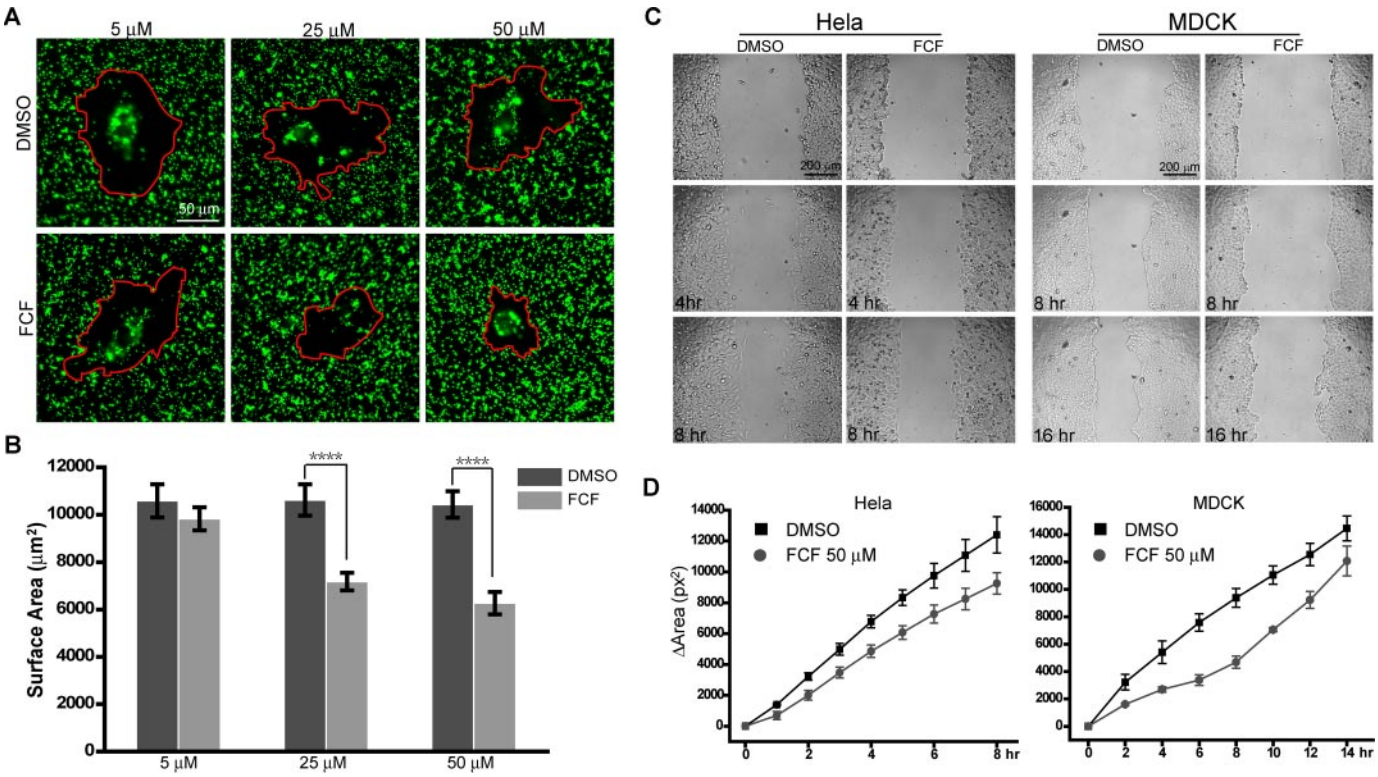

FIGURE 5. **FCF impairs cell migration.** *A*, representative images from HeLa cell motility assays. HeLa cells were plated on glass coverslips coated with green fluorescent beads, incubated in medium containing DMSO or 5, 25, or 50 μM FCF, and fixed 16 h later. *Red lines* mark the areas traveled by HeLa cells. *B*, the bar graph shows the surface areas (mean ± S.E., $n = 20$) traveled by HeLa cells after treatment with different concentrations of DMSO or FCF; ****, $p < 0.0001$. *C*, representative differential interference contrast images from HeLa (*left*; supplemental movie 8) and MDCK (*right*; supplemental movie 9) wound-healing assays at different time points. Cell monolayers were wounded with a pipette tip and then imaged in medium containing DMSO or 50 μM FCF. *D*, the plots show the changes in wounded surface area (mean ± S.E.; three independent experiments for each cell type and eight areas imaged for each experiment) as a function of time in cell monolayers treated with DMSO (*black squares*) or 50 μM FCF (*gray circles*).

(*e.g.* Cdc3/10/11/12 (42), SEPT2, SEPT7) reversibly and across species.

To elucidate how FCF acts on septins, we examined SEPT2 dynamics *in vivo* using FRAP. The results reveal that FCF increased both the half-time of recovery and the immobile fraction, indicating an increase in the stability of septin filaments. This is consistent with the FCF-induced changes in septin organization observed both *in vitro* (Fig. 1) and in cells (Fig. 2). Moreover, our FRAP data indicate that the thick bundle-like septin filaments induced by FCF arise from a decrease in the k_{off} of septin assembly (lower dissociation rate), which progressively results in accumulation of abnormally large filamentous structures.

FCF-induced changes in septin dynamics and organization resulted in cell morphology changes, mitotic defects, and decreased cell migration. These phenotypes are similar to those reported from septin depletion and overexpression studies (13, 18, 21, 47). We suggest that stabilization of septin filaments by FCF reduces the turnover rate of septin filaments and therefore the relative abundance of cytoplasmic and filamentous septins, which is critical for their function. These results are in accordance with the effects of septin depletion or overexpression, which alter overall septin organization and function.

FCF provides a high degree of temporal control over septin function, acting within 1 h (Fig. 2*B*), and is reversible (Fig. 2*C*); therefore, it may prove more useful than siRNA as a probe for septin functions. Taken together, our results show that FCF alters mammalian septin assembly *in vitro* and alters septin organization and dynamics in cells by stabilizing septin filaments. These results suggest that FCF will be useful as a tool to study septin biology. With low levels of cytotoxicity, anti-mitotic, and anti-migratory efficacies, FCF could be considered as a septin-based anti-tumorigenic agent.

Acknowledgments—We are indebted to Florian Wessel (Max Planck Institute, Münster, Germany) for technical help and data analysis, Dr. Makoto Kinoshita (Kyoto University, Kyoto, Japan) for recombinant proteins, and Dr. Linda Wordeman (University of Washington) for HeLa cells expressing α-tubulin-GFP. We also thank Nafisa Ghori for technical assistance with transmission electron microscopy and members of the Nelson/Frydman laboratories for help and advice.

REFERENCES

1. Hartwell, L. H. (1971) *Exp. Cell Res.* **69,** 265–276
2. Longtine, M. S., DeMarini, D. J., Valencik, M. L., Al-Awar, O. S., Fares, H., De Virgilio, C., and Pringle, J. R. (1996) *Curr. Opin. Cell Biol.* **8,** 106–119
3. Gladfelter, A. S., Pringle, J. R., and Lew, D. J. (2001) *Curr. Opin. Microbiol.* **4,** 681–689
4. Faty, M., Fink, M., and Barral, Y. (2002) *Curr. Genet.* **41,** 123–131
5. Longtine, M. S., and Bi, E. (2003) *Trends Cell Biol.* **13,** 403–409
6. Versele, M., and Thorner, J. (2005) *Trends Cell Biol.* **15,** 414–424
7. Lindsey, R., and Momany, M. (2006) *Curr. Opin. Microbiol.* **9,** 559–565
8. Kinoshita, M. (2003) *Genome Biol.* **4,** 236
9. Kinoshita, M., Field, C. M., Coughlin, M. L., Straight, A. F., and Mitchison, T. J. (2002) *Dev. Cell* **3,** 791–802

10. Kremer, B. E., Adang, L. A., and Macara, I. G. (2007) *Cell* **130,** 837–850
11. Nagata, K.-I., and Inagaki, M. (2004) *Oncogene* **24,** 65–76
12. Kremer, B. E., Haystead, T., and Macara, I. G. (2005) *Mol. Biol. Cell* **16,** 4648–4659
13. Joo, E., Surka, M. C., and Trimble, W. S. (2007) *Dev. Cell* **13,** 677–690
14. Nagata, K.-I., Kawajiri, A., Matsui, S., Takagishi, M., Shiromizu, T., Saitoh, N., Izawa, I., Kiyono, T., Itoh, T. J., Hotani, H., and Inagaki, M. (2003) *J. Biol. Chem.* **278,** 18538–18543
15. Beites, C. L., Xie, H., Bowser, R., and Trimble, W. S. (1999) *Nat. Neurosci.* **2,** 434–439
16. Hsu, S.-C., Hazuka, C. D., Roth, R., Foletti, D. L., Heuser, J., and Scheller, R. H. (1998) *Neuron* **20,** 1111–1122
17. Spiliotis, E. T., Hunt, S. J., Hu, Q., Kinoshita, M., and Nelson, W. J. (2008) *J. Cell Biol.* **180,** 295–303
18. Spiliotis, E. T., Kinoshita, M., and Nelson, W. J. (2005) *Science* **307,** 1781–1785
19. Zhu, M., Wang, F., Yan, F., Yao, P. Y., Du, J., Gao, X., Wang, X., Wu, Q., Ward, T., Li, J., Kioko, S., Hu, R., Xie, W., and Yao, X. (2008) *J. Biol. Chem.* M710591200
20. Kinoshita, M., Kumar, S., Mizoguchi, A., Ide, C., Kinoshita, A., Haraguchi, T., Hiraoka, Y., and Noda, M. (1997) *Genes Dev.* **11,** 1535–1547
21. Surka, M. C., Tsang, C. W., and Trimble, W. S. (2002) *Mol. Biol. Cell* **13,** 3532–3545
22. Spiliotis, E. T., and Nelson, W. J. (2006) *J. Cell Sci.* **119,** 4–10
23. Weirich, C. S., Erzberger, J. P., and Barral, Y. (2008) *Nat. Rev. Mol. Cell Biol.* **9,** 478–489
24. Barral, Y., and Kinoshita, M. (2008) *Curr. Opin. Cell Biol.* **20,** 12–18
25. Sheffield, P. J., Oliver, C. J., Kremer, B. E., Sheng, S., Shao, Z., and Macara, I. G. (2003) *J. Biol. Chem.* **278,** 3483–3488
26. Mendoza, M., Hyman, A. A., and Glotzer, M. (2002) *Curr. Biol.* **12,** 1858–1863
27. Sirajuddin, M., Farkasovsky, M., Hauer, F., Kuhlmann, D., Macara, I. G., Weyand, M., Stark, H., and Wittinghofer, A. (2007) *Nature* **449,** 311–315
28. Russell, S. E. H., and Hall, P. A. (2005) *Br. J. Cancer* **93,** 499–503
29. Hall, P. A., and Russell, S. E. H. (2004) *J. Pathol.* **204,** 489–505
30. Montagna, C., Lyu, M.-S., Hunter, K., Lukes, L., Lowther, W., Reppert, T., Hissong, B., Weaver, Z., and Ried, T. (2003) *Cancer Res.* **63,** 2179–2187
31. Larisch, S. (2004) *Cell Cycle* **3,** 1021–1023
32. Craven, R. A., Stanley, A. J., Hanrahan, S., Dods, J., Unwin, R., Totty, N., Harnden, P., Eardley, I., Selby, P. J., and Banks, R. E. (2006) *Proteomics* **6,** 2853–2864
33. Capurso, G., Crnogorac-Jurcevic, T., Milione, M., Panzuto, F., Campanini, N., Dowen, S. E., Di Florio, A., Sette, C., Bordi, C., Lemoine, N. R., and Delle Fave, G. (2005) *Neuroendocrinology* **81,** 311–321
34. Burrows, J. F., Chanduloy, S., McIlhatton, M. A., Nagar, H., Yeates, K., Donaghy, P., Price, J., Godwin, A. K., Johnston, P. G., and Russell, S. E. H. (2003) *J. Pathol.* **201,** 581–588
35. Gonzalez, M. E., Peterson, E. A., Privette, L. M., Loffreda-Wren, J. L., Kalikin, L. M., and Petty, E. M. (2007) *Cancer Res.* **67,** 8554–8564
36. Amir, S., and Mabjeesh, N. J. (2007) *Cancer Biol. Ther.* **6,** 1926–1931
37. Kinoshita, A., Kinoshita, M., Akiyama, H., Tomimoto, H., Akiguchi, I., Kumar, S., Noda, M., and Kimura, J. (1998) *Am. J. Pathol.* **153,** 1551–1560
38. Ihara, M., Tomimoto, H., Kitayama, H., Morioka, Y., Akiguchi, I., Shibasaki, H., Noda, M., and Kinoshita, M. (2003) *J. Biol. Chem.* **278,** 24095–24102
39. Ihara, M., Yamasaki, N., Hagiwara, A., Tanigaki, A., Kitano, A., Hikawa, R., Tomimoto, H., Noda, M., Takanashi, M., Mori, H., Hattori, N., Miyakawa, T., and Kinoshita, M. (2007) *Neuron* **53,** 519–533
40. Kim, C. S., Seol, S. K., Song, O. K., Park, J. H., and Jang, S. K. (2007) *J. Virol.* **81,** 3852–3865
41. Pizarro-Cerda, J., Jonquieres, R., Gouin, E., Vandekerckhove, J., Garin, J., and Cossart, P. (2002) *Cell. Microbiol.* **4,** 101–115
42. Iwase, M., Okada, S., Oguchi, T., and Toh-e, A. (2004) *Genes Genet. Syst.* **79,** 199–206
43. Yamada, S., Pokutta, S., Drees, F., Weis, W. I., and Nelson, W. J. (2005) *Cell* **123,** 889–901
44. Bulinski, J. C., Odde, D. J., Howell, B. J., Salmon, T. D., and Waterman-Storer, C. M. (2001) *J. Cell Sci.* **114,** 3885–3897
45. Sprague, B. L., and McNally, J. G. (2005) *Trends Cell Biol.* **15,** 84–91
46. Turner, D. P., Moussa, O., Sauane, M., Fisher, P. B., and Watson, D. K. (2007) *Cancer Res.* **67,** 1618–1625
47. Chacko, A. D., Hyland, P. L., McDade, S. S., Hamilton, P. W., Russell, S. H., and Hall, P. A. (2005) *J. Pathol.* **206,** 458–465

Epithelial polarity requires septin coupling of vesicle transport to polyglutamylated microtubules

Elias T. Spiliotis,[1] Stephen J. Hunt,[1] Qicong Hu,[1] Makoto Kinoshita,[2] and W. James Nelson[1]

[1]Departments of Biology, and Molecular and Cellular Physiology, Stanford University, Stanford, CA 94305
[2]Biochemistry and Cell Biology Unit, HMRO, Kyoto University, Kyoto 606-8501, Japan

In epithelial cells, polarized growth and maintenance of apical and basolateral plasma membrane domains depend on protein sorting from the trans-Golgi network (TGN) and vesicle delivery to the plasma membrane. Septins are filamentous GTPases required for polarized membrane growth in budding yeast, but whether they function in epithelial polarity is unknown. Here, we show that in epithelial cells septin 2 (SEPT2) fibers colocalize with a subset of microtubule tracks composed of polyglutamylated (polyGlu) tubulin, and that vesicles containing apical or basolateral proteins exit the TGN along these SEPT2/polyGlu microtubule tracks. Tubulin-associated SEPT2 facilitates vesicle transport by maintaining polyGlu microtubule tracks and impeding tubulin binding of microtubule-associated protein 4 (MAP4). Significantly, this regulatory step is required for polarized, columnar-shaped epithelia biogenesis; upon SEPT2 depletion, cells become short and fibroblast-shaped due to intracellular accumulation of apical and basolateral membrane proteins, and loss of vertically oriented polyGlu microtubules. We suggest that septin coupling of the microtubule cytoskeleton to post-Golgi vesicle transport is required for the morphogenesis of polarized epithelia.

Introduction

The plasma membrane of polarized columnar-shaped epithelial cells is segregated into functionally distinct apical and basolateral domains that face different biological compartments and regulate vectorial transport of ions and solutes. Biogenesis of these membrane domains and maintenance of cell shape depend on protein sorting during vesicle budding from the TGN and endosomes, transport of vesicles along the actin and microtubule cytoskeleton, and their fusion with the appropriate membrane domain (Griffiths and Simons, 1986; Matter and Mellman, 1994; Mostov et al., 2000; Rodriguez-Boulan et al., 2005).

The microtubule cytoskeleton is involved in long-range transport of vesicular carriers and in the morphogenesis of columnar-shaped, polarized epithelial cells (Musch, 2004). During polarization, microtubules are organized into a vertical network that orients along the apicobasal cell axis (Musch, 2004; Rodriguez-Boulan et al., 2005). TGN-derived vesicular carriers associate with microtubules (Van der Sluijs et al., 1990; Hirschberg et al., 1998; Toomre et al., 1999), and disruption of the microtubule cytoskeleton and its motor proteins reduces the efficiency of apical and basolateral protein delivery to their respective membrane domains (Rindler et al., 1987; Lafont et al., 1994; Grindstaff et al., 1998; Kreitzer et al., 2000; Jaulin et al., 2007). How release and transport of vesicles from the Golgi complex to the plasma membrane are coordinated with microtubule organization is unknown.

In the budding yeast *Saccharomyces cerevisiae*, polarized membrane growth is spatiotemporally coordinated by septins (Barral et al., 2000; Gladfelter et al., 2001), a family of conserved filamentous GTPases that associate with cell membranes and the cytoskeleton (Spiliotis and Nelson, 2006). In mammalian cells, septins bind to microtubules (Surka et al., 2002; Nagata et al., 2003; Spiliotis et al., 2005), but the functional significance of this association in interphase cells and the role of septins in the morphogenesis of polarized epithelia are unknown. Here, we examine the distribution and function of the mammalian SEPT2 with respect to the microtubule cytoskeleton of Madin-Darby canine kidney (MDCK) cells. We show that SEPT2 associates with a distinct subset of microtubule tracks and is required for efficient Golgi-to-plasma membrane transport and the morphogenesis of columnar-shaped epithelial cells.

S. Hunt and Q. Hu contributed equally to this paper.

Correspondence to Elias T. Spiliotis: eliass@stanford.edu; or W. James Nelson: wjnelson@stanford.edu

Abbreviations used in this paper: C-MBD-MAP4, C-terminal microtubule binding domain of microtubule-associated protein 4; GalTase, galactosyltransferase; gpi, glycosyl phosphatidylinositol; LDL-R, low density lipoprotein receptor; MAP, microtubule-associated protein; p75, neurotrophin receptor protein 75; PKD, protein kinase D1; polyGlu, polyglutamylated; VSV-G, vesicular stomatitis virus G protein.

The online version of this paper contains supplemental material.

The Journal of Cell Biology, Vol. 180, No. 2, January 28, 2008 295–303
http://www.jcb.org/cgi/doi/10.1083/jcb.200710039

Supplemental Material can be found at:
http://www.jcb.org/cgi/content/full/jcb.200710039/DC1

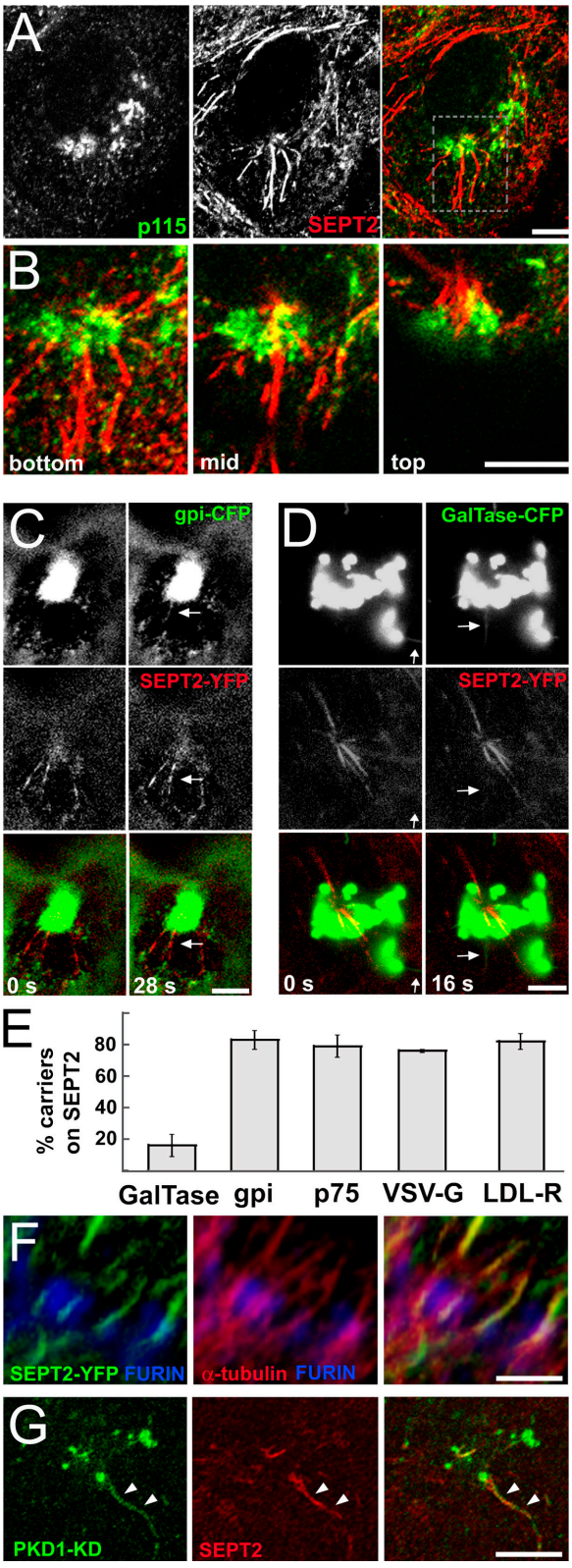

Figure 1. **SEPT2 fibers localize to TGN sites of apical and basolateral protein export.** (A and B) Subconfluent monolayers of MDCK cells were stained with SEPT2 and p115 antibodies, and imaged by confocal microscopy. Optical sections from the bottom, middle, and top of the highlighted Golgi region are shown at higher magnification (B). (C and D) MDCK-SEPT2-YFP cells were transiently transfected with gpi-CFP or GalTase-CFP, and imaged by time-lapse microscopy at 37°C. Non-neighbor deconvolution was applied and linear dynamic ranges were renormalized equally across the entire image to enhance the fluorescence intensity of tubular–vesicular structures. Arrows point to tubular vesicular elements extending from the Golgi complex. (E) Tubular–vesicular carriers containing CFP-tagged gpi, GalTase, VSV-G, and p75 were scored for overlap with SEPT2-YFP fibers (n = 80–100; mean values ± SEM from three independent experiments). (F) 3D-rendered confocal images of a Golgi region from MDCK-SEPT2-YFP cells stained with α-tubulin and furin convertase antibodies. (G) HeLa cells were transfected with the protein kinase D1 mutant PKD-K618N (PKD1-KD) tagged with GST. Cells were stained with GST and SEPT2 antibodies. Arrowheads point to a PKD-K618N–containing tubular extension. Bars, ~5 μm.

Results and discussion

Immunofluorescence microscopy of nonpolarized MDCK cells with antibodies to SEPT2 and the Golgi resident protein p115 revealed a juxtanuclear tuft of SEPT2 fibers closely apposed to the Golgi complex (Fig. 1, A and B). SEPT2 fibers co-aligned with microtubules (Fig. S1 A, available at http://www.jcb.org/cgi/content/full/jcb.200710039/DC1), and their distribution was dependent on microtubule structural integrity (Fig. S1 B). Because formation and transport of Golgi-derived vesicles occur along microtubules (Hirschberg et al., 1998; Toomre et al., 1999), we determined if SEPT2 localized to sites of vesicle export from the Golgi complex. We used high resolution live-cell imaging of MDCK cells that stably expressed a YFP-tagged SEPT2 at sub-endogenous levels (Spiliotis et al., 2005) and transiently co-expressed marker proteins of either the apical (CFP-tagged glycosyl phosphatidylinositol [gpi] or neurotrophin receptor protein 75 [p75]) or basolateral membrane (CFP-tagged vesicular stomatitis virus G protein [VSV-G] or low density lipoprotein receptor [LDL-R]). Note that SEPT2-YFP fibers colocalized with microtubules around the TGN similar to endogenous SEPT2 (Fig. 1 F). Strikingly, the majority of tubular–vesicular carriers containing apical (Fig. 1 C; Video 1 and Fig. S2, B and D) or basolateral marker proteins (Fig. S2, C and E) exited the Golgi complex along SEPT2-YFP fibers (Fig. 1 E). In contrast, membrane tubules containing a TGN resident protein (galactosyltransferase; GalTase) rarely overlapped with SEPT2-YFP fibers (Fig. 1, D and E; Video 2; Fig. S2 A).

In some instances SEPT2-YFP was not static but traversed the cytoplasm as tubular–vesicular elements (Video 3) with instantaneous velocities (0.38 ± 0.16 μm/s; n = 33) similar to those of kinesin-driven vesicles (Toomre et al., 1999). Consistent with this observation, and with septin binding to membrane phosphoinositides (Zhang et al., 1999) and synaptic vesicles (Beites et al., 1999), SEPT2 cofractionated with vesicle membranes that contained exocytic cargo (E-cadherin) and the small GTPase Rab8 (Fig. S3). SEPT2 also colocalized with Golgi-derived membrane tubules induced by expression of the inactive form of protein kinase D1 (PKD-K618N; Fig. 1 G), which blocks fission from the TGN of vesicles that are specifically destined for the plasma membrane (Liljedahl et al., 2001).

To test if SEPT2 is required for vesicle transport from the TGN to the plasma membrane, SEPT2 organization was disrupted by microinjecting cells with anti-SEPT2 IgGs and examining the effects on trafficking of the basolateral membrane marker VSV-G (ts045-VSV-G-YFP) and the apical membrane marker p75-GFP. In the presence of anti-SEPT2 IgGs, delivery

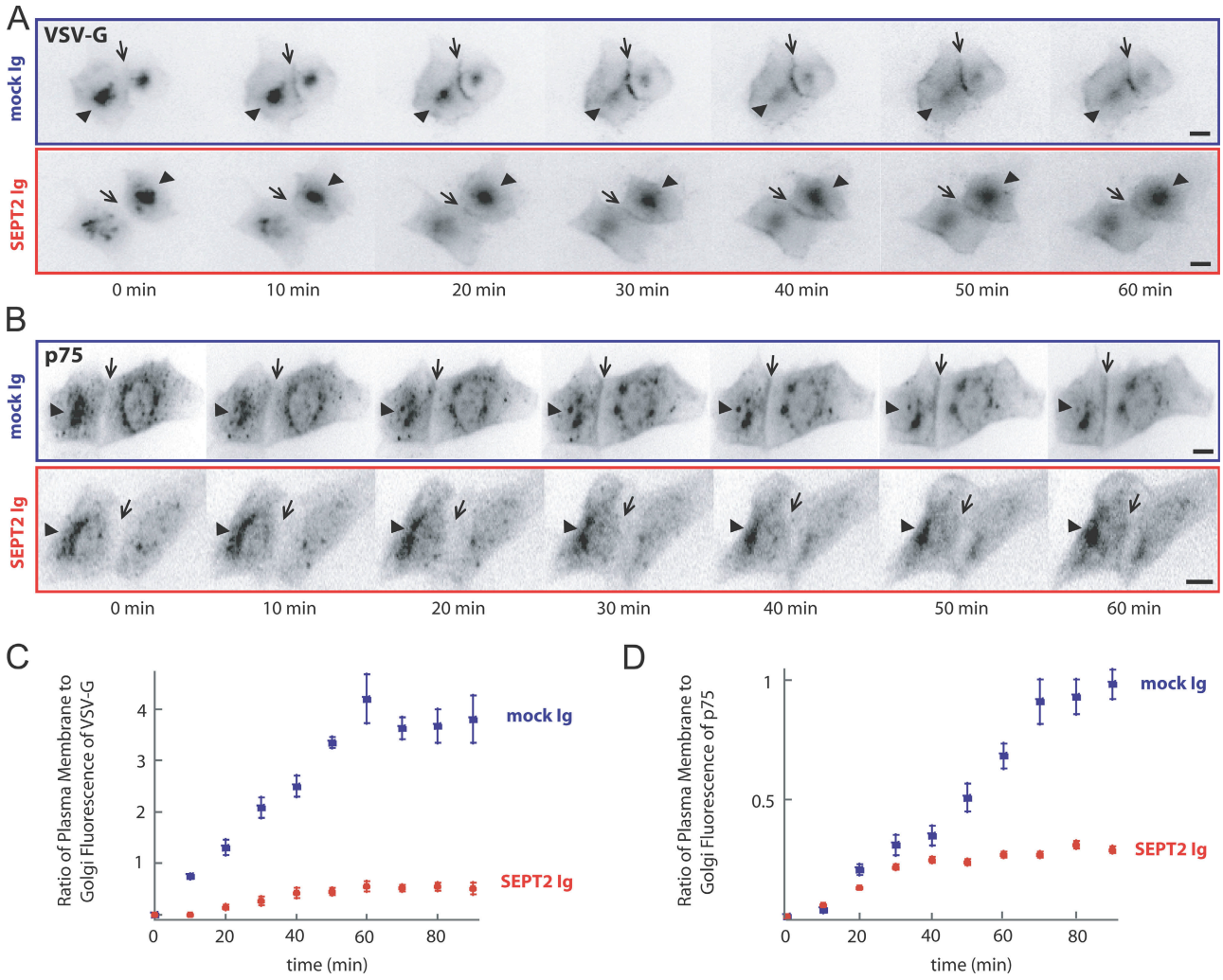

Figure 2. **SEPT2 is required for efficient Golgi-to-plasma membrane transport of basolateral and apical membrane proteins.** (A and B) Preimmune (mock; blue) or anti-SEPT2 (red) IgGs were microinjected into MDCK cells with plasmid vectors encoding for the temperature-sensitive mutant of the basolateral membrane protein VSV-G (ts045-VSV-G-YFP; A) or the apical protein p75-GFP (B). After accumulation of tsO45-VSV-G-YFP and p75-GFP in the Golgi complex at 19°C, live cells were imaged at 32°C. Arrows point to the plasma membrane of cell–cell contacts; arrowheads point to juxtanuclear Golgi regions. Bars, ~5 µm. (C and D) Net fluorescence intensities of cell surface (plasma membrane) and juxtanuclear Golgi regions were measured. Scatter plots show ratios (mean values ± SEM; *n* = 6) of plasma membrane to Golgi fluorescence for ts045-VSV-G-YFP– (C) and p75-GFP–expressing cells (D). Data are representative of three different experiments.

of ts045-VSV-G-YFP (Fig. 2, A and C) and p75-GFP (Fig. 2, B and D) from the Golgi to the plasma membrane was greatly reduced compared with that in the presence of control IgGs.

Co-alignment of SEPT2 with microtubules near the TGN (Fig. 1 F and Fig. S1 A) raised the possibility that SEPT2 might enhance vesicle transport on a qualitatively and/or functionally distinct subset of microtubule tracks. Immunofluorescence with antibodies to acetylated and detyrosinated tubulin revealed little or no colocalization between these post-translationally modified microtubules and SEPT2 fibers (unpublished data). In contrast, the preponderance of juxtanuclear/Golgi-proximal SEPT2 fibers colocalized with microtubules composed of polyglutamylated (polyGlu) tubulin (Fig. 3 A), which contains C-terminal side chains with 2–6 glutamate residues (Edde et al., 1990). When levels of SEPT2 were reduced by SEPT2 siRNAs, there was a concomitant decrease in the level of polyGlu microtubules (Fig. 3, B and E), indicating that SEPT2 is required for the maintenance of polyGlu microtubules. To further test whether SEPT2 is required for tubulin polyglutamylation, SEPT2 was buffered away from microtubules by overexpressing its cytoplasmic binding partner MAP4-GFP (Kremer et al., 2005). Excess cytoplasmic MAP4-GFP (high levels of expression; Fig. 3, C and F) not only eliminated SEPT2 association with microtubules as revealed by loss of juxtanuclear/Golgi-proximal SEPT2 fibers, but also decreased the level of polyGlu microtubules (Fig. 3, C and F). These effects were specific for MAP4 because overexpression of the neuronal MAP1B (Ding et al., 2002) (Fig. 3 D) or MAP8 (unpublished data) light chains did not disrupt SEPT2 fibers or polyGlu microtubules.

We next examined whether loss of SEPT2 fibers and polyGlu microtubules affected vesicular transport between the Golgi and the plasma membrane. Indeed, loss of SEPT2 fibers and polyGlu microtubule tracks upon MAP4-GFP overexpression resulted in decreased delivery of ts045-VSV-G-YFP to the

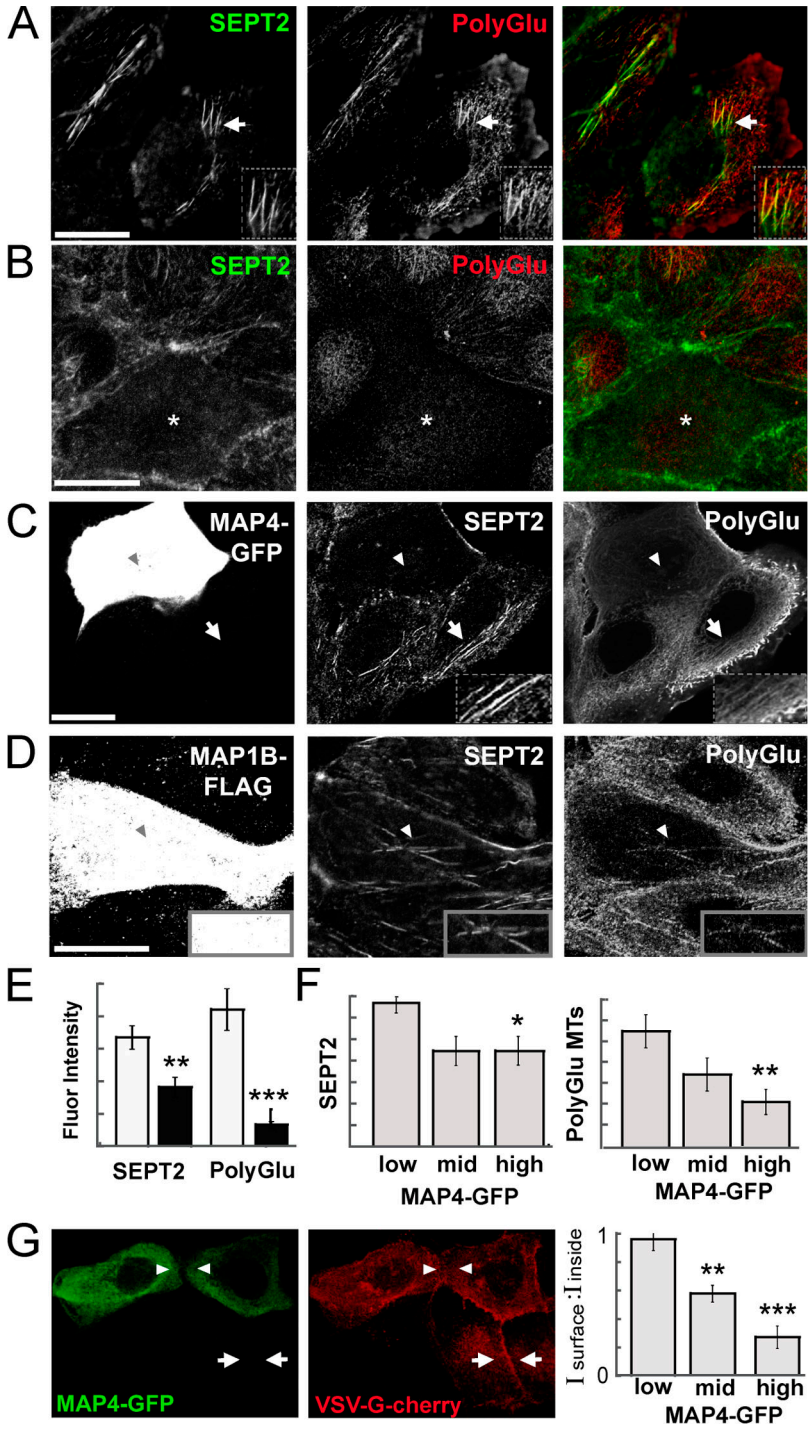

Figure 3. **SEPT2 fibers colocalize with, and are required for, polyglutamylated microtubule tracks.** (A and B) Untreated (A) and SEPT2-siRNA-treated (B) MDCK cells were stained with SEPT2 and polyGlu (≥2 glutamate residues) tubulin (mAb B3) antibodies and imaged by confocal microscopy. In A, arrows point to juxtanuclear/Golgi SEPT2 filaments that colocalize with polyGlu-microtubule tracks (see insets for higher magnification). In B, the asterisk marks a SEPT2-depleted cell. (C and D) MDCK cells were transfected with MAP4-GFP and FLAG-tagged MAP1B light chain (MAP1B-FLAG), and stained with SEPT2, polyGlu-tubulin, and FLAG antibodies. Arrows point to polyGlu microtubules and SEPT2 filaments (see insets for higher magnification), and arrowheads point to the juxtanuclear/Golgi regions of MAP-expressing cells. (E) Bar graph shows mean SEPT2 and polyGlu tubulin fluorescence (± SEM) in control (white columns; $n = 11$) and SEPT2 (black columns; $n = 13$) siRNA-treated cells. **, P = 0.0042; ***, P < 0.0001. (F) Bar graphs show mean SEPT2 ($n = 19$) and polyGlu tubulin ($n = 25$) fluorescence (± SEM) as a function of MAP4-GFP expression after binning GFP fluorescence into low, mid, and high range values. *, P = 0.04; **, P = 0.003. (G) MDCK cells were transfected with MAP4-GFP and ts045-VSV-G-cherry at 41°C and then shifted to 32°C for 1.5 h. Arrowheads (MAP4-GFP-expressing cells) and arrows (nonexpressing cells) point to the plasma membrane at cell–cell contacts. Bar graph shows mean (± SEM) ratios of plasma membrane to intracellular fluorescence for cells ($n = 30$) with low, middle, and high levels of MAP4-GFP expression from three independent experiments. **; P = 0.001; ***; P < 0.0001.

plasma membrane (Fig. 3 G). Direct disruption of SEPT2 fibers in cells cotransfected with SEPT2 siRNAs and ts045-VSV-G-YFP also reduced Golgi-to-plasma membrane transport of VSV-G (ratio of plasma membrane [PM] to intracellular [IC] fluorescence of 0.6 ± 0.04 [$n = 21$] vs. 1 ± 0.1 [$n = 9$] in control cells; P < 0.0001). However, cotransfection of a mixture of SEPT2 and MAP4 siRNAs resulted in an intermediate VSV-G delivery phenotype (PM:IC fluorescence 0.81 ± 0.1 [$n = 22$]; P < 0.003), indicating that SEPT2 and MAP4 counteract each other in regulating vesicle transport along microtubules. Therefore, in addition to the previously characterized role of cytoplasmic septins in sequestering MAP4 from microtubules (Kremer et al., 2005), which controls the stability of microtubules, microtubule-associated SEPT2 is required for the maintenance of a distinct subset of microtubules (polyGlu microtubules) that facilitate efficient vesicle transport.

To further examine whether the polyGlu side chains of tubulin or polyGlu tubulin-bound SEPT2 directly affect MAP4–tubulin binding, we used a competitive blot overlay assay, which has been used previously to map tubulin binding sites of motors and MAPs and quantitatively examine the effect of tubulin polyglutamylation on their binding (Larcher et al., 1996;

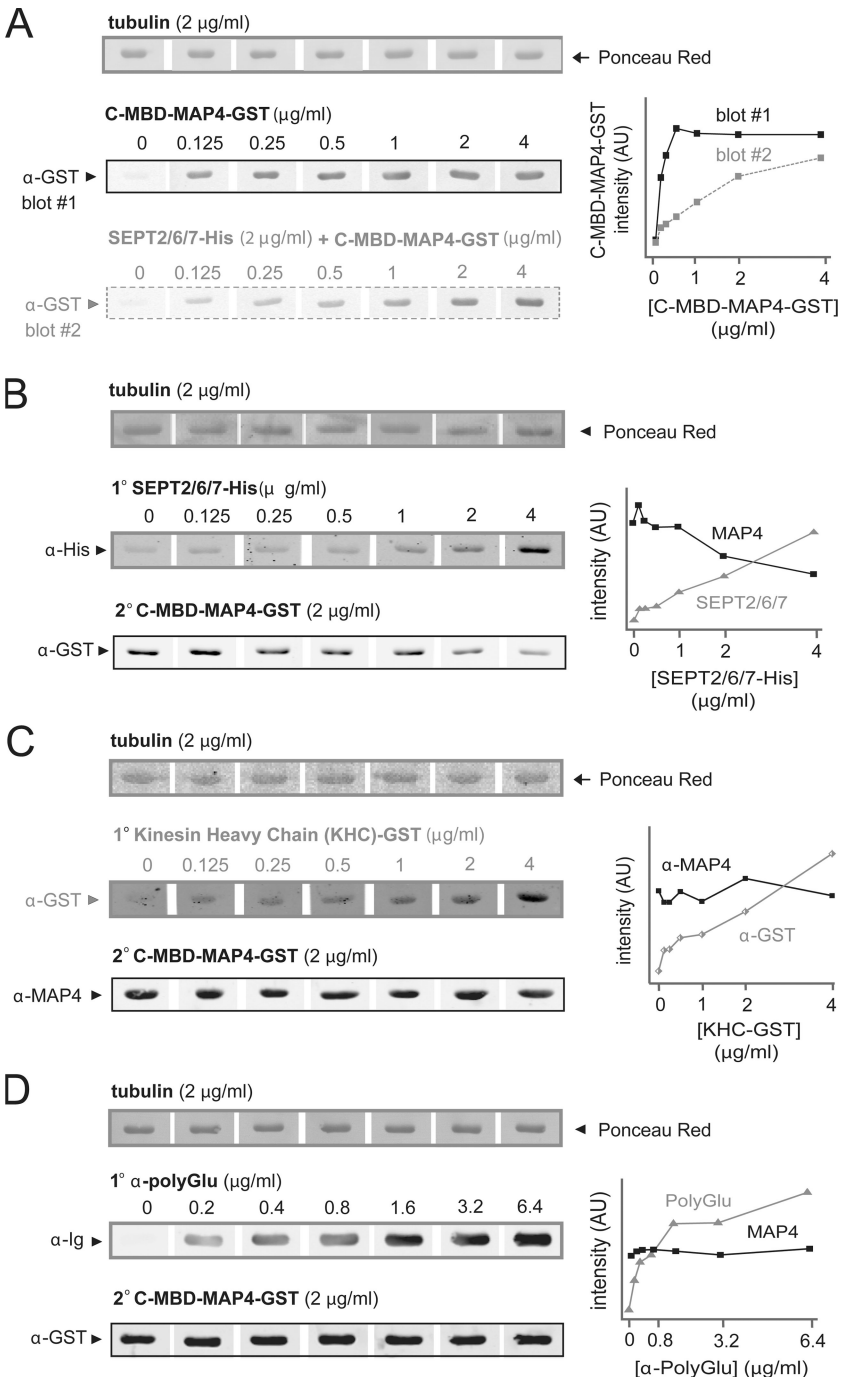

Figure 4. **Tubulin-bound SEPT2 complexes inhibit binding of the microtubule-binding domain of MAP4 (C-MBD-MAP4) to tubulin.** Equal amounts (2 μg) of purified tubulin were separated by 10% SDS-PAGE, transferred to nitrocellulose, and stained with Ponceau red. (A) Tubulin-containing strips were overlaid with increasing concentrations (0–4 μg/ml) of GST-tagged C-MBD-MAP4 directly (solid line; blot #1), or first overlaid with His-tagged SEPT2/6/7 (2 μg/ml) and then increasing concentrations of C-MBD-MAP4-GST (dotted line; blot #2). (B) Tubulin-containing strips were overlaid with increasing concentrations (0–4 μg/ml) of His-SEPT2/6/7 (1° overlay) and then with C-MBD-MAP4-GST (2 μg/ml; 2° overlay). (C) Tubulin strips were overlaid with increasing concentrations (0–4 μg/ml) of GST-tagged kinesin heavy chain (KHC-GST; 1° overlay) and then, with C-MBD-MAP4-GST (2 μg/ml; 2° overlay). (D) Tubulin was overlaid with an increasing concentration (0–6.4 μg/ml) of anti-polyGlu tubulin (mAb B3; 1° overlay) and then with C-MBD-MAP4-GST (2 μg/ml; 2° overlay). Tubulin-bound proteins were detected with GST, His, MAP4, and Ig antibodies. Band intensities were quantified and plotted against protein concentrations.

Bonnet et al., 2001). Overlaying purified brain tubulin (high polyGlu content) with recombinant SEPT2/6/7 complex decreased tubulin binding of the C-terminal microtubule binding domain of MAP4 (C-MBD-MAP4) (Fig. 4 A); note that in vivo SEPT2 functions as a heterotrimer with SEPT6 and SEPT7 (SEPT2/6/7 complex; see Kinoshita et al., 2002). SEPT2 complexes also decreased C-MBD-MAP4 binding to tubulin in a concentration-dependent manner (Fig. 4 B). In contrast, increasing concentrations of anti-polyGlu antibody (Fig. 4 D) or kinesin heavy chain (Fig. 4 C) did not interfere with binding of C-MBD-MAP4 to tubulin. Thus, polyGlu tubulin-bound SEPT2 can directly interfere with MAP4–tubulin binding.

Having shown that SEPT2 plays roles in vesicular transport, we tested whether SEPT2 is required for the establishment of epithelial membrane polarity and columnar cell shape. We depleted endogenous SEPT2 from nonpolarized, "contact-naïve" MDCK cells with siRNAs, and then assayed cell polarity and shape in monolayers of polarized cells grown on filters (Fig. 5, A and B). In contrast to the columnar morphology of cells treated with control siRNAs, SEPT2-depleted cells lacked an apical dome and honeycomb morphology characteristic of a polarized, columnar epithelium (Fig. 5 C). Significantly, SEPT2-depleted cells were elongated along their long axis and were shorter compared with control cells (Fig. 5 D). These defects

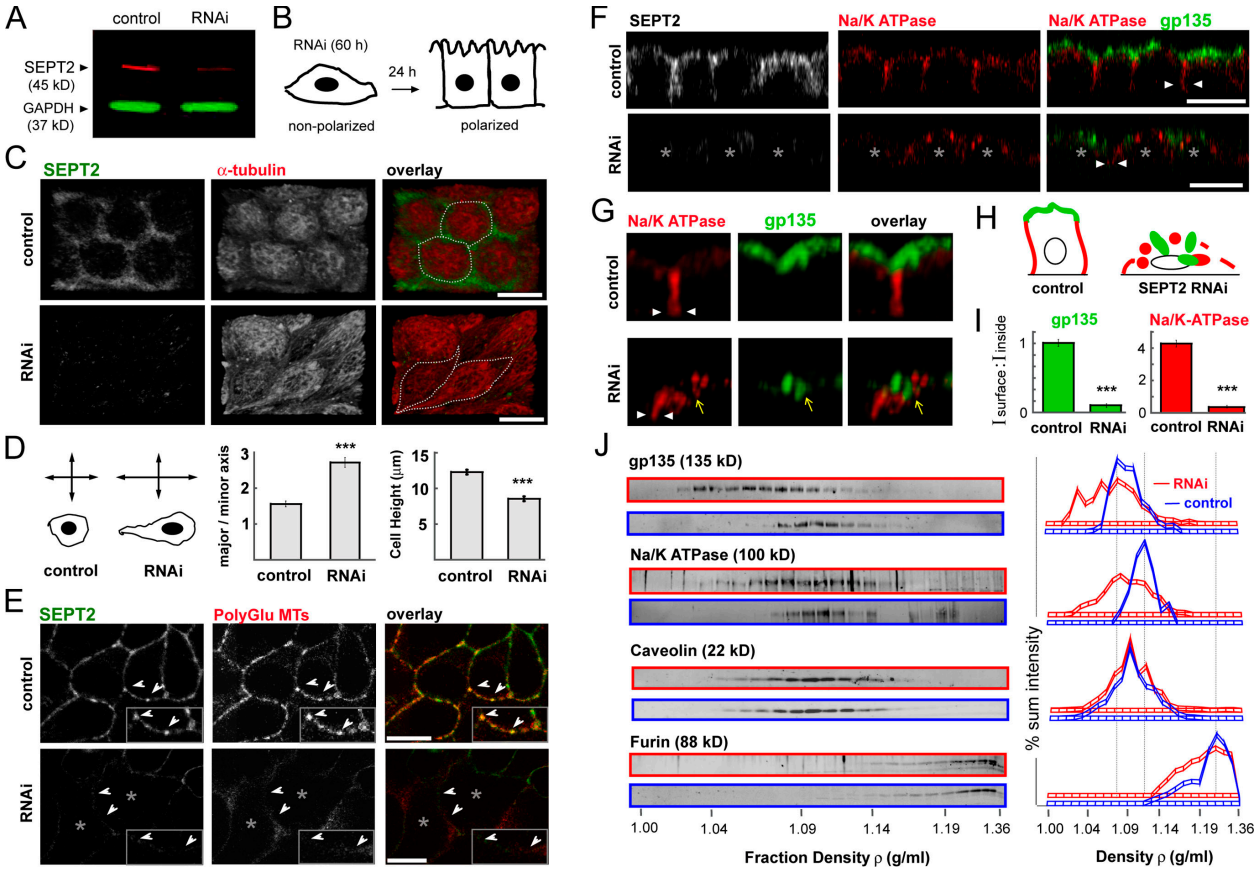

Figure 5. **SEPT2 is required for the morphogenesis of polarized, columnar-shaped epithelia.** (A) Non-polarized, "contact-naïve" MDCK cells were transfected with control and SEPT2 siRNAs for 60 h. Cell extracts were analyzed by SDS-PAGE and Western blotting with antibodies to SEPT2 (red) and glyceraldehyde-3-phosphate dehydrogenase (GAPDH; green). (B) Schematic of the experimental setup. (C) Representative dorsal views of 3D-rendered confocal images of MDCK cells stained for SEPT2 and α-tubulin. (D) Representative contour sketches of control and SEPT2-depleted cells. The ratios (mean ± SEM) of lengths of major-to-minor cell axes are shown for control (n = 33) and SEPT2-depleted (n = 30) cells from three independent experiments ($P < 0.0001$). Cell heights were measured from cross sections (xz) of confocal images and their values (mean ± SEM) are shown for control (n = 20) and SEPT2-depleted (n = 20) cells ($P < 0.0001$). (E) Representative mid-section confocal images of MDCK cells stained for SEPT2 and polyGlu tubulin; fixation/permeabilization conditions differed from those in F (see Materials and methods). Arrowheads point to SEPT2 and polyGlu microtubules that run parallel to the lateral membrane in the apicobasal axis. (F) Representative confocal cross sections (xz) of MDCK cells stained for SEPT2, Na/K-ATPase, and gp135/podocalyxin. Asterisks outline SEPT2-depleted cells; arrowheads point to lateral cell–cell contacts. (G) High resolution 3D-rendered images of the regions outlined by arrows in F. Yellow arrows point to punctate structures containing gp135/podocalyxin and Na/K-ATPase. (H) Cartoons of Na/K-ATPase (green) and gp135/podocalyxin (red) localizations in control and SEPT2-depleted cells. (I) Apical (gp135/podocalyxin) and basolateral (Na/K-ATPase) membrane and intracellular fluorescence intensities were measured from confocal cross sections (xz) of control (n = 23) and SEPT2-depleted (n = 23) cells. Bar graphs show ratios (mean values ± SEM) of plasma membrane to intracellular fluorescence from three independent experiments (***, $P < 0.0001$). (J) Post-nuclear homogenates from control (red) and SEPT2-depleted (blue) MDCK monolayers separated in iodixanol (OptiPrep) gradients, and analyzed by SDS-PAGE and blotted with antibodies to gp135/podocalyxin (apical), Na/K-ATPase (basolateral), caveolin (apical and basolateral), and furin convertase (TGN). Protein band intensities were plotted as a percentage of their sum intensity. Vertical lines demarcate the peak fractions of apical, basolateral, and Golgi proteins in gradients from control cells. Data are representative of three independent experiments.

correlated with a lack of vertically oriented polyGlu microtubules; note that in columnar-shaped control cells polyGlu microtubules colocalized with SEPT2 fibers parallel to the lateral membrane in the apicobasal cell axis (Fig. 5 E). Moreover, in SEPT2-depleted cells, levels of endogenous apical (gp135/podocalyxin) and basolateral (Na/K-ATPase) membrane markers were significantly reduced from their respective membrane domains (Fig. 5, F and I), and these proteins accumulated intracellularly in punctate structures (Fig. 5, G and H); this was not due to loss of the diffusion barrier between the apical and basolateral membrane domains as tight junctions were unaffected in SEPT2-depleted cells (unpublished data). In OptiPrep density gradients of membranes from control and SEPT2 siRNA-treated cells (Fig. 5 J), the distribution of membranes containing gp135/podocalyxin and Na/K-ATPase shifted toward fractions of low buoyant density (ρ = 1.03–1.08 g/ml) compared with controls. These fractions did not contain the TGN resident protein furin (Fig. 5 J) and their low densities resembled those of post-Golgi vesicle membranes (Wandinger-Ness et al., 1990; Deretic and Papermaster, 1991), which is consistent with the accumulation of gp135/podocalyxin and Na/K-ATPase in punctate intracellular structures (Fig. 5 G). Note that caveolin, which traffics from the Golgi to both the apical and basolateral membranes in stable microdomains distinct from the dynamic mechanisms of vesicle formation that characterize most membrane proteins (Tagawa et al., 2005), was unaffected by SEPT2 depletion (Fig. 5 J).

Based on these data, we suggest that SEPT2 is required for efficient Golgi-to-plasma membrane transport of vesicles

containing apical or basolateral membrane proteins. This is supported by: (1) presence of SEPT2 at TGN sites of plasma membrane protein export (Fig. 1); (2) decreased post-Golgi vesicle traffic in nonpolarized MDCK cells upon microinjection of function-blocking SEPT2 antibodies (Fig. 2); and (3) reduced membrane growth (Fig. 5, G and H) and columnarization (Fig. 5, C and D) of MDCK cell monolayers upon SEPT2 depletion. Although SEPT2 is involved in microtubule-dependent vesicle transport at TGN exit sites, we cannot exclude the possibility that SEPT2 also functions in vesicular transport from and to post-Golgi compartments (e.g., recycling endosomes) en route to the plasma membrane. Recent studies indicate that apical and basolateral proteins traffic through transport intermediates upon exit from the TGN (Ang et al., 2004; Fields et al., 2007; Gravotta et al., 2007). Interestingly, SEPT2 localization to endosomes and cell–cell junctions has been observed in MDCK cells by immuno-EM (unpublished data). Future studies will test whether septins regulate vesicle transport at these sites of membrane fission and fusion.

Similar to the Ras-like (e.g., Rab, Rho/Rac) and myosin-kinesin superfamilies of P-loop NTPases, septins comprise a unique superfamily of GTPases (Leipe et al., 2002). Although cytoplasmic septin complexes have been shown to regulate microtubule stability (Kremer et al., 2005), the function of the microtubule-associated, filamentous septins is unknown. We suggest that SEPT2 regulates the efficiency of vesicle transport by antagonizing MAP4, whose inhibitory role in vesicle transport is independent of its role in microtubule stability (Bulinski et al., 1997). Because microtubule-associated proteins inhibit the binding of TGN-derived vesicles to microtubules in vitro (Van der Sluijs et al., 1990) and membrane motility and traffic in vivo (Bulinski et al., 1997), we suggest that SEPT2 binding to polyglutamylated microtubules specifies a functionally distinct subset of microtubule tracks on which "fast track" vesicle transport occurs without the impediment of MAP "speed bumps." Therefore, the balance between the levels of polyGlu microtubules, SEPT2, and MAP4 may control the amount of vesicle transport to the plasma membrane. For example, different amounts of vesicle transport may be required for rapid membrane growth during morphogenesis of a columnar epithelium compared with those required to maintain homeostasis or in response to physiological stress (wound healing). This type of regulation may be important in other cell types, as microtubule-dependent vesicle transport in neurons requires polyGlu microtubules (Ikegami et al., 2007) and the dissociation of MAPs from microtubules (Mandelkow et al., 2004).

Materials and methods

Cell culture and DNA constructs

HeLa and MDCK clone II cells were maintained as described previously (Spiliotis et al., 2005). The plasmid vector encoding for ts045-VSVG3-SP-cherry was constructed by subcloning mCherry into pVSVG3-SP-YFP-N1 (a gift from K. Simons, Max Planck Institute of Molecular Cell Biology and Genetics, Dresden, Germany).

Plasmid DNA and siRNA transfections

Plasmids for ts045-VSVG3-SP-cherry, GST-tagged PKD1-K618N (a gift from V. Malhotra, CRG, Barcelona, Spain), MAP4-GFP (a gift from I. Macara, University of Virginia, Charlottesville, VA), and FLAG-tagged MAP1B and MAP8 (gifts from Y. Yang, Stanford University, Stanford, CA) were transfected using the Lipofectamine 2000 reagent (Invitrogen). MDCK cells were transfected with siCONTROL nontargeting siRNA #1 (Dharmacon RNA Technologies), MAP4 (ON-TARGET plus SMART pool; Dharmacon RNA Technologies), and SEPT2 siRNA oligonucleotides as described previously (Spiliotis et al., 2005).

Immunofluorescence microscopy

Subconfluent cell monolayers (Figs. 1, 3, and S1) were fixed with warm PHEM (60 mM Pipes-KOH, pH 6.9, 25 mM Hepes, 10 mM EGTA, and 1 mM $MgCl_2$) containing 3% paraformaldehyde (PFA; EM Sciences) and 0.1% Triton X-100, and stained with antisera to SEPT2 (N5N; rabbit polyclonal), α-tubulin (DM1A; Sigma-Aldrich), p115 (a gift from S. Pfeffer, Stanford University), furin convertase (ABR), GST (mAb B-14; Santa Cruz Biotechnology, Inc.), polyglutamylated tubulin (IgM clone B3; Sigma-Aldrich), FLAG (mAb M2; Sigma-Aldrich), and with secondary FITC- or Rhodamine red X–conjugated $F(ab')_2$ goat or donkey anti–mouse and anti–rabbit IgGs, Rhodamine red X–conjugated $F(ab')_2$ goat anti–mouse IgM and Cy5-conjugated $F(ab')_2$ donkey anti–rabbit IgG (Jackson ImmunoResearch Laboratories).

Confluent MDCK monolayers grown on Transwell filters (Figs. 5 F and S4) were fixed in PBS containing 3% PFA and stained with antibodies to SEPT2, gp135/podocalyxin (3F2/D8 mouse hybridoma supernatant), and Na/K-ATPase (chicken polyclonal; Novus). To stain for α-tubulin and polyGlu tubulin (Fig. 5, C and E), cells were fixed with warm microtubule stabilizing buffer (80 mM Pipes-KOH; pH 6.8, 5 mM EDTA, and 2 mM $MgCl_2$) containing 0.5% Triton X-100 and 0.3% glutaraldehyde (EM Sciences).

Samples were imaged in Vectashield mounting medium (Vector Laboratories) with a confocal laser scanning microscope (LSM 510; Carl Zeiss, Inc.) by obtaining 0.4–0.8-μm optical sections with a 100× 1.4 NA oil objective. Fluorescence quantifications (Fig. 3) were performed after importing LSM images into Slidebook 4.2 software (Intelligent Imaging Innovations). Data were binned into three categories based on the range of GFP fluorescence intensities; 0–20 arbitrary units (low; e.g., top right cell in Fig. 3 G), 20–40 arbitrary units (mid; e.g., top left cell in Fig. 3 G), or >40 arbitrary units (high; e.g., top cell in Fig. 3 C). Cell heights were measured using LSM software (Carl Zeiss, Inc.). The lengths of the major and minor cell axes were automatically calculated using the ellipse best-fit module of the Slidebook 4.2 software. 3D volume rendering and fluorescence quantifications (Fig. 5 and S4) were performed with Volocity 4.2 software (Improvision). Data were statistically analyzed using an automated unpaired *t* test (http://www.physics.csbsju.edu/stats/t-test.html). Image manipulations were limited to renormalization of linear dynamic ranges and applied equally across the entire image. No gamma corrections were applied.

Microinjections and live-cell imaging

Preimmune and anti-SEPT2 (N5N; 0.5–1 mg/ml needle concentration) sera were dialyzed, concentrated on Microcon 50.000 MW columns (Millipore), mixed with plasmid DNA in 10 mM Hepes, 140 mM KCl, pH 7.4, and injected into the cytoplasm and nuclei of cells with an Eppendorf microinjection system. In Fig. 1, MDCK-SEPT2-YFP cells were transfected with plasmids for CFP-tagged p75, LDL-R (gifts from E. Rodriguez-Boulan, Weill Medical College of Cornell University, New York, NY), gpi (a gift from M. Edidin, The Johns Hopkins University, Baltimore, MD), VSV-G or GalTase (gifts from J. Lippincott-Schwartz, NICHD, National Institutes of Health, Bethesda, MD). In Fig. 2, tsO45-VSV-G-YFP–injected cells were maintained at 41°C for 2 h before shifting the temperature to 32°C for 10 min, and then to 19°C for 30 min in the presence of cycloheximide (50 μg/ml); p75-GFP-injected cells were maintained at 19°C before transferring to media with cycloheximide for 30 min. Subsequently, cells were imaged in cycloheximide (10 μg/ml) containing media.

Cells were imaged in phenol red–free DME supplemented with 25 mM Hepes using the Marianas system (Intelligent Imaging Innovations) equipped with a 175-Watt Xenon light source, a dual galvanometric filter changer with CFP and YFP excitation/emission filters, CoolSNAP HQ interline CCD camera, and a Plan-Apo 100× 1.4 NA oil objective. No-neighbors deconvolution and post-acquisition analysis were performed using Slidebook 4.2. Sum fluorescence intensities for Golgi and plasma membrane regions were measured after image segmentation using the mask and pencil tools of Slidebook. Spatial overlap between tubular–vesicular structures and SEPT2 filaments was determined by the overlap of YFP and CFP fluorescence.

Recombinant proteins and blot overlay assays

Bovine brain tubulin and GST-human kinesin heavy chain motor domain were purchased from Cytoskeleton, Inc. The C-terminal microtubule-binding domain of human MAP4 (aa 654–1090; a gift from I. Macara) and

His-SEPT2/6/7 complexes were purified as previously described (Kinoshita et al., 2002; Kremer et al., 2005).

In blot overlay assays, brain tubulin was separated by 10% SDS-PAGE and transferred onto nitrocellulose membranes, which were stained with Ponceau S (Sigma-Aldrich). Membranes were scanned, cut into strips, destained, and incubated overnight at 4°C in blocking buffer (10 mM Tris HCl, pH 6.8, 150 mM NaCl, 1 mM DTT, 0.1% Tween 20, 5% nonfat dry milk, and 0.5% BSA). Recombinant proteins and antibodies were diluted in blocking buffer and overlaid onto membrane strips. To visualize tubulin-bound proteins, membranes were washed with TBS, 0.1% Tween 20, and incubated in the same buffer containing 2% BSA and antibodies. Blots were subsequently incubated with secondary AlexaFluor 680 and IRDye800-conjugated antibodies and scanned in a Li-COR infrared imager. Quantification of protein bands was performed with the Odyssey Infrared Imaging System (LI-COR Biosciences).

MDCK cell fractionation on OptiPrep density gradients and Western blotting

Non-polarized "contact naïve" MDCKs were transfected with siCONTROL and SEPT2 siRNAs, and passaged twice while being maintained in regular medium for 60 h. Cells (15×10^6) were plated onto collagen-coated 75-mm Transwell filters (Costar) for 24 h, and ball-bearing homogenized in buffer I (25 mM sucrose, 20 mM Hepes KOH, pH 7.1, 90 mM potassium acetate, 2 mM magnesium acetate, 2 mM Pefabloc, and protease inhibitors). Post-nuclear supernatants were adjusted with buffer I and OptiPrep (Axis-Shield) to 30% (wt/vol) iodixanol, overlaid with equal volumes of 20 and 10% iodixanol solutions, and centrifuged at 350,000 *g* for 3 h in a VTI 65.1 rotor (Beckman Coulter). Equal volume fractions were collected from the top ($\rho \sim 1$ g/ml) through the bottom ($\rho \sim 1.3$ g/ml) of the gradient, and the refractive index (η) of each fraction was measured using a refractometer (Bausch & Lomb). Densities were determined in g/ml [$\rho = (\eta \times 3.443) - 3.599$]. For the linear portions of these gradients (fractions 1–23), the densities for the same numbered fractions were equivalent across gradients. Fractions were boiled in SDS sample buffer and analyzed by SDS-PAGE and immunoblotting with antibodies to gp135/podocalyxin, Na/K-ATPase (α3NKA), caveolin (Transduction Laboratories), furin convertase (ABR-Affinity BioReagents), glyceraldehyde-3-phosphate dehydrogenase (6C5; Abcam), and AlexaFluor 680 goat anti–rabbit and anti–mouse IgGs (Invitrogen). Scanning of membranes and quantification of protein bands were performed with the Odyssey Infrared Imaging System (LI-COR Biosciences).

Subcellular fractionation of vesicle membranes

MDCK cells were homogenized in buffer containing 10 mM Hepes-NaOH, pH 7.4, 140 mM KCl, 5 mM EGTA, 1 mM DTT, 2 mM Pefabloc, and protease inhibitors. Post-18,000 *g* supernatants were adjusted with OptiPrep to 30% iodixanol, overlaid with equal volumes of 25 and 5% iodixanol, and centrifuged at 300,000 *g* for 3 h to obtain a fourth layer (clathrin-free vesicle fraction) at the interphase between the 5 and 25% iodixanol solutions. Vesicle fractions were drawn with a syringe and centrifuged at 100,000 *g* for 1 h in a TL-100 Tabletop Ultracentrifuge (Beckman Coulter). Membrane pellets and cytosolic supernatants were boiled in SDS sample buffer before SDS-PAGE and immunoblotting with antibodies to E-cadherin (rabbit polyclonal E2), clathrin heavy chain (Clone 23; BD Biosciences), Rab8 (BD Biosciences), and membrin (Assay Designs).

Online supplemental material

Fig. S1 shows localization of SEPT2 fibers with respect to microtubules in untreated and nocodazole-treated MDCK cells. Fig. S2 is a gallery of still images from time-lapse movies of SEPT2-YFP and Golgi-derived vesicular–tubular carriers containing CFP-tagged GalTase, gpi, ts045-VSV-G, p75, and LDL-R. Fig. S3 demonstrates SEPT2 co-fractionation with vesicle membranes. Videos 1 and 2 are time-lapse movies of SEPT2-YFP and Golgi-derived vesicular carriers that contain CFP-tagged gpi and GalTase, respectively. Video 3 shows vesicular movement of SEPT2-YFP. Online supplemental material is available at http://www.jcb.org/cgi/content/full/jcb.200710039/DC1.

We thank V. Varenika and members of the Nelson laboratory for technical help and advice; and Drs. S. Pfeffer, E. Rodriguez-Boulan, J. Lippincott-Schwartz, K. Simons, I. Macara, V. Malhotra, and Y. Yang for reagents.

This work was supported by NIH grant GM35527 (W.J. Nelson), a postdoctoral fellowship from the Jane Coffin Childs Fund for Medical Research (E.T. Spiliotis), and NIH MSTP (S.J. Hunt) and Cell and Molecular Biology (Q. Hu) training grants. Data cited as unpublished are available upon reader's request.

Submitted: 5 October 2007
Accepted: 28 December 2007

References

Ang, A.L., T. Taguchi, S. Francis, H. Folsch, L.J. Murrells, M. Pypaert, G. Warren, and I. Mellman. 2004. Recycling endosomes can serve as intermediates during transport from the Golgi to the plasma membrane of MDCK cells. *J. Cell Biol.* 167:531–543.

Barral, Y., V. Mermall, M.S. Mooseker, and M. Snyder. 2000. Compartmentalization of the cell cortex by septins is required for maintenance of cell polarity in yeast. *Mol. Cell.* 5:841–851.

Beites, C.L., H. Xie, R. Bowser, and W.S. Trimble. 1999. The septin CDCrel-1 binds syntaxin and inhibits exocytosis. *Nat. Neurosci.* 2:434–439.

Bonnet, C., D. Boucher, S. Lazereg, B. Pedrotti, K. Islam, P. Denoulet, and J.C. Larcher. 2001. Differential binding regulation of microtubule-associated proteins MAP1A, MAP1B, and MAP2 by tubulin polyglutamylation. *J. Biol. Chem.* 276:12839–12848.

Bulinski, J.C., T.E. McGraw, D. Gruber, H.L. Nguyen, and M.P. Sheetz. 1997. Overexpression of MAP4 inhibits organelle motility and trafficking in vivo. *J. Cell Sci.* 110:3055–3064.

Deretic, D., and D.S. Papermaster. 1991. Polarized sorting of rhodopsin on post-Golgi membranes in frog retinal photoreceptor cells. *J. Cell Biol.* 113:1281–1293.

Ding, J., J.J. Liu, A.S. Kowal, T. Nardine, P. Bhattacharya, A. Lee, and Y. Yang. 2002. Microtubule-associated protein 1B: a neuronal binding partner for gigaxonin. *J. Cell Biol.* 158:427–433.

Edde, B., J. Rossier, J.P. Le Caer, E. Desbruyeres, F. Gros, and P. Denoulet. 1990. Posttranslational glutamylation of alpha-tubulin. *Science.* 247:83–85.

Fields, I.C., E. Shteyn, M. Pypaert, V. Proux-Gillardeaux, R.S. Kang, T. Galli, and H. Folsch. 2007. v-SNARE cellubrevin is required for basolateral sorting of AP-1B-dependent cargo in polarized epithelial cells. *J. Cell Biol.* 177:477–488.

Gladfelter, A.S., J.R. Pringle, and D.J. Lew. 2001. The septin cortex at the yeast mother-bud neck. *Curr. Opin. Microbiol.* 4:681–689.

Gravotta, D., A. Deora, E. Perret, C. Oyanadel, A. Soza, R. Schreiner, A. Gonzalez, and E. Rodriguez-Boulan. 2007. AP1B sorts basolateral proteins in recycling and biosynthetic routes of MDCK cells. *Proc. Natl. Acad. Sci. USA.* 104:1564–1569.

Griffiths, G., and K. Simons. 1986. The trans Golgi network: sorting at the exit site of the Golgi complex. *Science.* 234:438–443.

Grindstaff, K.K., R.L. Bacallao, and W.J. Nelson. 1998. Apiconuclear organization of microtubules does not specify protein delivery from the trans-Golgi network to different membrane domains in polarized epithelial cells. *Mol. Biol. Cell.* 9:685–699.

Hirschberg, K., C.M. Miller, J. Ellenberg, J.F. Presley, E.D. Siggia, R.D. Phair, and J. Lippincott-Schwartz. 1998. Kinetic analysis of secretory protein traffic and characterization of golgi to plasma membrane transport intermediates in living cells. *J. Cell Biol.* 143:1485–1503.

Ikegami, K., R.L. Heier, M. Taruishi, H. Takagi, M. Mukai, S. Shimma, S. Taira, K. Hatanaka, N. Morone, I. Yao, et al. 2007. Loss of alpha-tubulin polyglutamylation in ROSA22 mice is associated with abnormal targeting of KIF1A and modulated synaptic function. *Proc. Natl. Acad. Sci. USA.* 104:3213–3218.

Jaulin, F., X. Xue, E. Rodriguez-Boulan, and G. Kreitzer. 2007. Polarization-dependent selective transport to the apical membrane by KIF5B in MDCK cells. *Dev. Cell.* 13:511–522.

Kinoshita, M., C.M. Field, M.L. Coughlin, A.F. Straight, and T.J. Mitchison. 2002. Self- and actin-templated assembly of Mammalian septins. *Dev. Cell.* 3:791–802.

Kreitzer, G., A. Marmorstein, P. Okamoto, R. Vallee, and E. Rodriguez-Boulan. 2000. Kinesin and dynamin are required for post-Golgi transport of a plasma-membrane protein. *Nat. Cell Biol.* 2:125–127.

Kremer, B.E., T. Haystead, and I.G. Macara. 2005. Mammalian septins regulate microtubule stability through interaction with the microtubule-binding protein MAP4. *Mol. Biol. Cell.* 16:4648–4659.

Lafont, F., J.K. Burkhardt, and K. Simons. 1994. Involvement of microtubule motors in basolateral and apical transport in kidney cells. *Nature.* 372:801–803.

Larcher, J.C., D. Boucher, S. Lazereg, F. Gros, and P. Denoulet. 1996. Interaction of kinesin motor domains with alpha- and beta-tubulin subunits at a tau-independent binding site. Regulation by polyglutamylation. *J. Biol. Chem.* 271:22117–22124.

Leipe, D.D., Y.I. Wolf, E.V. Koonin, and L. Aravind. 2002. Classification and evolution of P-loop GTPases and related ATPases. *J. Mol. Biol.* 317:41–72.

Liljedahl, M., Y. Maeda, A. Colanzi, I. Ayala, J. Van Lint, and V. Malhotra. 2001. Protein kinase D regulates the fission of cell surface destined transport carriers from the trans-Golgi network. *Cell.* 104:409–420.

Mandelkow, E.M., E. Thies, B. Trinczek, J. Biernat, and E. Mandelkow. 2004. MARK/PAR1 kinase is a regulator of microtubule-dependent transport in axons. *J. Cell Biol.* 167:99–110.

Matter, K., and I. Mellman. 1994. Mechanisms of cell polarity: sorting and transport in epithelial cells. *Curr. Opin. Cell Biol.* 6:545–554.

Mostov, K.E., M. Verges, and Y. Altschuler. 2000. Membrane traffic in polarized epithelial cells. *Curr. Opin. Cell Biol.* 12:483–490.

Musch, A. 2004. Microtubule organization and function in epithelial cells. *Traffic.* 5:1–9.

Nagata, K., A. Kawajiri, S. Matsui, M. Takagishi, T. Shiromizu, N. Saitoh, I. Izawa, T. Kiyono, T.J. Itoh, H. Hotani, and M. Inagaki. 2003. Filament formation of MSF-A, a mammalian septin, in human mammary epithelial cells depends on interactions with microtubules. *J. Biol. Chem.* 278:18538–18543.

Rindler, M.J., I.E. Ivanov, and D.D. Sabatini. 1987. Microtubule-acting drugs lead to the nonpolarized delivery of the influenza hemagglutinin to the cell surface of polarized Madin-Darby canine kidney cells. *J. Cell Biol.* 104:231–241.

Rodriguez-Boulan, E., G. Kreitzer, and A. Musch. 2005. Organization of vesicular trafficking in epithelia. *Nat. Rev. Mol. Cell Biol.* 6:233–247.

Spiliotis, E.T., and W.J. Nelson. 2006. Here come the septins: novel polymers that coordinate intracellular functions and organization. *J. Cell Sci.* 119:4–10.

Spiliotis, E.T., M. Kinoshita, and W.J. Nelson. 2005. A mitotic septin scaffold required for Mammalian chromosome congression and segregation. *Science.* 307:1781–1785.

Surka, M.C., C.W. Tsang, and W.S. Trimble. 2002. The mammalian septin MSF localizes with microtubules and is required for completion of cytokinesis. *Mol. Biol. Cell.* 13:3532–3545.

Tagawa, A., A. Mezzacasa, A. Hayer, A. Longatti, L. Pelkmans, and A. Helenius. 2005. Assembly and trafficking of caveolar domains in the cell: caveolae as stable, cargo-triggered, vesicular transporters. *J. Cell Biol.* 170:769–779.

Toomre, D., P. Keller, J. White, J.C. Olivo, and K. Simons. 1999. Dual-color visualization of trans-Golgi network to plasma membrane traffic along microtubules in living cells. *J. Cell Sci.* 112:21–33.

Van der Sluijs, P., M.K. Bennett, C. Antony, K. Simons, and T.E. Kreis. 1990. Binding of exocytic vesicles from MDCK cells to microtubules in vitro. *J. Cell Sci.* 95:545–553.

Wandinger-Ness, A., M.K. Bennett, C. Antony, and K. Simons. 1990. Distinct transport vesicles mediate the delivery of plasma membrane proteins to the apical and basolateral domains of MDCK cells. *J. Cell Biol.* 111:987–1000.

Zhang, J., C. Kong, H. Xie, P.S. McPherson, S. Grinstein, and W.S. Trimble. 1999. Phosphatidylinositol polyphosphate binding to the mammalian septin H5 is modulated by GTP. *Curr. Biol.* 9:1458–1467.

REVIEW ARTICLE
Cytoskeleton, June 2011 68:313–324 (doi: 10.1002/cm.20514)

Ciliary Diffusion Barrier: The Gatekeeper for the Primary Cilium Compartment

Qicong Hu[1] and W. James Nelson[1,2]*

[1]Department of Biology, Stanford University, Stanford, California
[2]Department of Molecular and Cellular Physiology, Stanford University, Stanford, California

Received 8 March 2011; Accepted 4 May 2011
Monitoring Editor: Ritsu Kamiya

The primary cilium is a cellular antenna that detects and transmits chemical and mechanical cues in the environment through receptors and downstream signal proteins enriched along the ciliary membrane. While it is known that ciliary membrane proteins enter the cilium by way of vesicular and intraflagellar transport, less is known about how ciliary membrane proteins are retained in, and how apical membrane proteins are excluded from the cilium. Here, we review evidence for a membrane diffusion barrier at the base of the primary cilium, and highlight the recent finding of a septin cytoskeleton diffusion barrier. We also discuss candidate ciliopathy genes that may be involved in formation of the barrier, and the role of a diffusion barrier as a common mechanism for compartmentalizing membranes and lipid domains. © 2011 Wiley-Liss, Inc.

Key Words: primary cilium, ciliary membrane proteins, ciliopathy, diffusion barrier, basal body, ciliary pocket, ciliary necklace, transition zone, septins, GTPases

Introduction

Cilia are rod-like membrane projections of several microns in length on the apical surface of many, if not all cell types in vertebrates [Pazour and Bloodgood, 2008]. They are composed of a cylindrically organized microtubule axoneme that emanates from a centriole-derived structure called the basal body [Satir and Christensen, 2007; Marshall, 2008]. The ciliary membrane surrounds the axoneme and is contiguous with the surrounding plasma membrane (Fig. 1).

Cilia are assembled and maintained through a bidirectional transportation system called intraflagellar trafficking (IFT) mediated by IFT complexes and molecular motors moving along axonemal microtubules [Fig. 1; Rosenbaum and Witman, 2002; Pedersen and Rosenbaum, 2008; Pigino et al., 2009; Ishikawa and Marshall, 2011]. IFT regulates cilia assembly, resorption and signaling, and defects in IFT proteins are found in a variety of cilium-related diseases [Pazour and Rosenbaum, 2002; Snell et al., 2004; Scholey and Anderson, 2006; Wang et al., 2006; Pedersen and Rosenbaum, 2008].

Cilia are categorized into motile or multi-cilia (9 + 2 pattern of microtubule structure), and immotile or primary cilia (9 + 0 pattern of microtubule structure) based on the mobility and number of cilia, and the organization of axonemal microtubules (Fig. 1). Motile cilia in the respiratory airway clear mucus by beating constantly in coordinated waves [Shah et al., 2009], and nodal cilia generate flow to specify left-right asymmetry [Nonaka et al., 1998; Basu and Brueckner, 2008]. Sperm has a specialized cilium that is motile and drives sperm motility. This class of motile cilia will not be discussed further, and the reader is directed to several a recent review of this field [Salathe, 2007].

The primary cilium in mammals was first identified over 100 years ago [Zimmermann, 1898]. However, it was considered a vestigial appendage of little importance and was largely ignored until the last decade when studies began to link ciliary dysfunction with genetic diseases such as polycystic kidney disease (PKD) [Pazour et al., 2000; Bloodgood, 2009].

Recent studies have revealed that the primary cilium is the cell's antenna which receives and transmits extracellular signals through specific receptors on the ciliary membrane that initiate cell signaling cascades critical for normal development and homeostasis [Pazour and Witman, 2003; Marshall and Nonaka, 2006; Singla and Reiter, 2006; Eggenschwiler and Anderson, 2007; Sloboda and Rosenbaum, 2007; Gerdes et al., 2009; Lancaster and Gleeson, 2009]. Also mediated by the primary cilium [Eggenschwiler and Anderson, 2007; Pazour and Bloodgood, 2008] are mechanoreception [Schwartz et al., 1997; Praetorius and Spring, 2001; Nauli et al., 2003; Malone et al., 2007],

*Address correspondence to: W. James Nelson, Department of Biology, 318 Campus Drive, James H. Clark Center, E200 Stanford University, Stanford, California 94305. E-mail: wjnelson@stanford.edu

Published online 1 June 2011 in Wiley Online Library (wileyonlinelibrary.com).

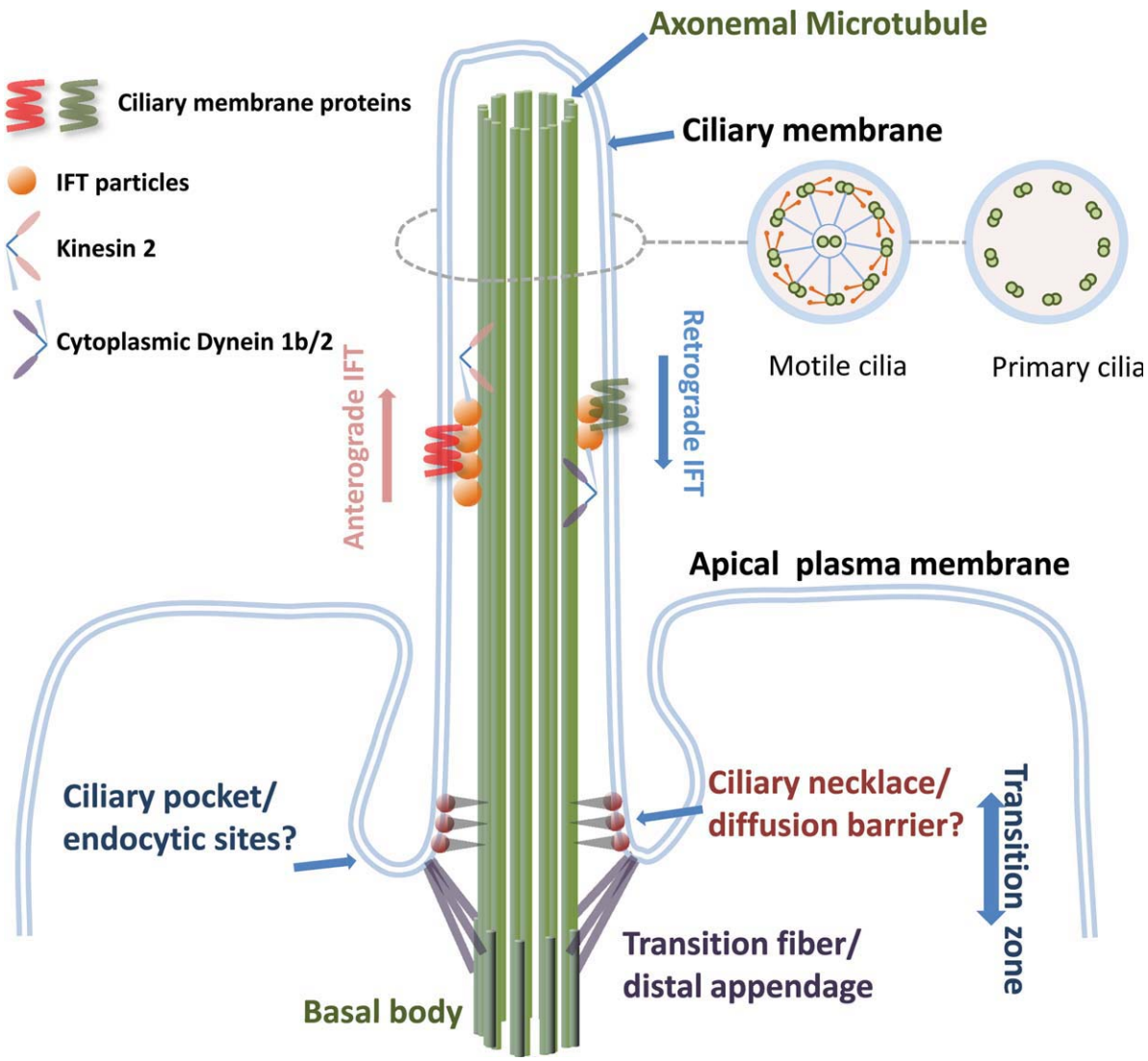

Fig. 1. Scheme of a fully assembled primary cilium and ciliary base structures. IFT particles move with their cargos (e.g., ciliary membrane proteins) within the cilia by the molecular motors kinesin 2 (anterograde trafficking) and cytoplasmic dynein 1b/2 (retrograde trafficking). At the ciliary base, transition fiber/distal appendages link the basal body to the ciliary base, and together with ciliary necklace they form the transition zone and a diffusion barrier for ciliary proteins. Plasma membrane invagination (ciliary pocket) at the ciliary base appears to be sites for endocytosis. The illustration is based on Rosenbaum and Witman [2002] and EM images from Gilula and Satir [1972].

chemoreception [Mombaerts, 1999; McEwen et al., 2008], photoreception [Besharse and Horst, 1990], and extracellular signaling by Sonic Hedgehog [Shh; Huangfu et al., 2003; Rohatgi et al., 2007; Wong and Reiter, 2008] and Wnt [Gerdes and Katsanis, 2008], Planar Cell Polarity (PCP) [Ross et al., 2005; Jones and Chen, 2008], and Platelet-Derived Growth Factor-AA (PDGF-AA) [Schneider et al., 2005].

Heritable diseases, called ciliopathies, are associated with ciliary dysfunction. They present clinically with a complex combination of phenotypes including cystic kidneys, retinal degeneration, hearing loss, situs inversus, and other defects: for example, PKD [Pazour et al., 2000; Yoder et al., 2002; Nauli et al., 2003], Bardet-Biedl syndrome (BBS) [Kulaga et al., 2004; Mykytyn and Sheffield, 2004], Nephronophthisis (NPHP) [Hildebrandt et al., 2009], Meckel-Gruber syndrome (MKS) [Kyttala et al., 2006; Delous et al., 2007], Joubert syndrome [Baala et al., 2007; Parisi et al., 2007], Usher syndrome [Yan and Liu, 2010]. Each syndrome is caused by mutations in a number of genes, and in general the normal proteins encoded by those genes localize to the primary cilium or basal body [Badano et al., 2006; Fliegauf et al., 2007; Sharma et al., 2008].

Distinct Protein and Lipid Compositions of the Ciliary Membrane and Surrounding Plasma Membrane

The ciliary membrane is contiguous with the surrounding plasma membrane but retains a distinct composition of

lipids and proteins required for cilia-mediated sensing/signaling events, ciliary membrane trafficking and ciliogenesis. However, mechanisms for retaining these proteins and lipids in the primary cilia are not clear.

In tissue culture cell lines, many proteins and signaling pathways are concentrated in the primary cilium including: the PKD-causing proteins polycystin-1, polycystin-2, cystin and polaris [Pazour et al., 2002; Yoder et al., 2002; Nauli et al., 2003]; Shh signaling components Smoothened (Smo), Patched1 (Ptc1), Gli2, Gli3 and β-arrestin [Corbit et al., 2005; Haycraft et al., 2005; Rohatgi et al., 2007; Kovacs et al., 2008]; platelet-derived growth factor receptor α [Schneider et al., 2005]; the angiopoietin receptors tyrosine kinases Tie-1 and Tie-2 [Teilmann and Christensen, 2005]; and melanin-concentrating hormone receptor 1 (Mchr1) [Berbari et al., 2008b]. Specialized membrane signaling proteins are also found in olfactory cilia such as membrane and olfactory transduction proteins [Mayer et al., 2008], in the olfactory sensory neurons of *C. elegans* such as the odorant receptor cyclic nucleotide-gated channel CNGB1b [Jenkins et al., 2006], in motile cilia in airway epithelial such as sensory bitter taste receptors [Shah et al., 2009], and in the outer segment, a specialized cilium of rod photoreceptors that contain the photosensor, rhodopsin [Tam et al., 2000].

Small GTPases that mediate trafficking and biogenesis of ciliary membrane are also enriched in the primary cilium. Rab8a is present in primary cilia of cultured cells and coordinates with BBS proteins to promote ciliary membrane growth [Nachury et al., 2007; Knödler et al., 2010; Westlake et al., 2011]. Proteomic analyses of photoreceptors and *Chlamydomonas reinhardtii* revealed that Rab subfamily members, ADP-ribosylation factor (ARF) subfamily members, RAN, and SNARE proteins are present in the sensory cilium and flagellum, respectively [Pazour et al., 2005; Liu et al., 2007a; Kwok et al., 2008]. The ARF-like family of small GTPases of the Ras superfamily are enriched in the cilium and mutations in Arl13b gives rise to PKD phenotype in Zebrafish [Duldulao et al., 2009]. BBS proteins are present in primary cilium and assemble as a coat on vesicles that deliver membrane proteins to the cilium [Nachury et al., 2007; Jin et al., 2010]. Some polarity protein complexes such as the transmembrane protein Crumbs3 localize to cilia of cultured Madin–Darby canine kidney (MDCK) cells, and are required for ciliogenesis [Fan et al., 2007; Sfakianos et al., 2007].

The ciliary membrane also maintains a lipid composition different from that of the apical plasma membrane. In quail oviduct, a high concentration of cholesterol was found on the shaft of ciliary membrane but not in the ciliary necklace enriched in intramembrane particles [Chailley and Boisvieux-Ulrich, 1985]. The trypanosome flagellar membrane is enriched in sterols and saturated fatty acids [Tyler et al., 2009]. In addition, lipid-raft associated proteins such as palmitoylated and myristoylated proteins are targeted to the ciliary membranes [Janich and Corbeil, 2007; Emmer et al., 2009, 2010]. Several studies have linked ciliopathy with defective phosphotidylinositol (PtdIns) signaling by inositol polyphosphate-5-phosphatase E (INPP5E), which mediates PtdIns metabolism and localizes in the primary cilia. Mutations of INPP5E were found in ciliopathy patients and impaired INPP5E phosphatase activity [Bielas et al., 2009; Jacoby et al., 2009]. Therefore, cilia should be enriched in INPP5E product PI(4)P and PI(3,4)P_2. A number of cilium-related proteins have been shown to bind phospholipids including Tubby-like protein 3 and BBSome proteins [Nachury et al., 2007; Jin et al., 2010; Mukhopadhyay et al., 2010].

Lipid rafts and lipid microdomains may organize a microenvironment for signal transduction complexes [Simons and Toomre, 2000]. It remains to be determined if the primary ciliary membrane contains lipid rafts and if so, whether they play roles in cilia sensory functions. Difficulties in purifying primary cilia and the lack of tools to detect or manipulate lipids have impeded our understanding the function of lipids in the ciliary membrane [Mitchell et al., 2009]. Nevertheless, the concentration and restricted distribution of proteins and lipids in the ciliary membrane indicate that the contents of the ciliary membrane and the surrounding plasma membrane are physically and functionally separated.

Early Evidence of a Membrane Diffusion Barrier in the Primary Cilium

Early studies suggested that the presence of a membrane diffusion barrier at the base of the primary cilium that physically and functionally separated the surrounding apical plasma membrane and ciliary membrane.

In *C. reinhardtii*, glycoprotein agglutinins which mediate the adhesion of two algae during mating are segregated into two pools comprising an active fraction on flagella and an inactive fraction on the plasma membrane. However, cell body agglutinins move into the flagellum in response to mating signal, demonstrating that the function barrier can be opened by regulatory signals [Hunnicutt et al., 1990]. In *Chlamydomonas eugametos*, the agglutination antigens present on the cell body are unable to diffuse into the flagellar/ciliary membrane, suggesting a physical barrier at the base of the ciliary membrane [Musgrave et al., 1986]. In MDCK cells, Laurdan staining showed that the ciliary membrane has a condensed lipid zone of high lipid order at the base of primary cilium, regarded as the periciliary membrane domain [Pazour and Bloodgood, 2008] and glycosylphosphatidylinositol (GPI) anchored proteins, while can diffuse in the surrounding

plasma membrane, were excluded from the ciliary membrane in fixed cells [Vieira et al., 2006] although a recent study using live cell microscopy indicated that GPI-Green Fluorescent Protein (GFP) is in the ciliary membrane of MDCK cells [Francis et al., 2011].

The outer segment of photoreceptor cells in the retina is a specialized primary cilium that concentrates the membrane protein rhodopsin [Besharse et al., 1977]. In photoreceptor rod cells, rhodopsin is compartmentalized in the outer segment yet diffuses into the inner segment after breaching the connecting cilium, suggesting that the connecting cilium serves as a membrane diffusion barrier between the inner and outer segments [Spencer et al., 1988]. Interestingly, in retinal rod photoreceptors the small soluble protein GFP is able to diffuse between the outer and inner segments across the connecting cilium, but it remains to be determined if larger soluble proteins have the same property [Calvert et al., 2010]. It is possible, therefore, that mechanisms involved in retaining membrane proteins and soluble proteins in primary cilium are different. Nevertheless, these data suggest the presence of a membrane diffusion barrier surrounding the ciliary membrane.

Direct Test of a Membrane Diffusion Barrier in the Primary Cilium of Mammalian Cells

Ciliary membrane proteins can be targeted to the ciliary membrane through ciliary targeting sequences, and they become enriched in the cilum [Tam et al., 2000; Geng et al., 2006; Rohatgi et al., 2007; Berbari et al., 2008a; Pazour and Bloodgood, 2008; Follit et al., 2009; Tao et al., 2009; Nachury et al., 2010]. Several hypotheses have been put forward to explain the retention and enrichment of ciliary membrane proteins: active transport, binding-retention, and a membrane diffusion barrier [Fig. 2; Emmer et al., 2010; Nachury et al., 2010]. The active transport hypothesis posits that newly synthesized proteins are actively transported into the primary cilia to offset the constant, free diffusion of proteins out of the primary cilia (Fig. 2A). In the binding-retention hypothesis, proteins once transported into the primary cilia are "fixed" in the primary cilia possibly by binding to a ciliary matrix or the microtubule axoneme (Fig. 2B). In diffusion barrier hypothesis, proteins are retained by a physical barrier that prevents proteins from diffusing from the ciliary membrane into the surrounding apical plasma membrane (Fig. 2C).

The diffusion of ciliary membrane proteins in the ciliary membrane and surrounding apical plasma membrane of polarized epithelial cells were measured directly using fluorescence recovery after photobleaching [FRAP; Hu et al., 2010]. Photobleaching of the whole cilium or part of primary cilia or plasma membrane pool revealed that four membrane proteins in the apical plasma membrane and ciliary membrane are mobile, but do not exchange, indicating the presence of a physical barrier that blocks the free diffusion of those membrane proteins between these two adjacent plasma membrane compartments. It should be noted, however IFT88 shows high turnover and mobility suggesting IFT complexes may adopt the active-transportation mechanism to enter and be retained within the primary cilium [Hu et al., 2010]. Interestingly, in *Chlamydomonas*, only a small portion of PKD2 is mobile within the flagella suggesting that distinct mechanisms may be involved in retaining different ciliary membrane proteins in the ciliary membrane [Huang et al., 2007]. *Chlamydomonas* flagellar proteome showed that a subset of membrane proteins are more enriched in the axonemal fraction than in the membrane and matrix fraction suggesting their anchorage to the axoneme [Pazour et al., 2005]. Taken together, these results indicate that at least some membrane proteins are retained in the ciliary membrane by a diffusion barrier, and not by the active transportation or binding-retention hypothesis, whereas a subset of membrane proteins such as PKD2 may utilize the binding-retention mechanism to maintain ciliary localization.

Septins as a Component of the Membrane Diffusion Barrier in the Ciliary Membrane

Septins comprise a large, conserved family of GTPases that form linear heterotrimers (heterotetramers in budding yeast) which in turn assemble into apolar filaments, bundles and rings [Versele and Thorner, 2005; Sirajuddin et al., 2007; Bertin et al., 2008]. They play important roles in cell division, cell migration, and cell morphogenesis by forming scaffolds and diffusion barriers [Kinoshita et al., 2002; Spiliotis et al., 2005, 2008; Joo et al., 2007; Kremer et al., 2007; Hu et al., 2008; Caudron and Barral, 2009; Oh and Bi, 2011].

Studies in a several biological systems indicate that septins assemble into structures that regulate the distribution of membrane proteins between different compartments of cells, and hence have characteristics of a diffusion barrier. In budding yeast, septins assemble into hourglass shape rings and ordered protein "gauzes" at the mother–daughter neck. There, septins act as a scaffold to restrict the distribution of polarity and exocytosis factors [Gladfelter et al., 2001; Faty et al., 2002; Rodal et al., 2005] and form a diffusion barrier between the mother and daughter cells for plasma membrane proteins, the nuclear envelop and the endoplasmic reticulum to maintain asymmetric cell division [Barral et al., 2000; Dobbelaere and Barral, 2004; Luedeke et al., 2005; Shcheprova et al., 2008].

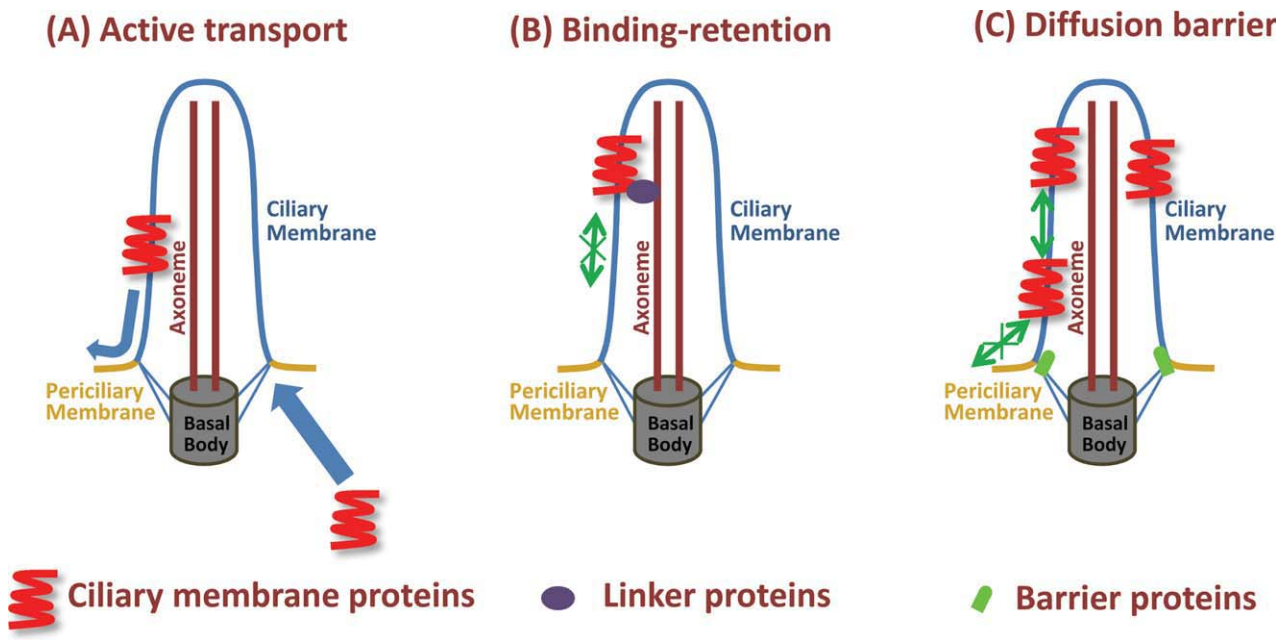

Fig. 2. Scheme of three hypotheses to retain ciliary membrane proteins. A: Active transportation hypothesis. Ciliary membrane proteins are actively targeted and transported into the ciliary membrane and they are able to diffuse out of the ciliary membrane into plasma membrane or endocytosed from the plasma membrane into cytoplasm. The transportation rate into ciliary membrane is faster than the diffusion rate out of the cilium, thereby resulting in the enrichment of proteins in the cilium. **B:** Binding-retention hypothesis. Ciliary membrane proteins, once transported into the ciliary membrane, bind stably to the axoneme and are retained. **C:** Diffusion barrier hypothesis. Ciliary membrane proteins, once transported into the ciliary membrane are prevented from diffusing from the ciliary membrane by a physical barrier but may actively move within ciliary membrane.

Disruption of the septin rings results in mislocalization of cortical proteins at the bud neck, and therefore a failure of cytokinesis [Dobbelaere and Barral, 2004; Versele and Thorner, 2005; Oh and Bi, 2011]. In mitotic mammalian cells, septins surround the midbody, and have been proposed to be a cortical barrier between the two daughter cells [Schmidt and Nichols, 2004]. In sperm, septin filaments encircle the cortical membrane between the middle and principle piece of sperm tail; septin gene knockout causes a defect in sperm motility due to cortical disorganization and dispersion of the membrane protein Basigin due to a loss of the septin-based diffusion barrier [Ihara et al., 2005; Kissel et al., 2005; Steels et al., 2007; Kwitny et al., 2010]. In hippocampal neurons, septins localize at the membrane and at the base of dendrite spines; depletion of septins affects dendritic branch morphogenesis [Tada et al., 2007; Xie et al., 2007]. In mouse epithelial cells, septins localize to the base of the primary cilia at the boundary between ciliary membrane and plasma membrane, and between the axoneme and distal/subdistal appendage proteins of basal body [Hu et al., 2010] (Fig. 3). In *Xenopus* epidermis, septins form ring-like structures at the base of cilia in multi-ciliated cells while exogenous, over-expressed SEPT2 localizes along the shaft of cilia suggesting septins may play a role in the axonemal matrix for ciliary function [Kim et al., 2010].

Depletion of septins in both mouse epithelial cells and *Xenopus* impairs the formation and organization of cilia. In epithelial cells with reduced levels of SEPT2, ciliary membrane proteins can diffuse across the barrier as measured using FRAP [Hu et al., 2010]. Similarly, the enrichment of ciliary membrane proteins involved in Shh signaling is partially lost, resulting in a reduced Shh signaling. Thus, SEPT2 contributes to the formation of the diffusion barrier at the base of the primary cilium. In *Xenopus*, septins interact with PCP signaling proteins and Fritz [Kim et al., 2010]. Septins and Fritz are in the same

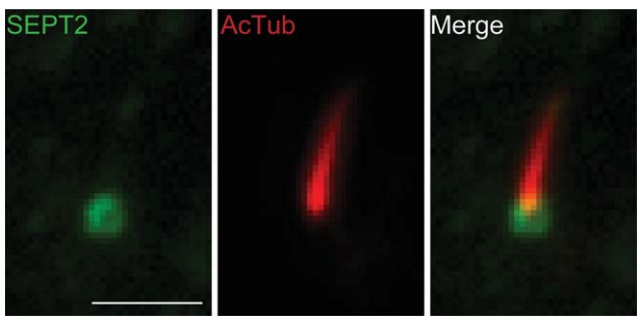

Fig. 3. SEPT2 forms a ring-like structure at the ciliary base of IMCD3 cells. IMCD3 cells were fixed and stained with anti-SEPT2 antibody (green) and anti-acetylated tubulin antibody (red). The image shows the primary cilium on the apical membrane. Scale bar ~2μm.

pathway to control convergent-extention and ciliogenesis in early *Xenopus* development. In addition, depletion of septins or Fritz impairs Shh signaling. Finally, mutations in the *Fritz* gene are found in patients with Meckel-Gruber and BBSs, although it is not known whether septin mutations also exist in patients with those ciliopathies and whether mutations in *Fritz* in those patients are pathogenic. The finding that a septin cytoskeleton is localized to sites of many of these barriers for membrane compartmentalization indicates an evolutionarily conserved mechanism to organize and compartmentalize membrane structure.

Despite these recent advances, several important questions remain. First, it remains unknown how septins contribute to the formation of the membrane diffusion barrier; there are no data to explain how septins are specifically recruited to the diffusion barrier at the base of primary cilia, sperm annulus, bases of dendritic spins or midbody of mitotic cells. Septins can interact with phospholipid membranes and mediate their tubulation [Zhang et al., 1999; Tanaka-Takiguchi et al., 2009], and phosphatidylinositol-4,5-bisphosphate ($PI(4,5)P_2$) promotes the assembly of yeast septins in vitro [Bertin et al., 2010]. It is possible that septins locally organize membrane lipids which in turn restrict the mobility of membrane proteins. Alternatively, septins may bind transmembrane proteins which serve as the diffusion barrier, although transmembrane proteins that interact with septins have not been identified.

Second, it is unknown whether the septin-mediated membrane diffusion barrier has selectivity for different membrane proteins, soluble (cytoplasmic) proteins of different molecular sizes, or peripheral membrane proteins that bind to different lipids.

Third, it is unknown whether and how ciliary diffusion barriers are regulated. For example, ciliary membrane proteins can be targeted and transported to the ciliary membrane during ciliogenesis indicating that the barrier either has not formed, or is permissive to the diffusion of ciliary membrane proteins. In another example, Shh binding to Ptc1 results in Ptc1 leaving the ciliary membrane causing Smo enrichment in the cilia [Corbit et al., 2005; Rohatgi et al., 2007; Wong and Reiter, 2008; Milenkovic et al., 2009]. How the ciliary barrier selectively gates these receptors remains unknown. In this context it is interesting to note that nuclear transport components RanGTP and importin-β2 mediate the shuttling of cytoplasmic kinesin-2 motor KIF17 into cilia [Dishinger et al., 2010; Hurd et al., 2011], but it is unknown how this complex bypasses the ciliary barrier.

Ultrastructure of the Ciliary Base

The diffusion barrier is localized at the boundary of apical plasma membrane and ciliary membrane [Hu et al., 2010] (Figs. 1–3). Ultrastructural studies of the ciliary base shed some light on the structural nature of the diffusion barrier. Freeze-fracture electron microscopy (EM) revealed a "ciliary necklace" surrounding the membrane at the base of cilia [Fig. 1; Gilula and Satir, 1972]. The necklace is composed of rows of particles associated with the membrane that are connected to the basal body by appendages, and was proposed to form the membrane diffusion barrier or organize lipids at the transitional zone between the basal body and axonemal microtubules [Satir and Christensen, 2007; Fig. 1]. However, the molecular identity of the ciliary necklace remains to be determined.

Another membrane structure at the base of the ciliary membrane comprises the ciliary membrane pocket (Fig. 1). Cross-sections of *Elliptio* lateral cilium revealed a pocket structure at the base of ciliary membrane with the ciliary necklace localized on the inner side of the pocket [Sorokin, 1962; Gilula and Satir, 1972]. In Trypanosomatid, a protozoan parasite which uses a single flagellum as an invasion tool, a ciliary/flagellar pocket also exists and appears as a site for protein endocytosis and exocytosis [Overath et al., 1997; Gull, 2003; Kohl et al., 2005; Gadelha et al., 2009]. A cytoskeleton protein BILBO1 at the ciliary pocket was identified and plays an important role in ciliary pocket biogenesis [Bonhivers et al., 2008]. A membrane pocket was also identified in *Xenopus* rod photoreceptor at the base of connecting cilum [Papermaster et al., 1985]. Additional ultrastructural studies showed a similar structure in human retinal pigment epithelial cells, mouse 3T3 cells and some mouse kidney epithelial (IMCD3) cells [Molla-Herman et al., 2010; Rohatgi and Snell, 2010]. Actin filaments were observed in the vicinity of ciliary pocket, possibly mediating the position of cilium. Remarkably, clathrin-coated pits and vesicles were also found exclusively at the ciliary pocket, further indicating that they are sites of endocytic targeting and recycling of ciliary membrane proteins [Molla-Herman et al., 2010].

Taken together, a ciliary diffusion barrier protein complex may be localized at the transition zone (TZ) consisting of the basal body, its accessory appendages (also called transition fibers) connected to the ciliary pocket, the proximal region of the axoneme, the ciliary necklace membrane region, and the Y-connector between axonemal microtubules and ciliary necklace membrane (Fig. 1). This complex may be the main site for trafficking in and out of ciliary membrane and, as a diffusion barrier, regulate membrane and cytosolic protein diffusion [Nachury et al., 2010].

Additional Candidates for the Ciliary Diffusion Barrier

Several proteins, in addition to septins, have been identified at the ciliary diffusion barrier complex/transitional zone [Sharma et al., 2008] and some may constitute the diffusion barrier. Interestingly, many of them are proteins encoded by

ciliopathy genes. In *C. elegans* and cilia of different mammalian tissues, the NPHP disease gene product NPHP1, NPHP2/Invesin, NPHP4/Nephroretinin, NPHP6/CEP290/MKS-4, NPHP8/RPGRIP1L/MKS-5, NPHP9/Nek8, and NPHP11/TMEM67/MKS-3/Meckelin are localized mainly at the transitional zone at the ciliary base [Otto et al., 2003, 2005, 2008; Mollet et al., 2005; Simons et al., 2005; Winkelbauer et al., 2005; Fliegauf et al., 2006; Sayer et al., 2006; Valente et al., 2006; Delous et al., 2007; Shiba et al., 2010]. Remarkably, in *C. reinhardtii*, CEP290 is an integral component of Y-shape connector that links the microtubule doublets to the ciliary necklace at the TZ; significantly, *cep290* mutant causes a loss of the Y-shape link and therefore the association between axonemal microtubules and ciliary membrane. Loss of CEPT290 leads to a reduction of IFT-associated and membrane proteins in the flagella [Craige et al., 2010]. Thus, CEP290 appears to function as a gatekeeper to regulate the delivery and exit of flagellar proteins [Betleja and Cole, 2010]. MKS proteins MKS-1, MKS-2/TMEM216, MKS-3/Meckelin/TMEM67 and their related proteins are also localized to the ciliary base and are required for ciliogenesis [Williams et al., 2008, 2009; Bialas et al., 2009; Dawe et al., 2009; Valente et al., 2010]. A recent study systematically characterized the localization and function interaction of MKS and NPHP proteins at the TZ in *C. elegans* and demonstrated they establish the attachment between basal body/TZ and ciliary membrane and ciliary gating function [Williams et al., 2011]. It would be of great interest to determine their ultrastructure localization and protein binding profiles. In *Xenopus* photoreceptors, the Usher syndrome gene products SANS (USH1G), Whirlin (USH2D), USH2A, and VLGR1b are in a complex that forms a bridge between the connecting cilium and periciliary membrane [Liu et al., 2007b; Maerker et al., 2008]; Usher syndrome is a disorder that causes combined deafness and blindness characterized with degeneration of retinal photoreceptors. Retinitis pigmentosa (RP) GTPase regulator (RPGR) localizes at the connecting cilium and maintains the polarized distribution of rhodopsin in the photoreceptor cells [Hong et al., 2001; Roepman et al., 2005; He et al., 2008]; mutations in RPGR are a frequent cause of RP, a retinal degeneration disease. Basal body distal appendage protein Cep164 forms a donut-shaped structure at the base of primary cilium [Graser et al., 2007]. Oral-facial-digital type I (OFD1) syndrome gene product OFD1 has basal body and centrosomal localizations [Romio et al., 2004].

Although these proteins are candidates for forming the diffusion barrier, details of the fine structure localization and functions of these proteins networks at the transitional zone and at the base of the cilia remain to be determined. Immuno-gold labeling and super-resolution microscopy could be used to further pinpoint their localization at the ciliary base. Tandem affinity purification system coupled with sequential mass spectrometry has been used successfully to identify BBSomes and their associated proteins [Nachury et al., 2007], and this might be an application useful for the purification of protein complex in the transitional zone. Protein interactions could be verified subsequently by biochemical methods and genetic interaction studies. In vitro purification, reconstitution, high resolution EM and crystal structures of those protein complexes would be helpful to study their structure–function relationships.

Conclusions and Perspectives

The ciliary diffusion barrier maintains the specific concentration of ciliary membrane proteins and associated signaling complexes within the cilium compared to the surrounding (apical) plasma membrane. The diffusion barrier appears to be localized to the TZ at the base of the ciliary membrane, and consist of ciliary necklace, the Y-link connecting ciliary necklace and axonemal microtubules, a septin cytoskeleton, and may include a complex protein network involving proteins encoded by ciliopathy genes.

Many important aspects of the diffusion barrier are poorly understood. First, selectivity of the diffusion barrier to different proteins remains to be determined. The diffusion of additional integral membrane proteins, peripheral proteins and IFT complex and associated proteins could be tested using FRAP. Soluble proteins of different sizes could be tagged with fluorophores and injected into or expressed in cells and their distribution observed in cilia. Interestingly, 10 kDa fluorescently labeled dextrans can enter mammalian primary cilia while dextrans of 40 kDa or larger are excluded from the ciliary compartment suggesting a size exclusion mechanism controlling the ciliary entry of soluble proteins [Kee et al., 2010]. The underlying mechanisms involved in selectivity should be addressed. Second, the signaling cascades regulating the assembly, disassembly, and permeability of the diffusion barrier are unknown. Third, the biochemical composition and structure of the diffusion barrier are unknown. Protein complexes encoded by ciliopathy genes at the TZ could be purified and identified, and their localization at the ciliary base could be pinpointed using high-resolution immuno-gold EM. Protein depletion or genetic knockouts of single or multiple components are needed to test the structural and functional importance of specific proteins and combinations of proteins at the TZ of the diffusion barrier. Once the molecular nature of the diffusion barrier is defined, animal models can be established to explore the physiological relevance of the ciliary diffusion barrier in development, homeostasis and diseases.

Acknowledgments

Work from the Nelson laboratory was supported by a grant from the NIH (GM35527), and Q.H. was also supported

by a US Department of Defense Breast Cancer Research Program Predoctoral Training Grant (BC083077). We thank Max V. Nachury, Hua Jin, Elias T. Spiliotis, and reviewers for helpful comments on the manuscript.

References

Baala L, Romano Sp, Khaddour R, Saunier S, Smith UM, Audollent S, Ozilou C, Faivre L, Laurent N, Foliguet B, et al. 2007. The Meckel-Gruber syndrome gene, MKS3, is mutated in Joubert syndrome. Am J Hum Genet 80(1):186–194.

Badano JL, Mitsuma N, Beales PL, Katsanis N. 2006. The ciliopathies: An emerging class of human genetic disorders. Annu Rev Genomics Hum Genet 7(1):125–148.

Barral Y, Mermall V, Mooseker MS, Snyder M. 2000. Compartmentalization of the cell cortex by septins is required for maintenance of cell polarity in yeast. Mol Cell 5(5):841–851.

Basu B, Brueckner M. 2008. Cilia: Multifunctional organelles at the center of vertebrate left-right asymmetry. Curr Top Dev Biol 85:151–174.

Berbari NF, Johnson AD, Lewis JS, Askwith CC, Mykytyn K. 2008a. Identification of ciliary localization sequences within the third intracellular loop of G protein-coupled receptors. Mol Biol Cell 19(4):1540–1547.

Berbari NF, Lewis JS, Bishop GA, Askwith CC, Mykytyn K. 2008b.Bardet-Biedl syndrome proteins are required for the localization of G protein-coupled receptors to primary cilia. Proc Natl Acad Sci USA 105(11):4242–4246.

Bertin A, McMurray MA, Grob P, Park S-S, Garcia G, Patanwala I, Ng H-L, Alber T, Thorner J, Nogales E. 2008. *Saccharomyces cerevisiae* septins: Supramolecular organization of heterooligomers and the mechanism of filament assembly. Proc Natl Acad Sci USA 105(24):8274–8279.

Bertin A, McMurray MA, Thai L, Garcia G, III, Votin V, Grob P, Allyn T, Thorner J, Nogales E. 2010. Phosphatidylinositol-4,5-bisphosphate promotes budding yeast septin filament assembly and organization. J Mol Biol 404(4):711–731.

Besharse JC, Hollyfield JG, Rayborn ME. 1977. Photoreceptor outer segments: Accelerated membrane renewal in rods after exposure to light. Science 196(4289):536–538.

Besharse JC, Horst CJ. 1990 The photoreceptor connecting cilium. A model for the transition zone. In: Bloodgood RA, editor. Ciliary and Flagellar Membranes. New York: Plenum Press. pp 389–417.

Betleja E, Cole DG. 2010. Ciliary trafficking: CEP290 guards a gated community. Curr Biol 20(21):R928–R931.

Bialas NJ, Inglis PN, Li C, Robinson JF, Parker JDK, Healey MP, Davis EE, Inglis CD, Toivonen T, Cottell DC, et al. 2009. Functional interactions between the ciliopathy-associated Meckel syndrome 1 (MKS1) protein and two novel MKS1-related (MKSR) proteins. J Cell Sci 122(5):611–624.

Bielas SL, Silhavy JL, Brancati F, Kisseleva MV, Al-Gazali L, Sztriha L, Bayoumi RA, Zaki MS, Abdel-Aleem A, Rosti RO, et al. 2009. Mutations in INPP5E, encoding inositol polyphosphate-5-phosphatase E, link phosphatidyl inositol signaling to the ciliopathies. Nat Genet 41(9):1032–1036.

Bloodgood RA. 2009. From central to rudimentary to primary: The history of an underappreciated organelle whose time has come. The primary cilium. Methods Cell Biol 94:2–52.

Bonhivers Ml, Nowacki S, Landrein N, Robinson DR. 2008. Biogenesis of the trypanosome endo-exocytotic organelle is cytoskeleton mediated. PLoS Biol 6(5):e105.

Calvert PD, Schiesser WE, Pugh EN, Jr. 2010. Diffusion of a soluble protein, photoactivatable GFP, through a sensory cilium. J Gen Physiol 135(3):173–196.

Caudron F, Barral Y. 2009. Septins and the lateral compartmentalization of eukaryotic membranes. Dev Cell 16(4):493–506.

Chailley B, Boisvieux-Ulrich E. 1985. Detection of plasma membrane cholesterol by filipin during microvillogenesis and ciliogenesis in quail oviduct. J Histochem Cytochem 33(1):1–10.

Corbit KC, Aanstad P, Singla V, Norman AR, Stainier DYR, Reiter JF. 2005. Vertebrate smoothened functions at the primary cilium. Nature 437(7061):1018–1021.

Craige B, Tsao C-C, Diener DR, Hou Y, Lechtreck K-F, Rosenbaum JL, Witman GB. 2010. CEP290 tethers flagellar transition zone microtubules to the membrane and regulates flagellar protein content. J Cell Biol 190(5):927–940.

Dawe HR, Adams M, Wheway G, Szymanska K, Logan CV, Noegel AA, Gull K, Johnson CA. 2009. Nesprin-2 interacts with meckelin and mediates ciliogenesis via remodelling of the actin cytoskeleton. J Cell Sci 122(15):2716–2726.

Delous M, Baala L, Salomon R, Laclef C, Vierkotten J, Tory K, Golzio C, Lacoste T, Besse L, Ozilou C, et al. 2007. The ciliary gene RPGRIP1L is mutated in cerebello-oculo-renal syndrome (Joubert syndrome type B) and Meckel syndrome. Nat Genet 39(7): 875–881.

Dishinger JF, Kee HL, Jenkins PM, Fan S, Hurd TW, Hammond JW, Truong YN, Margolis B, Martens JR, Verhey KJ. 2010. Ciliary entry of the kinesin-2 motor KIF17 is regulated by importin-β2 and RanGTP. Nat Cell Biol 12(7):703–710.

Dobbelaere J, Barral Y. 2004. Spatial coordination of cytokinetic events by compartmentalization of the cell cortex. Science 305(5682):393–396.

Duldulao NA, Lee S, Sun Z. 2009. Cilia localization is essential for in vivo functions of the Joubert syndrome protein Arl13b/Scorpion. Development 136(23):4033–4042.

Eggenschwiler JT, Anderson KV. 2007. Cilia and developmental signaling. Annu Rev Cell Dev Biol 23(1):345–373.

Emmer BT, Souther C, Toriello KM, Olson CL, Epting CL, Engman DM. 2009. Identification of a palmitoyl acyltransferase required for protein sorting to the flagellar membrane. J Cell Sci 122(6):867–874.

Emmer BT, Maric D, Engman DM. 2010. Molecular mechanisms of protein and lipid targeting to ciliary membranes. J Cell Sci 123(4):529–536.

Fan S, Fogg V, Wang Q, Chen X-W, Liu C-J, Margolis B. 2007. A novel Crumbs3 isoform regulates cell division and ciliogenesis via importin β interactions. J Cell Biol 178(3):387–398.

Faty M, Fink M, Barral Y. 2002. Septins: A ring to part mother and daughter. Curr Genet 41(3):123–131.

Fliegauf M, Benzing T, Omran H. 2007. When cilia go bad: Cilia defects and ciliopathies. Nat Rev Mol Cell Biol 8(11):880–893.

Fliegauf M, Horvath J, von Schnakenburg C, Olbrich H, Müller D, Thumfart J, Schermer B, Pazour GJ, Neumann HPH, Zentgraf H, et al. 2006. Nephrocystin specifically localizes to the transition zone of renal and respiratory cilia and photoreceptor connecting cilia. J Am Soc Nephrol 17(9):2424–2433.

Follit JA, Li L, Vucica Y, Pazour GJ. 2009. The cytoplasmic tail of fibrocystin contains a ciliary targeting sequence. J Cell Biol 188(1): 21–28.

Francis SS, Sfakianos J, Lo B, Mellman I. 2011. A hierarchy of signals regulates entry of membrane proteins into the ciliary membrane domain in epithelial cells. J Cell Biol 193(1):219–233.

Gadelha C, Rothery S, Morphew M, McIntosh JR, Severs NJ, Gull K. 2009. Membrane domains and flagellar pocket boundaries are influenced by the cytoskeleton in African trypanosomes. Proc Natl Acad Sci USA 106(41):17425–17430.

Geng L, Okuhara D, Yu Z, Tian X, Cai Y, Shibazaki S, Somlo S. 2006. Polycystin-2 traffics to cilia independently of polycystin-1 by using an N-terminal RVxP motif. J Cell Sci 119(7):1383–1395.

Gerdes JM, Katsanis N. 2008. Ciliary function and Wnt signal modulation. Curr Top Dev Biol 85:175–195.

Gerdes JM, Davis EE, Katsanis N. 2009. The vertebrate primary cilium in development, homeostasis, and disease. Cell 137(1): 32–45.

Gilula NB, Satir P. 1972. The ciliary necklace: A ciliary membrane specialization. J Cell Biol 53(2):494–509.

Gladfelter AS, Pringle JR, Lew DJ. 2001. The septin cortex at the yeast mother-bud neck. Curr Opin Microbiol 4(6):681–689.

Graser S, Stierhof Y-D, Lavoie SB, Gassner OS, Lamla S, Le Clech M, Nigg EA. 2007. Cep164, a novel centriole appendage protein required for primary cilium formation. J Cell Biol 179(2):321–330.

Gull K. 2003. Host–parasite interactions and trypanosome morphogenesis: A flagellar pocketful of goodies. Curr Opin Microbiol 6(4): 365–370.

Haycraft CJ, Banizs B, Aydin-Son Y, Zhang Q, Michaud EJ, Yoder BK. 2005. Gli2 and Gli3 localize to cilia and require the intraflagellar transport protein polaris for processing and function. PLoS Genet 1(4):e53.

He S, Parapuram SK, Hurd TW, Behnam B, Margolis B, Swaroop A, Khanna H. 2008. Retinitis pigmentosa GTPase regulator (RPGR) protein isoforms in mammalian retina: Insights into X-linked retinitis pigmentosa and associated ciliopathies. Vision Res 48(3):366–376.

Hildebrandt F, Attanasio M, Otto E. 2009. Nephronophthisis: Disease mechanisms of a ciliopathy. J Am Soc Nephrol 20(1):23–35.

Hong D-H, Yue G, Adamian M, Li T. 2001. Retinitis pigmentosa GTPase regulator (RPGR)-interacting protein is stably associated with the photoreceptor ciliary axoneme and anchors RPGR to the connecting cilium. J Biol Chem 276(15):12091–12099.

Hu Q, Nelson WJ, Spiliotis ET. 2008. Forchlorfenuron alters mammalian septin assembly, organization, and dynamics. J Biol Chem 283(43):29563–29571.

Hu Q, Milenkovic L, Jin H, Scott MP, Nachury MV, Spiliotis ET, Nelson WJ. 2010. A septin diffusion barrier at the base of the primary cilium maintains ciliary membrane protein distribution. Science 329(5990):436–439.

Huang K, Diener DR, Mitchell A, Pazour GJ, Witman GB, Rosenbaum JL. 2007. Function and dynamics of PKD2 in *Chlamydomonas reinhardtii* flagella. J Cell Biol 179(3):501–514.

Huangfu D, Liu A, Rakeman AS, Murcia NS, Niswander L, Anderson KV. 2003. Hedgehog signalling in the mouse requires intraflagellar transport proteins. Nature 426(6962):83–87.

Hunnicutt GR, Kosfiszer MG, Snell WJ. 1990. Cell body and flagellar agglutinins in *Chlamydomonas reinhardtii*: The cell body plasma membrane is a reservoir for agglutinins whose migration to the flagella is regulated by a functional barrier. J Cell Biol 111(4):1605–1616.

Hurd TW, Fan S, Margolis BL. 2011. Localization of retinitis pigmentosa 2 to cilia is regulated by Importin β2. J Cell Sci 124(5): 718–726.

Ihara M, Kinoshita A, Yamada S, Tanaka H, Tanigaki A, Kitano A, Goto M, Okubo K, Nishiyama H, Ogawa O, et al. 2005. Cortical organization by the septin cytoskeleton is essential for structural and mechanical integrity of mammalian spermatozoa. Dev Cell 8(3):343–352.

Ishikawa H, Marshall WF. 2011. Ciliogenesis: Building the cell's antenna. Nat Rev Mol Cell Biol 12(4):222–234.

Jacoby M, Cox JJ, Gayral Sp, Hampshire DJ, Ayub M, Blockmans M, Pernot E, Kisseleva MV, Compere P, Schiffmann SN, et al. 2009. INPP5E mutations cause primary cilium signaling defects, ciliary instability and ciliopathies in human and mouse. Nat Genet 41(9):1027–1031.

Janich P, Corbeil D. 2007. GM1 and GM3 gangliosides highlight distinct lipid microdomains within the apical domain of epithelial cells. FEBS Lett 581(9):1783–1787.

Jenkins PM, Hurd TW, Zhang L, McEwen DP, Brown RL, Margolis B, Verhey KJ, Martens JR. 2006. Ciliary targeting of olfactory CNG channels requires the CNGB1b subunit and the kinesin-2 motor protein, KIF17. Curr Biol 16(12):1211–1216.

Jin H, White SR, Shida T, Schulz S, Aguiar M, Gygi SP, Bazan JF, Nachury MV. 2010. The conserved Bardet-Biedl syndrome proteins assemble a coat that traffics membrane proteins to cilia. Cell 141(7):1208–1219.

Jones C, Chen P. 2008. Primary cilia in planar cell polarity regulation of the inner ear. Curr Top Dev Biol 85:197–224.

Joo E, Surka MC, Trimble WS. 2007. Mammalian SEPT2 is required for scaffolding nonmuscle myosin ii and its kinases. Dev Cell 13(5):677–690.

Kee H, McIntyre J, Jenkins P, Verhey K, Martens JR. 2010. Size exclusion and fatty acylation control ciliary protein entry. Mol Biol Cell 21(Suppl); Abstract No. 1108/B283.

Kim SK, Shindo A, Park TJ, Oh EC, Ghosh S, Gray RS, Lewis RA, Johnson CA, Attie-Bittach T, Katsanis N, et al. 2010. Planar cell polarity acts through septins to control collective cell movement and ciliogenesis. Science 329(5997):1337–1340.

Kinoshita M, Field CM, Coughlin ML, Straight AF, Mitchison TJ. 2002. Self- and actin-templated assembly of mammalian septins. Dev Cell 3(6):791–802.

Kissel H, Georgescu MM, Larisch S, Manova K, Hunnicutt GR, Steller H. 2005. The Sept4 septin locus is required for sperm terminal differentiation in mice. Dev Cell 8(3):353–364.

Knödler A, Feng S, Zhang J, Zhang X, Das A, Peränen J, Guo W. 2010. Coordination of Rab8 and Rab11 in primary ciliogenesis. Proc Natl Acad Sci USA 107(14):6346–6351.

Kohl L, Bastin P, Kwang WJ. 2005. The Flagellum of Trypanosomes. Int Rev Cytol 244:227–285.

Kovacs JJ, Whalen EJ, Liu R, Xiao K, Kim J, Chen M, Wang J, Chen W, Lefkowitz RJ. 2008. b-Arrestin mediated localization of smoothened to the primary cilium. Science 320(5884):1777–1781.

Kremer BE, Adang LA, Macara IG. 2007. Septins regulate actin organization and cell-cycle arrest through nuclear accumulation of NCK mediated by SOCS7. Cell 130(5):837–850.

Kulaga HM, Leitch CC, Eichers ER, Badano JL, Lesemann A, Hoskins BE, Lupski JR, Beales PL, Reed RR, Katsanis N. 2004. Loss of BBS proteins causes anosmia in humans and defects in olfactory cilia structure and function in the mouse. Nat Genet 36(9): 994–998.

Kwitny S, Klaus AV, Hunnicutt GR. 2010. The annulus of the mouse sperm tail is required to establish a membrane diffusion barrier that is engaged during the late steps of spermiogenesis. Biol Reprod 82(4):669–678.

Kwok MCM, Holopainen JM, Molday LL, Foster LJ, Molday RS. 2008. Proteomics of photoreceptor outer segments identifies a subset of SNARE and Rab proteins implicated in membrane vesicle trafficking and fusion. Mol Cell Proteomics 7(6): 1053–1066.

Kyttala M, Tallila J, Salonen R, Kopra O, Kohlschmidt N, Paavola-Sakki P, Peltonen L, Kestila M. 2006. MKS1, encoding a component of the flagellar apparatus basal body proteome, is mutated in Meckel syndrome. Nat Genet 38(2):155–157.

Lancaster MA, Gleeson JG. 2009. The primary cilium as a cellular signaling center: Lessons from disease. Curr Opin Genet Dev 19(3):220–229.

Liu Q, Tan G, Levenkova N, Li T, Pugh EN, Rux JJ, Speicher DW, Pierce EA. 2007a.The proteome of the mouse photoreceptor sensory cilium complex. Mol Cell Proteomics 6(8):1299–1317.

Liu X, Bulgakov OV, Darrow KN, Pawlyk B, Adamian M, Liberman MC, Li T. 2007b.Usherin is required for maintenance of retinal photoreceptors and normal development of cochlear hair cells. Proc Natl Acad Sci USA 104(11):4413–4418.

Luedeke C, Frei SB, Sbalzarini I, Schwarz H, Spang A, Barral Y. 2005. Septin-dependent compartmentalization of the endoplasmic reticulum during yeast polarized growth. J Cell Biol 169(6): 897–908.

Maerker T, van Wijk E, Overlack N, Kersten FFJ, McGee J, Goldmann T, Sehn E, Roepman R, Walsh EJ, Kremer H, et al. 2008. A novel Usher protein network at the periciliary reloading point between molecular transport machineries in vertebrate photoreceptor cells. Hum Mol Genet 17(1):71–86.

Malone AMD, Anderson CT, Tummala P, Kwon RY, Johnston TR, Stearns T, Jacobs CR. 2007. Primary cilia mediate mechanosensing in bone cells by a calcium-independent mechanism. Proc Natl Acad Sci USA 104(33):13325–13330.

Marshall WF. 2008. Basal bodies: Platforms for building cilia. Curr Top Dev Biol 85:1–22.

Marshall WF, Nonaka S. 2006. Cilia: Tuning in to the cell's antenna. Curr Biol 16(15):R604–R614.

Mayer U, Ungerer N, Klimmeck D, Warnken U, Schnölzer M, Frings S, Möhrlen F. 2008. Proteomic analysis of a membrane preparation from rat olfactory sensory cilia. Chem Senses 33(2):145–162.

McEwen DP, Jenkins PM, Martens JR. 2008. Olfactory cilia: Our direct neuronal connection to the external World. Curr Top Dev Biol 85:333–370.

Milenkovic L, Scott MP, Rohatgi R. 2009. Lateral transport of Smoothened from the plasma membrane to the membrane of the cilium. J Cell Biol 187(3):365–374.

Mitchell KAP, Szabo G, Otero AdS. 2009. Methods for the isolation of sensory and primary cilia: An overview. Methods Cell Biol 94:87–101.

Molla-Herman A, Ghossoub R, Blisnick T, Meunier A, Serres C, Silbermann F, Emmerson C, Romeo K, Bourdoncle P, Schmitt A, et al. 2010. The ciliary pocket: An endocytic membrane domain at the base of primary and motile cilia. J Cell Sci 123(10):1785–1795.

Mollet G, Silbermann F, Delous M, Salomon Rm, Antignac C, Saunier S. 2005. Characterization of the nephrocystin/nephrocystin-4 complex and subcellular localization of nephrocystin-4 to primary cilia and centrosomes. Hum Mol Genet 14(5):645–656.

Mombaerts P. 1999. Molecular biology of odorant receptors in vertebrates. Annu Rev Neurosci 22(1):487–509.

Mukhopadhyay S, Wen X, Chih B, Nelson CD, Lane WS, Scales SJ, Jackson PK. 2010. TULP3 bridges the IFT-A complex and membrane phosphoinositides to promote trafficking of G protein-coupled receptors into primary cilia. Genes Dev 24(19):2180–2193.

Musgrave A, Wildt P, Etten I, Pijst H, Scholma C, Kooyman R, Homan W, Ende H. 1986. Evidence for a functional membrane barrier in the transition zone between the flagellum and cell body of *Chlamydomonas eugametos* gametes. Planta 167(4):544–553.

Mykytyn K, Sheffield VC. 2004. Establishing a connection between cilia and Bardet-Biedl syndrome. Trends Mol Med 10(3):106–109.

Nachury MV, Loktev AV, Zhang Q, Westlake CJ, Peränen J, Merdes A, Slusarski DC, Scheller RH, Bazan JF, Sheffield VC, et al. 2007. A core complex of BBS proteins cooperates with the GTPase Rab8 to promote ciliary membrane biogenesis. Cell 129(6): 1201–1213.

Nachury MV, Seeley ES, Jin H. 2010. Trafficking to the ciliary membrane: How to get across the periciliary diffusion barrier? Annu Rev Cell Dev Biol 26(1):59–87.

Nauli SM, Alenghat FJ, Luo Y, Williams E, Vassilev P, Li X, Elia AEH, Lu W, Brown EM, Quinn SJ, et al. 2003. Polycystins 1 and 2 mediate mechanosensation in the primary cilium of kidney cells. Nat Genet 33(2):129–137.

Nonaka S, Tanaka Y, Okada Y, Takeda S, Harada A, Kanai Y, Kido M, Hirokawa N. 1998. Randomization of left-right asymmetry due to loss of nodal cilia generating leftward flow of extraembryonic fluid in mice lacking KIF3B motor protein. Cell 95(6):829–837.

Oh Y, Bi E. 2011. Septin structure and function in yeast and beyond. Trends Cell Biol 21(3):141–148.

Otto EA, Schermer B, Obara T, O'Toole JF, Hiller KS, Mueller AM, Ruf RG, Hoefele J, Beekmann F, Landau D, et al. 2003. Mutations in INVS encoding inversin cause nephronophthisis type 2, linking renal cystic disease to the function of primary cilia and left-right axis determination. Nat Genet 34(4):413–420.

Otto EA, Loeys B, Khanna H, Hellemans J, Sudbrak R, Fan S, Muerb U, O'Toole JF, Helou J, Attanasio M, et al. 2005. Nephrocystin-5, a ciliary IQ domain protein, is mutated in Senior-Loken syndrome and interacts with RPGR and calmodulin. Nat Genet 37(3):282–288.

Otto EA, Trapp ML, Schultheiss UT, Helou J, Quarmby LM, Hildebrandt F. 2008. NEK8 mutations affect ciliary and centrosomal localization and may cause nephronophthisis. J Am Soc Nephrol 19(3):587–592.

Overath P, Stierhof Y-D, Wiese M. 1997. Endocytosis and secretion in trypanosomatid parasites—Tumultuous traffic in a pocket. Trends Cell Biol 7(1):27×33.

Papermaster DS, Schneider BG, Besharse JC. 1985. Vesicular transport of newly synthesized opsin from the Golgi apparatus toward the rod outer segment. Ultrastructural immunocytochemical and autoradiographic evidence in *Xenopus* retinas. Invest Ophthalmol Vis Sci 26(10):1386–404.

Parisi MA, Doherty D, Chance PF, Glass IA. 2007. Joubert syndrome (and related disorders) (OMIM 213300). Eur J Hum Genet 15(5):511–521.

Pazour GJ, Agrin N, Leszyk J, Witman GB. 2005. Proteomic analysis of a eukaryotic cilium. J Cell Biol 170(1):103–113.

Pazour GJ, Bloodgood RA. 2008. Targeting proteins to the ciliary membrane. Curr Top Dev Biol 85:115–149.

Pazour GJ, Rosenbaum JL. 2002. Intraflagellar transport and cilia-dependent diseases. Trends Cell Biol 12(12):551–555.

Pazour GJ, Witman GB. 2003. The vertebrate primary cilium is a sensory organelle. Curr Opin Cell Biol 15(1):105–110.

Pazour GJ, Dickert BL, Vucica Y, Seeley ES, Rosenbaum JL, Witman GB, Cole DG. 2000. Chlamydomonas IFT88 and its mouse homologue, polycystic kidney disease gene Tg737, are required for assembly of cilia and flagella. J Cell Biol 151(3):709–718.

Pazour GJ, San Agustin JT, Follit JA, Rosenbaum JL, Witman GB. 2002. Polycystin-2 localizes to kidney cilia and the ciliary level is elevated in orpk mice with polycystic kidney disease. Curr Biol 12(11):R378–R380.

Pedersen LB, Rosenbaum JL. 2008. Intraflagellar transport (IFT): Role in ciliary assembly, resorption and signalling. Curr Top Dev Biol 85: 23–61.

Pigino G, Geimer S, Lanzavecchia S, Paccagnini E, Cantele F, Diener DR, Rosenbaum JL, Lupetti P. 2009. Electron-tomographic analysis of intraflagellar transport particle trains in situ. J Cell Biol 187(1):135–148.

Praetorius HA, Spring KR. 2001. Bending the MDCK cell primary cilium increases intracellular calcium. J Membr Biol 184(1):71–79.

Rodal AA, Kozubowski L, Goode BL, Drubin DG, Hartwig JH. 2005. Actin and septin ultrastructures at the budding yeast cell cortex. Mol Biol Cell 16(1):372–384.

Roepman R, Letteboer SJF, Arts HH, van Beersum SEC, Lu X, Krieger E, Ferreira PA, Cremers FPM. 2005. Interaction of nephrocystin-4 and RPGRIP1 is disrupted by nephronophthisis or Leber congenital amaurosis-associated mutations. Proc Natl Acad Sci USA 102(51):18520–18525.

Rohatgi R, Milenkovic L, Scott MP. 2007. Patched1 regulates Hedgehog signaling at the primary cilium. Science 317(5836):372–376.

Rohatgi R, Snell WJ. 2010. The ciliary membrane. Curr Opin Cell Biol 22(4):541–546.

Romio L, Fry AM, Winyard PJD, Malcolm S, Woolf AS, Feather SA. 2004. OFD1 is a centrosomal/basal body protein expressed during mesenchymal-epithelial transition in human nephrogenesis. J Am Soc Nephrol 15(10):2556–2568.

Rosenbaum JL, Witman GB. 2002. Intraflagellar transport. Nat Rev Mol Cell Biol 3(11):813–825.

Ross AJ, May-Simera H, Eichers ER, Kai M, Hill J, Jagger DJ, Leitch CC, Chapple JP, Munro PM, Fisher S, et al. 2005. Disruption of Bardet-Biedl syndrome ciliary proteins perturbs planar cell polarity in vertebrates. Nat Genet 37(10):1135–1140.

Salathe M. 2007. Regulation of mammalian ciliary beating. Annu Rev Physiol 69(1):401–422.

Satir P, Christensen ST. 2007. Overview of structure and function of mammalian cilia. Annu Rev Physiol 69(1):377–400.

Sayer JA, Otto EA, O'Toole JF, Nurnberg G, Kennedy MA, Becker C, Hennies HC, Helou J, Attanasio M, Fausett BV, et al. 2006. The centrosomal protein nephrocystin-6 is mutated in Joubert syndrome and activates transcription factor ATF4. Nat Genet 38(6): 674–681.

Schmidt K, Nichols BJ. 2004. A barrier to lateral diffusion in the cleavage furrow of dividing mammalian cells. Curr Biol 14(11): 1002–1006.

Schneider L, Clement CA, Teilmann SC, Pazour GJ, Hoffmann EK, Satir P, Christensen ST. 2005. PDGFRαα signaling is regulated through the primary cilium in fibroblasts. Curr Biol 15(20):1861–1866.

Scholey JM, Anderson KV. 2006. Intraflagellar transport and cilium-based signaling. Cell 125(3):439–442.

Schwartz EA, Leonard ML, Bizios R, Bowser SS. 1997. Analysis and modeling of the primary cilium bending response to fluid shear. Am J Physiol 272(1):F132–F138.

Sfakianos J, Togawa A, Maday S, Hull M, Pypaert M, Cantley L, Toomre D, Mellman I. 2007. Par3 functions in the biogenesis of the primary cilium in polarized epithelial cells. J Cell Biol 179(6): 1133–1140.

Shah AS, Ben-Shahar Y, Moninger TO, Kline JN, Welsh MJ. 2009. Motile cilia of human airway epithelia are chemosensory. Science 325(5944):1131–1134.

Sharma N, Berbari NF, Yoder BK. 2008. Ciliary dysfunction in developmental abnormalities and diseases. Curr Top Dev Biol 85: 371–427.

Shcheprova Z, Baldi S, Frei SB, Gonnet G, Barral Y. 2008. A mechanism for asymmetric segregation of age during yeast budding. Nature 454(7205):728–734.

Shiba D, Manning DK, Koga H, Beier DR, Yokoyama T. 2010. Inv acts as a molecular anchor for Nphp3 and Nek8 in the proximal segment of primary cilia. Cytoskeleton 67(2):112–119.

Simons K, Toomre D. 2000. Lipid rafts and signal transduction. Nat Rev Mol Cell Biol 1(1):31–39.

Simons M, Gloy J, Ganner A, Bullerkotte A, Bashkurov M, Kronig C, Schermer B, Benzing T, Cabello OA, Jenny A, et al. 2005. Inversin, the gene product mutated in nephronophthisis type II, functions as a molecular switch between Wnt signaling pathways. Nat Genet 37(5):537–543.

Singla V, Reiter JF. 2006. The primary cilium as the cell's antenna: Signaling at a sensory organelle. Science 313(5787):629–633.

Sirajuddin M, Farkasovsky M, Hauer F, Kuhlmann D, Macara IG, Weyand M, Stark H, Wittinghofer A. 2007. Structural insight into filament formation by mammalian septins. Nature 449(7160): 311–315.

Sloboda RD, Rosenbaum JL. 2007. Making sense of cilia and flagella. J Cell Biol 179(4):575–582.

Snell WJ, Pan J, Wang Q. 2004. Cilia and flagella revealed: From flagellar assembly in *Chlamydomonas* to human obesity disorders. Cell 117(6):693–697.

Sorokin S. 1962. Centrioles and the formation of rudimentary cilia by fibroblasts and smooth muscle cells. J Cell Biol 15(2):363–377.

Spencer M, Detwiler PB, Bunt-Milam AH. 1988. Distribution of membrane proteins in mechanically dissociated retinal rods. Invest Ophthalmol Vis Sci 29(7):1012–1020.

Spiliotis ET, Kinoshita M, Nelson WJ. 2005. A mitotic septin scaffold required for mammalian chromosome congression and segregation. Science 307(5716):1781–1785.

Spiliotis ET, Hunt SJ, Hu Q, Kinoshita M, Nelson WJ. 2008. Epithelial polarity requires septin coupling of vesicle transport to polyglutamylated microtubules. J Cell Biol 180(2):295–303.

Steels JD, Estey MP, Froese CD, Reynaud D, Pace-Asciak C, Trimble WS. 2007. Sept12 is a component of the mammalian sperm tail annulus. Cell Motil Cytoskeleton 64(10):794–807.

Tada T, Simonetta A, Batterton M, Kinoshita M, Edbauer D, Sheng M. 2007. Role of septin cytoskeleton in spine morphogenesis and dendrite development in neurons. Curr Biol 17(20):1752–1758.

Tam BM, Moritz OL, Hurd LB, Papermaster DS. 2000. Identification of an outer segment targeting signal in the cooh terminus of rhodopsin using transgenic *Xenopus laevis*. J Cell Biol 151(7): 1369–1380.

Tanaka-Takiguchi Y, Kinoshita M, Takiguchi K. 2009. Septin-mediated uniform bracing of phospholipid membranes. Curr Biol 19(2): 140–145.

Tao B, Bu S, Yang Z, Siroky B, Kappes JC, Kispert A, Guay-Woodford LM. 2009. Cystin localizes to primary cilia via membrane microdomains and a targeting motif. J Am Soc Nephrol 20(12):2570–2580.

Teilmann SC, Christensen ST. 2005. Localization of the angiopoietin receptors Tie-1 and Tie-2 on the primary cilia in the female reproductive organs. Cell Biol Int 29(5):340–346.

Tyler KM, Fridberg A, Toriello KM, Olson CL, Cieslak JA, Hazlett TL, Engman DM. 2009. Flagellar membrane localization via association with lipid rafts. J Cell Sci 122(6):859–866.

Valente EM, Silhavy JL, Brancati F, Barrano G, Krishnaswami SR, Castori M, Lancaster MA, Boltshauser E, Boccone L, Al-Gazali L, et al. 2006. Mutations in CEP290, which encodes a centrosomal

protein, cause pleiotropic forms of Joubert syndrome. Nat Genet 38(6):623–625.

Valente EM, Logan CV, Mougou-Zerelli S, Lee JH, Silhavy JL, Brancati F, Iannicelli M, Travaglini L, Romani S, Illi B, et al. 2010. Mutations in TMEM216 perturb ciliogenesis and cause Joubert, Meckel and related syndromes. Nat Genet 42(7):619–625.

Versele M, Thorner J. 2005. Some assembly required: Yeast septins provide the instruction manual. Trends Cell Biol 15(8):414–424.

Vieira OV, Gaus K, Verkade P, Fullekrug J, Vaz WLC, Simons K. 2006. FAPP2, cilium formation, and compartmentalization of the apical membrane in polarized Madin-darby canine kidney (MDCK) cells. Proc Natl Acad Sci USA 103(49):18556–18561.

Wang Q, Pan J, Snell WJ. 2006. Intraflagellar transport particles participate directly in cilium-generated signaling in *Chlamydomonas*. Cell 125(3):549–562.

Westlake CJ, Baye LM, Nachury MV, Wright KJ, Ervin KE, Phu L, Chalouni C, Beck JS, Kirkpatrick DS, Slusarski DC, et al. 2011. Primary cilia membrane assembly is initiated by Rab11 and transport protein particle II (TRAPPII) complex-dependent trafficking of Rabin8 to the centrosome. Proc Natl Acad Sci USA 108(7): 2759–2764.

Williams CL, Winkelbauer ME, Schafer JC, Michaud EJ, Yoder BK. 2008. Functional redundancy of the B9 proteins and nephrocystins in *Caenorhabditis elegans* ciliogenesis. Mol Biol Cell 19(5): 2154–2168.

Williams CL, Masyukova SV, Yoder BK. 2009. Normal ciliogenesis requires synergy between the cystic kidney disease genes MKS-3 and NPHP-4. J Am Soc Nephrol 21(5):782–793.

Williams CL, Li C, Kida K, Inglis PN, Mohan S, Semenec L, Bialas NJ, Stupay RM, Chen N, Blacque OE., et al. 2011. MKS and NPHP modules cooperate to establish basal body/transition zone membrane associations and ciliary gate function during ciliogenesis. J Cell Biol 192(6):1023–1041.

Winkelbauer ME, Schafer JC, Haycraft CJ, Swoboda P, Yoder BK. 2005. The C. elegans homologs of nephrocystin-1 and nephrocystin-4 are cilia transition zone proteins involved in chemosensory perception. J Cell Sci 118(23):5575–5587.

Wong SY, Reiter JF. 2008. The primary cilium: At the crossroads of mammalian Hedgehog signaling. Curr Top Dev Biol 85: 225–260.

Xie Y, Vessey JP, Konecna A, Dahm R, Macchi P, Kiebler MA. 2007. The GTP-binding protein Septin 7 is critical for dendrite branching and dendritic-spine morphology. Curr Biol 17(20): 1746–1751.

Yan D, Liu XZ. 2010. Genetics and pathological mechanisms of Usher syndrome. J Hum Genet 55(6):327–335.

Yoder BK, Hou X, Guay-Woodford LM. 2002. The polycystic kidney disease proteins, Polycystin-1, Polycystin-2, Polaris, and Cystin, are co-localized in renal cilia. J Am Soc Nephrol 13(10): 2508–2516.

Zhang J, Kong C, Xie H, McPherson PS, Grinstein S, Trimble WS. 1999. Phosphatidylinositol polyphosphate binding to the mammalian septin H5 is modulated by GTP. Curr Biol 9(24): 1458–1467.

Zimmermann KW. 1898. Beitrage zur Kenntniss einiger Drusen und epithelien. Arch Mikrosk Anat 52:552–706.

A Septin Diffusion Barrier at the Base of the Primary Cilium Maintains Ciliary Membrane Protein Distribution

Qicong Hu,[1] Ljiljana Milenkovic,[2,3] Hua Jin,[4] Matthew P. Scott,[2,3,5–8] Maxence V. Nachury,[4] Elias T. Spiliotis,[9]* W. James Nelson[1,4]*

In animal cells, the primary cilium transduces extracellular signals through signaling receptors localized in the ciliary membrane, but how these ciliary membrane proteins are retained in the cilium is unknown. We found that ciliary membrane proteins were highly mobile, but their diffusion was impeded at the base of the cilium by a diffusion barrier. Septin 2 (SEPT2), a member of the septin family of guanosine triphosphatases that form a diffusion barrier in budding yeast, localized at the base of the ciliary membrane. SEPT2 depletion resulted in loss of ciliary membrane protein localization and Sonic hedgehog signal transduction, and inhibited ciliogenesis. Thus, SEPT2 is part of a diffusion barrier at the base of the ciliary membrane and is essential for retaining receptor-signaling pathways in the primary cilium.

The primary cilium is an antenna-like organelle protruding from the apical surface of almost every cell in a wide variety of organisms. The ciliary membrane is contiguous with the apical plasma membrane but has a unique set of proteins that sense and transduce a variety of extracellular signals, such as Sonic hedgehog (Shh) (*1*). These signaling pathways regulate gene expression during development and in adult life, and mutations in ciliary proteins give rise to a range of developmental defects (*2*, *3*).

Signal transduction by the primary cilium depends on the enrichment of specific proteins in the ciliary membrane. Protein trafficking and intraflagellar transport from the cytoplasm into the cilium establish the characteristic intracellular distributions of ciliary membrane proteins (*4*, *5*), but it is unknown how these proteins are subsequently retained in the ciliary membrane: For example, they might be immobilized in the cilium or impeded by a diffusion barrier (*6–10*).

To investigate these possible mechanisms, we used fluorescence recovery after photobleaching (FRAP) (*11*) to measure the diffusional mobility of four ciliary membrane proteins tagged with green fluorescent protein (GFP): two G protein–coupled receptors [serotonin receptor 6 (^{FI}Htr6^{SEP}) and somatostatin receptor (Sstr3^{GFP}) (*12*)], and the membrane-anchored and ciliary-targeted cytoplasmic tail (amino acids 1 to 193) of fibrocystin ($_{CTS}$PKHD1^{GFP}) (*13*) in primary kidney inner medullary collecting duct (IMCD3)

[1]Department of Biology, Stanford University, Stanford, CA 94305, USA. [2]Department of Developmental Biology, Stanford University School of Medicine, Stanford, CA 94305, USA. [3]Howard Hughes Medical Institute, Stanford University, Stanford, CA 94305, USA. [4]Department of Molecular and Cellular Physiology, Stanford University School of Medicine, Stanford, CA 94305, USA. [5]Department of Genetics, Stanford University School of Medicine, Stanford, CA 94305, USA. [6]Department of Bioengineering, Stanford University, Stanford, CA 94305, USA. [7]Department of Medicine, Stanford University School of Medicine, Stanford, CA 94305, USA. [8]Department of Biochemistry, Stanford University School of Medicine, Stanford, CA 94305, USA. [9]Department of Biology, Drexel University, Philadelphia, PA 19104, USA.

*To whom correspondence should be addressed. E-mail: wjnelson@stanford.edu (W.J.N.); ets33@drexel.edu (E.T.S.)

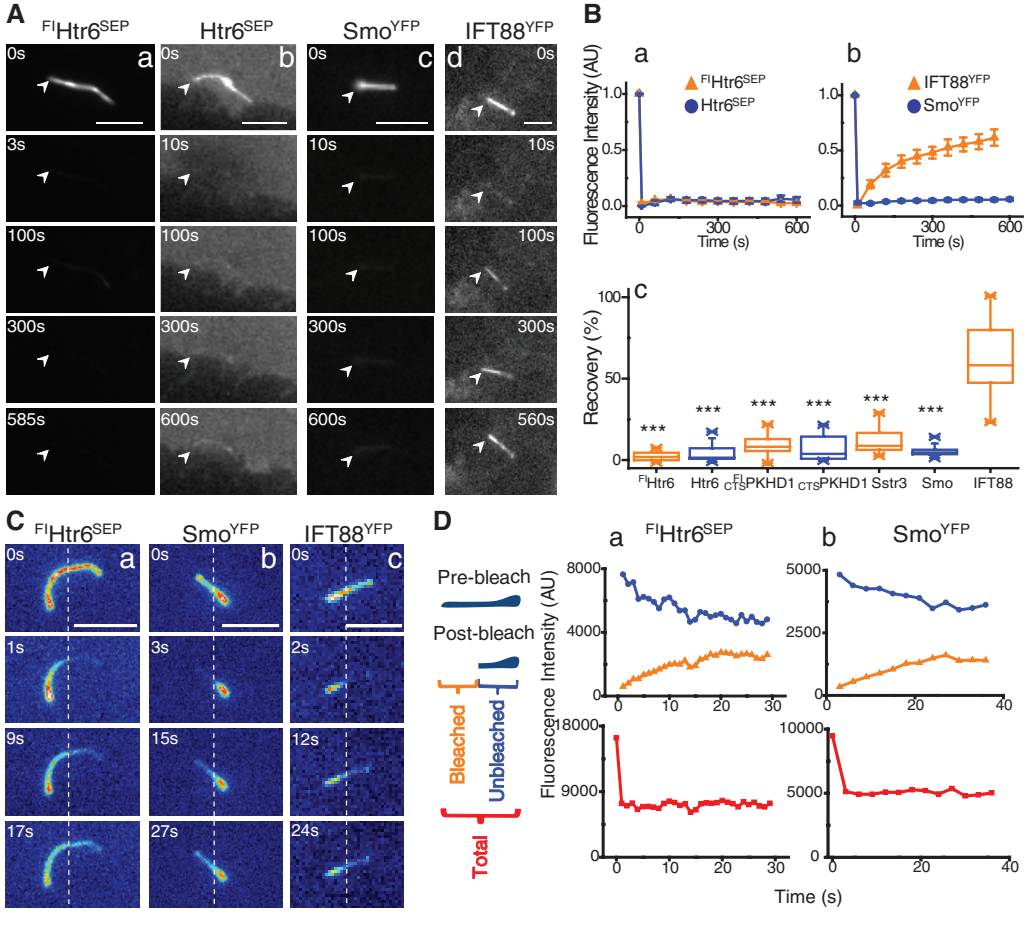

Fig. 1. (**A**) FRAP of proteins in the whole cilium 24 hours after serum starvation. IMCD3 cells stably (a) or transiently (b) expressing Htr6^{SEP} or IFT88^{YFP} (d), and Smo^{YFP} stably expressed in MEFs treated with 100 nM SAG for 24 hours (c); arrowheads mark one end of the cilium. Scale bars, 5 μm. (**B**) Kinetics of average (±SEM) fluorescence recovery of proteins photobleached in the whole cilium (a, b; n = 8 to 12). Summary of fluorescence recovery of ciliary membrane proteins as a percentage of the initial unbleached fluorescence level compared with IFT88^{YFP} distribution (c; ***$P < 0.0001$). (**C**) FRAP of Htr6^{SEP} (a), Smo^{YFP} (b), and IFT88^{YFP} (c) represented as heat-map images after photobleaching part of the cilium in IMCD3 cells; dotted lines mark the photobleached/unbleached boundary. Scale bars, 5 μm. (**D**) Representative example of kinetics of fluorescence recovery of photobleached region (orange curve), unbleached region (blue curve), and the two regions combined (red curve) of a primary cilium (n = 12 to 13).

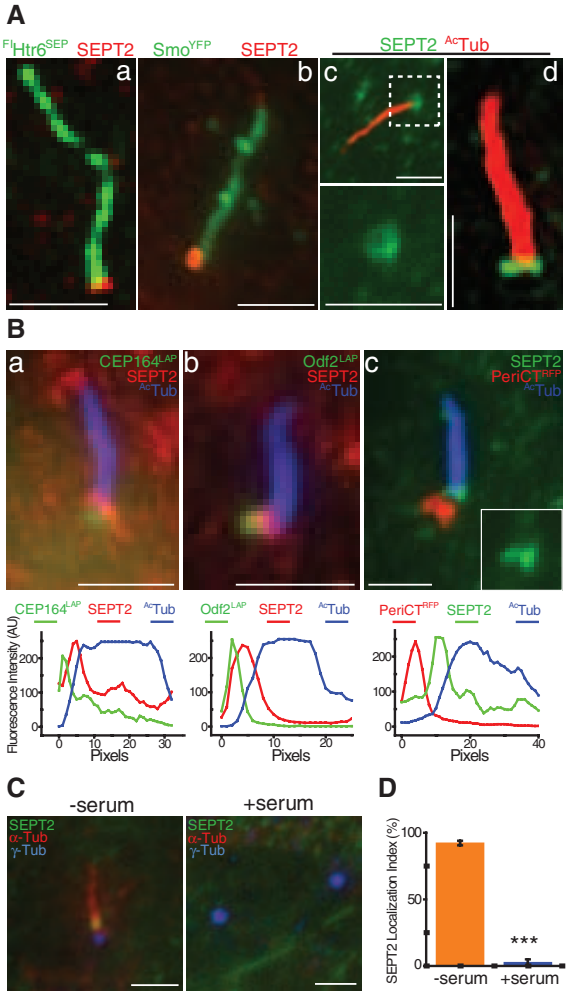

Fig. 2. (**A**) SEPT2 localization at the cilium of IMCD3 cells stably expressing ^{Fl}Htr6^{SEP} (a), MEFs stably expressing Smo^{YFP} treated with 100 nM SAG for 24 hours (b), and IMCD3 cells stained for acetylated α-tubulin (^{Ac}Tub) (c; higher magnification of boxed region shown at the bottom), and imaged with a super-resolution Optical Microscope Experimental (OMX) system using three-dimensional structured illumination (d). Scale bars, 2 μm. (**B**) SEPT2 and ^{Ac}Tub localization at the cilium of IMCD3 cells transiently expressing CEP164^{LAP} (a), Odf2^{LAP} (b) or PeriCT^{RFP} (c). Scale bars, 2 μm. (Lower panels) Fluorescence intensity profiles of protein staining from the basal body to the tip of the cilium. (**C**) IMCD3 cells grown for 24 hours without (–) or with (+) serum and stained for SEPT2, α-tubulin (α-tub), and γ-tubulin (γ-tub). Scale bars, 2 μm. (**D**) Percentage of cells with SEPT2 localized at the base of primary cilia (–serum) or pericentriolar region (+serum). Error bars represent SD of three independent experiments (n = 60 to 178 each; ***P < 0.0001).

cells, and the Shh signaling pathway transducer smoothened (Smo^{YFP}) (*14*) in mouse embryonic fibroblasts (MEF). All of these proteins localized to the cilium, but none recovered fluorescence when the whole cilium was photobleached (Fig. 1, A and B; fig. S1, A and B; and movies S1 to S6) (*15*), even though their mobility was high in the periciliary membrane, as shown for Htr6^{SEP} (fig. S1C, table S1, and movie S7). In contrast, fluorescence recovery of the intraflagellar transport complex protein IFT88 (IFT88^{YFP}) (*16*, *17*) was high (Fig. 1, A and B, table S1, and movie S8).

The low diffusional mobility of these ciliary membrane proteins might be due to their immobilization within the primary cilium or to the presence of a diffusion barrier at the base of the ciliary membrane. To distinguish between these possibilities, we photobleached part of the cilium and measured the fluorescence recovery of ciliary membrane proteins (Fig. 1, C and D; fig. S1, D and E; and movies S9 to S13). Strikingly, all proteins were highly mobile within the ciliary membrane (fig. S1F and table S2), although fluorescence recovery was still confined within the cilium (Fig. 1, C and D, and fig. S1, D and E). Note that constituent plasma membrane proteins (GPI^{YFP} and VSV-G^{GFP}) were also excluded from the ciliary membrane (fig. S2). Therefore, the diffusion of membrane proteins between the ciliary and periciliary membrane, unlike the movement of IFT88 and cytoplasmic GFP (*18*), is impeded at the base of the cilium by a diffusion barrier.

To identify molecular components of this ciliary membrane diffusion barrier, we focused on septins. Septins are oligomeric guanosine

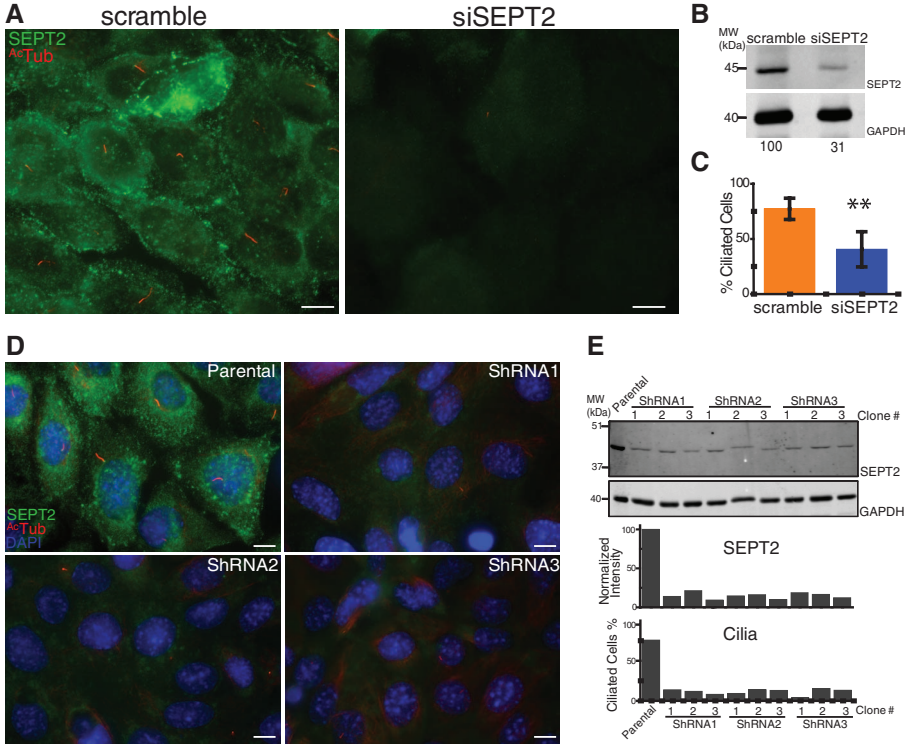

Fig. 3. (**A**) IMCD3 cells transfected with scrambled (scramble) or SEPT2 siRNA (siSEPT2), serum-starved to induce ciliogenesis, and stained for SEPT2 and ^{Ac}Tub. Scale bars, 10 μm. (**B**) Whole-cell lysates of scramble and siSEPT2 cells immunoblotted for SEPT2 and glyceraldehyde phosphate dehydrogenase (GAPDH); lower panel, SEPT2 band intensities normalized to GAPDH. (**C**) Percentage of scramble and siSEPT2 cells with a cilium >1 μm long (±SD of three independent experiments; n = 101 to 205 each; **P = 0.0098). (**D**) IMCD3 cells (Parental), and IMCD3 cells stably depleted of SEPT2 using shRNA1, shRNA2, or shRNA3, stained for SEPT2, ^{Ac}Tub, and 4′,6′-diamidino-2-phenylindole (DAPI). Scale bars, 10 μm. (**E**) Whole-cell lysates of parental IMCD3 cells and three arbitrarily chosen clones of shRNA1, 2, or 3 cells immunoblotted for SEPT2 and GAPDH; lower panel, SEPT2 band intensities normalized to GAPDH, and percentage of parental and shRNA1, 2, and 3 IMCD3 cells with a cilium (n = 115 to 282).

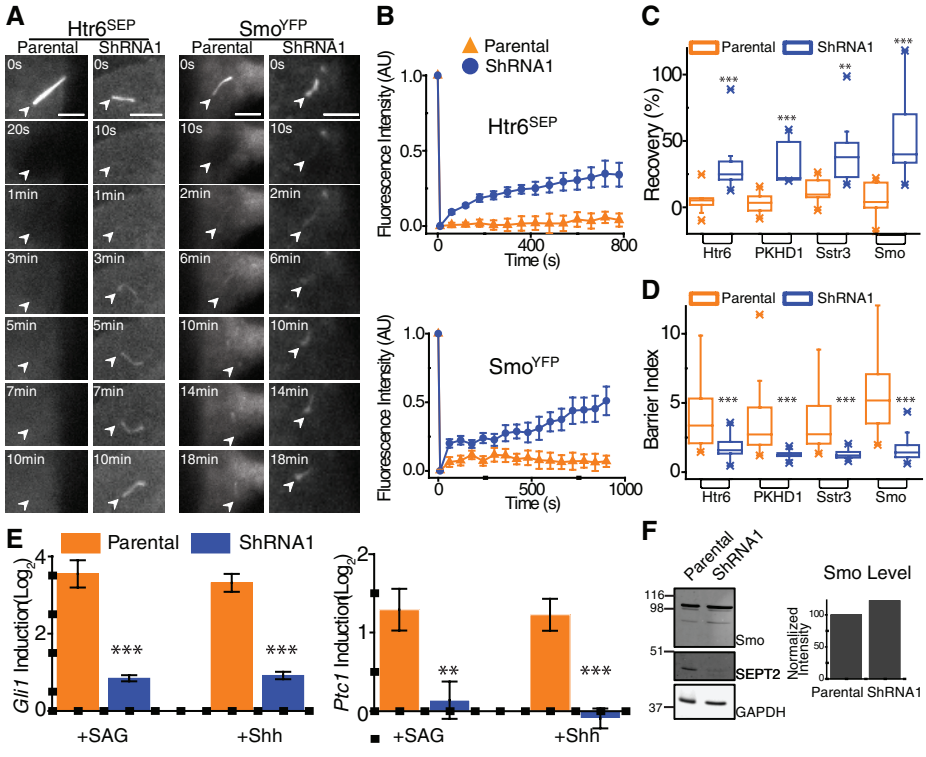

Fig. 4. (**A** and **B**) FRAP of the whole cilium of parental IMCD3 (Parental) and shRNA1 IMCD3 cells transiently expressing $Htr6^{SEP}$ or Smo^{YFP} and treated with 100 nM SAG for 24 hours. Scale bars, 5 μm. (B) Kinetics of average (±SEM) fluorescence recovery of photobleached proteins (n = 9 to 12). (**C**) Summary of percentage of fluorescence recovery of photobleached ciliary membrane proteins in parental and shRNA1 cells (**P < 0.002; ***P < 0.0005). (**D**) Summary of barrier index in parental and shRNA1 cells (n = 31 to 59; ***P < 0.0001). (**E**) *Gli1* (left) and *Ptc1* (right) mRNA induction in parental and shRNA1 cells after 100 nM SAG or Shh treatment for 24 hours (average of three independent experiments ±SD; **P = 0.005; ***P < 0.0007). (**F**) Whole-cell lysates of parental and shRNA1 cells immunoblotted for Smo, SEPT2, and GAPDH; normalized Smo levels in parental and shRNA1 cells (right).

triphosphatases (GTPases) that form a diffusion barrier at the mother-bud neck of budding yeast (*10*, *19*, *20*) and localize at the annulus that may form a diffusion barrier between the middle and principal piece of the mammalian sperm flagellum (*21*, *22*). Septin 2 (SEPT2) (*23*) localized to the base of the cilium at the boundary between the ciliary and periciliary membrane in IMCD3 cells (Fig. 2A and fig. S3A) and in MEFs stably expressing Smo^{YFP} (Fig. 2A). In some optical sections SEPT2 staining appeared as a ringlike structure of ~500 nm diameter (Fig. 2A), reminiscent of structures formed by recombinant septins in vitro (*24*), and as two fused dots (Fig. 2A and movies S14 and S15), similar to septin staining at the sperm annulus (*21*). In ~10% of cells, punctate SEPT2 also localized along and at the tip of the axoneme (fig. S3B).

SEPT2 localization at the base of the axoneme is similar to basal body distal appendage proteins. SEPT2, however, clearly localized between the ciliary axoneme [marked by acetylated α-tubulin (^{Ac}Tub)] and structures marked by the distal appendage protein CEP164 (*25*), the subdistal/distal appendage protein outer dense fiber 2 (Odf2) (*26*), and the pericentriolar protein pericentrin (PeriCT) (*27*) (Fig. 2B and fig. S3, C to E). SEPT2, but not the ciliary axoneme or these basal body proteins, was solubilized in buffer containing 0.5% TritonX-100 (fig. S3F), indicating that SEPT2, like other septins (*28*, *29*), is associated with membrane. In addition, SEPT2 did not localize to the centrosome in nonciliated cells (Fig. 2, C and D), further indicating that it is not a constituent centrosomal protein.

To investigate whether SEPT2 is required for cilium formation and ciliary membrane barrier function, we used transient transfection with small interfering RNA (siRNA) oligonucleotides to deplete ~69% SEPT2 from serum-starved IMCD3 cells (Fig. 3, A and B). In general, cells that were completely depleted of SEPT2 lacked a cilium (Fig. 3C and fig. S4, A and B), whereas cells that were partially depleted (~54.3% depletion at the base of primary cilia) had a cilium that was significantly shorter (3.46 ± 0.20 μm) than controls (4.78 ± 0.31 μm). We also established stable IMCD3 cell lines depleted of SEPT2 using three different short hairpin RNAs (shRNAs), which reduced SEPT2 levels by 80 to 90% (Fig. 3, D and E) and resulted in a more complete defect in ciliogenesis across the cell population (Fig. 3E and fig. S4, C and D).

To investigate whether SEPT2 is part of a diffusion barrier at the base of the ciliary membrane, we measured ciliary membrane protein mobility in the 10 to 15% of the stable SEPT2-depleted IMCD3 cells (shRNA1) that had a short cilium but did not have significant SEPT2 staining near the basal body (fig. S4C). We detected a significant increase in the diffusional mobility of four ciliary membrane proteins when the whole cilium was photobleached in SEPT2-depleted cells, compared with controls (Fig. 4, A to C; fig. S5, A and B; table S3; and movies S16 to S23). Furthermore, the barrier index, defined as the ratio of mean fluorescence intensity of these proteins in the ciliary membrane to surrounding periciliary membrane, was reduced significantly in SEPT2-depleted cells compared with controls (Fig. 4D and fig. S5C). Thus, SEPT2 depletion removed the ciliary membrane diffusion barrier in cells that could still assemble a cilium. Because the cilium was shorter in these cells, and absent in most SEPT2-depleted cells, it is possible that loss of the diffusion barrier contributed to the overall defect in ciliogenesis.

We investigated whether loss of the ciliary membrane diffusion barrier after SEPT2 depletion affected cilium-dependent receptor signal transduction. Shh signaling requires enrichment of Smo in the ciliary membrane, and signal transduction results in increased *Gli1* and *Patched1* (*Ptc1*) mRNA levels (*14*, *30*). In SEPT2-depleted cells, Smo accumulation in cilia was reduced, although total cellular levels were unaffected (Fig. 4, D and F, and fig. S5C). After induction with Shh or Smo agonist (SAG), *Gli1* and *Ptc1* mRNA levels were reduced significantly in SEPT2-depleted cells compared with controls (Fig. 4E). Thus, the SEPT2 diffusion barrier is required for cilium-dependent Shh signal transduction.

Here, we have identified a septin-containing diffusion barrier at the base of the ciliary membrane that is required to retain receptor-signaling pathways in the primary cilium. This diffusion barrier restricts the diffusion of ciliary membrane proteins between the ciliary and periciliary membrane but permits the diffusion of ciliary transport proteins (IFT88). This implies that newly synthesized ciliary membrane proteins are most likely inserted by IFT and Bardet-Biedl Syndrome proteins into the ciliary membrane above the diffusion barrier (*7*). Thus, septins appear to have evolutionarily conserved roles from fungi to animals in the functional compartmentalization of membrane domains.

References and Notes

1. J. T. Eggenschwiler, K. V. Anderson, *Annu. Rev. Cell Dev. Biol.* **23**, 345 (2007).
2. W. F. Marshall, S. Nonaka, *Curr. Biol.* **16**, R604 (2006).
3. M. A. Lancaster, J. G. Gleeson, *Curr. Opin. Genet. Dev.* **19**, 220 (2009).
4. B. T. Emmer, D. Maric, D. M. Engman, *J. Cell Sci.* **123**, 529 (2010).
5. R. D. Sloboda, J. L. Rosenbaum, *J. Cell Biol.* **179**, 575 (2007).
6. G. R. Hunnicutt, M. G. Kosfiszer, W. J. Snell, *J. Cell Biol.* **111**, 1605 (1990).
7. M. V. Nachury, E. S. Seeley, H. Jin, *Annu. Rev. Cell Dev. Biol.* **26** (2010), 10.1146/annurev.cellbio.042308.113337.
8. A. Musgrave *et al.*, *Planta* **167**, 544 (1986).
9. O. V. Vieira *et al.*, *Proc. Natl. Acad. Sci. U.S.A.* **103**, 18556 (2006).
10. F. Caudron, Y. Barral, *Dev. Cell* **16**, 493 (2009).
11. Q. Hu, W. J. Nelson, E. T. Spiliotis, *J. Biol. Chem.* **283**, 29563 (2008).
12. N. F. Berbari, A. D. Johnson, J. S. Lewis, C. C. Askwith, K. Mykytyn, *Mol. Biol. Cell* **19**, 1540 (2008).
13. J. A. Follit, L. Li, Y. Vucica, G. J. Pazour, *J. Cell Biol.* **188**, 21 (2010).
14. R. Rohatgi, L. Milenkovic, M. P. Scott, *Science* **317**, 372 (2007).
15. K. Huang *et al.*, *J. Cell Biol.* **179**, 501 (2007).
16. P. V. Tran *et al.*, *Nat. Genet.* **40**, 403 (2008).
17. G. J. Pazour *et al.*, *J. Cell Biol.* **151**, 709 (2000).
18. P. D. Calvert, W. E. Schiesser, E. N. Pugh Jr., *J. Gen. Physiol.* **135**, 173 (2010).
19. Y. Barral, V. Mermall, M. S. Mooseker, M. Snyder, *Mol. Cell* **5**, 841 (2000).
20. P. A. Takizawa, J. L. DeRisi, J. E. Wilhelm, R. D. Vale, *Science* **290**, 341 (2000).
21. M. Ihara *et al.*, *Dev. Cell* **8**, 343 (2005).
22. H. Kissel *et al.*, *Dev. Cell* **8**, 353 (2005).
23. E. T. Spiliotis, S. J. Hunt, Q. Hu, M. Kinoshita, W. J. Nelson, *J. Cell Biol.* **180**, 295 (2008).
24. M. Kinoshita, C. M. Field, M. L. Coughlin, A. F. Straight, T. J. Mitchison, *Dev. Cell* **3**, 791 (2002).
25. S. Graser *et al.*, *J. Cell Biol.* **179**, 321 (2007).
26. H. Ishikawa, A. Kubo, S. Tsukita, S. Tsukita, *Nat. Cell Biol.* **7**, 517 (2005).
27. A. K. Gillingham, S. Munro, *EMBO Rep.* **1**, 524 (2000).
28. J. Zhang *et al.*, *Curr. Biol.* **9**, 1458 (1999).
29. Y. Tanaka-Takiguchi, M. Kinoshita, K. Takiguchi, *Curr. Biol.* **19**, 140 (2009).
30. K. C. Corbit *et al.*, *Nature* **437**, 1018 (2005).

31. We thank M. Kinoshita, S. Munro, G. J. Pazour, K. Mykytyn, D. R. Beier, C. Janke, J. Christianson, R. Kopito, and T. Stearns for reagents, and J. Atkins (Applied Precision, Inc.) for technical support. Supported by NIH grant GM35527 (W.J.N.), Department of Defense Breast Cancer Research Program Predoctoral Fellowship BC083077 (Q.H.), and Drexel CURE award from the State of Pennsylvania Tobacco Settlement Funds (E.T.S.). Supported in part by grants (M.V.N.) from the American Heart Association, the March of Dimes, NIH (GM089933), and the Sloan, Klingenstein and Searle Foundations. L.M. is a Research Specialist, and M.P.S. an Investigator of the Howard Hughes Medical Institute.

Supporting Online Material

www.sciencemag.org/cgi/content/full/science.1191054/DC1
Materials and Methods
Figs. S1 to S5
Tables S1 to S3
References
Movies S1 to S23

19 April 2010; accepted 8 June 2010
Published online 17 June 2010;
10.1126/science.1191054
Include this information when citing this paper.

Integrative Modeling Defines the Nova Splicing-Regulatory Network and Its Combinatorial Controls

Chaolin Zhang,* Maria A. Frias, Aldo Mele, Matteo Ruggiu, Taesun Eom, Christina B. Marney, Huidong Wang, Donny D. Licatalosi, John J. Fak, Robert B. Darnell*

The control of RNA alternative splicing is critical for generating biological diversity. Despite emerging genome-wide technologies to study RNA complexity, reliable and comprehensive RNA-regulatory networks have not been defined. Here, we used Bayesian networks to probabilistically model diverse data sets and predict the target networks of specific regulators. We applied this strategy to identify ~700 alternative splicing events directly regulated by the neuron-specific factor Nova in the mouse brain, integrating RNA-binding data, splicing microarray data, Nova-binding motifs, and evolutionary signatures. The resulting integrative network revealed combinatorial regulation by Nova and the neuronal splicing factor Fox, interplay between phosphorylation and splicing, and potential links to neurologic disease. Thus, we have developed a general approach to understanding mammalian RNA regulation at the systems level.

RNA-binding proteins (RBPs) regulate alternative splicing (AS) and processing of RNA to generate biological complexity (*1*). Inferring RNA target networks regulated by these splicing factors may provide general insights into the mechanisms of regulation and their role in disease (*2*–*5*). Several global approaches have recently been applied toward this aim (*2*), including bioinformatic predictions driven by analysis of RBP motifs (*6*–*8*), profiling of RNA isoforms based on splicing microarrays (*9*–*11*) or RNA-Seq (*12*–*14*), and biochemical footprints derived from high-throughput sequencing of RNA isolated by crosslinking immunoprecipitation (HITS-CLIP) (*9*, *15*). These methods have been applied to identify and genetically validate ~90 alternative exons regulated by Nova1/2 (*9*, *10*), a family of neuron-specific splicing factors. Nova regulates a biologically coherent set of transcripts encoding synaptic proteins (*10*), and an RNA-regulatory map predicts that Nova-regulated splicing is position dependent, such that alternative exons are included when Nova binds to downstream introns and are excluded via binding within the exons or to upstream introns (*9*, *16*).

Each of these methods is limited in its signal-to-noise ratio and scope: RBP motifs generally have very low sequence specificity [e.g., YCAY for Nova, ~1 site per 64 nucleotides (nt)]; microarray or RNA-Seq data are noisy at the exon level beyond a small set of top candidates and are correlative in nature; and biochemical protein-RNA interactions do not necessarily imply functional regulation. Consequently, only a small set of targets have been confidently identified for most splicing factors (*4*, *17*). An alternative strategy is to integrate multiple sources of information, so that individually weak bits of evidence can be combined to generate confident predictions, as demonstrated in studies of protein-protein interactions (*18*) and transcription factor networks (*19*). Here, we set out to develop such an integrative approach to probabilistically model a diverse set of genomic, experimental, and evolutionary data, using Bayesian networks to define and understand the function of RNA networks.

We studied the Nova splicing-regulatory network as an exemplar and compiled four types of data important for inferring direct Nova-RNA interactions coupled with defined Nova-dependent AS events: (i) 279,631 CLIP tag clusters, ranked by peak height, derived from 20 independent HITS-CLIP experiments (figs. S1 and S2, table S1, and datasets S1 and S2); (ii) 841,501 Nova-binding sites (YCAY clusters) bioinformatically predicted and scored from the clustering, accessibility, and conservation of YCAY elements (fig. S3); (iii) four splicing-microarray data sets comparing wild-type and Nova knockout (KO) brains, which detected 1331 exons showing significant Nova-dependent splicing, in addition to many exons with moderate but potentially functional changes (fig. S4 and table S2); and (iv) evolutionary signatures of regulated splicing, including conservation of AS in humans or rats, and preservation of reading frame (*20*). Each individual data set suggested

Laboratory of Molecular Neuro-Oncology, Howard Hughes Medical Institute, The Rockefeller University, 1230 York Avenue, New York, NY 10021, USA.

*To whom correspondence should be addressed. E-mail: czhang@rockefeller.edu (C.Z.); darnelr@rockefeller.edu (R.B.D.)